MEASUREMENTS OF UNSTEADY PRESSURES AND WAKE FLUCTUATIONS FOR FLOW OVER A CYLINDER AT SUPERCRITICAL REYNOLDS NUMBER

Thesis by

Robert Edward Spitzer

In Partial Fulfillment of the Requirements

For the Degree of

Aeronautical Engineer

California Institute of Technology

Pasadena, California

1965

(Submitted December 31, 1964)

ABSTRACT

A test was conducted to measure and map the unsteady pressure fluctuations over the surface of a smooth, cantilevered, circular cylinder in the supercritical Reynolds number range from 2.5×10^5 to 7.5×10^5. Lift fluctuations were measured, hot-wire wake surveys were made, and the effects of boundary-layer tripping were investi - gated. Power spectral densities were computed from recordings of the fluctuations, and cross-correlation coefficients were determined.

Pressure fluctuations were found to be small in magnitude but with relatively high axial correlation except at the points of flow separation. Definite evidence of periodicity was found in the pressure fluctuations excluding those in the region of flow separation. Fluctuating lift was found to be random in nature in the supercritical regime. Power spectra of wake velocity fluctuations after transition showed largely turbulent patterns with perhaps some dominance at Strouhal number near 0.4 seen on occasion. Localized boundary-layer tripping caused earlier flow separation, significant increases in pressure and lift fluctuations, a greater degree of axial correlation, and a shift in the power spectra to indicate periodic effects.

ACKNOWLEDGMENT

The author would like to express his appreciation to Dr. Y.C. Fung for his encouragement and guidance during this study and to the National Science Foundation for providing financial assistance. Special indebtedness is owed to Dr. L. V. Schmidt for his friendship and for his helpful advice on the experimental techniques used in this study. Much is owed to M.E. Jessey, C. Hemphill, and R. D. Luntz for their assistance with the data acquisition system, to G. F. Carlson for constructing model and transducer components, and to W.H. Bettes, Jr., W.L. McNay, A. McMeekin, R. Gauthier, and D. Meggitt for their competent handling of the wind tunnel test. Sincere gratitude is owed to my wife, Jean Marie, for help throughout the program, especially in the preparation of the manuscript.

TABLE OF CONTENTS

LIST OF FIGURES

LIST OF FIGURES (cont'd)

NOTATION

A. List of Symbols:

d	Diameter of cylinder
f	Frequency, cycles per second
P_x	Static pressure at location (x)
q	Dynamic pressure, $q = {}^1/_2 \rho \overline{V_\infty}^2$
t	Time
V	Velocity
$\overline{V_\infty}$	Velocity of free stream flow
x	Axial coordinate along cylinder axis, X =0 at the base
y	Lateral coordinate from tunnel (and cylinder) centerline
z	Streamwise coordinate from cylinder trailing edge
ρ	Mass density of air
ν	Kinematic viscosity of air
τ	Time shift
θ	Angular coordinate along cylinder surface, zero reference is forward stagnation point
ϕ	Power spectral density
Note:	Other symbols are defined in the text when introduced

B. Superscripts:

$\overline{(\ )}$	Mean average, equals $\lim_{T \to \infty} \frac{1}{2T} \int_{-T}^{T} (\ )\, dt$
$\sqrt{\overline{(\ )^2}}$	Root-mean square of ( )

C. Subscripts:

$(\ )_i$	Refers to position x_i

NOTATION (cont'd)

$( )_n$ Refers to normalized term, e.g., ϕ_n

D Dimensionless Coefficients:

C_L Local lift force coefficient = $\frac{\text{Lift force / unit span}}{q\,d}$

C_D Local drag force coefficient = $\frac{\text{Drag force / unit span}}{q\,d}$

C_p Static pressure coefficient = $\frac{Px - Pref.}{q}$

R_e Reynolds number of the cylinder = $\frac{\overline{V}_\infty\, d}{\nu}$

S Strouhal number (non-dimensional frequency) = $\frac{fd}{\overline{V}_\infty}$

SECTION I

INTRODUCTION

The study of flow over a circular cylinder is not a new subject in aerodynamics. The existence of tones produced by wind blowing over wires has been known for some time. Strouhal (1) (1878) carried out experiments which showed that the frequency of these tones was directly proportional to the air velocity and inversely proportional to the cylinder diameter. Experiments by Lord Rayleigh (2) showed that loads on a cylinder caused oscillations in a direction perpendicular to the flow. In 1912 von Karman (3) published his theory of the vortex street which stimulated a lengthy series of flow investigations. While many experiments have been conducted, the problem of periodicity and vortex shedding is still essentially unsolved.

Studies of flow over the cylinder were made to measure static or steady-state (i.e., long-time averages) phenomena such as drag coefficient and static pressure distributions. Relf (4) (1914) measured drag of wires for Reynolds numbers up to 10^4, whereas tests by Flachsbart (5) (1927) extended the data to about Re = 10^6. Similar investigations have been carried on by many others. Fage and Falkner (6, 7, 8) measured drag by integrating cylinder pressure distributions in the range $4 \times 10^4 \leq Re \leq 4 \times 10^5$. Goldstein (9) summarizes much of the work up to 1938. Studying compressibility effects Stack (10) (1941) measured cylinder drag for $4 \times 10^4 \leq Re \leq 10^6$, and Delany and Sorensen (11) (1953) measured drag for $10^4 \leq Re \leq 2 \times 10^6$. Roshko (12) (1960) measured drag for $2 \times 10^6 \leq Re \leq 8.4 \times 10^6$. Recently, Bohne (13a) and Buell, et al., (14) have also measured drag

in the range of Roshko's data.

The results of these studies define three major flow regimes. For $10^3 \leq Re \leq 3 \times 10^5$ the value of drag coefficient, $\overline{C_D}$, lies between 1.0 and 1.2 with the flow regime being called "subcritical." At about $Re = 3 \times 10^5$ a transition occurs and $\overline{C_D}$ drops to 0.20 - 0.35 yielding the "supercritical" Reynolds number range, and somewhere near $Re = 3 \times 10^6$ a second transition seems to occur giving rise to a third range called "transcritical" by Roshko where $\overline{C_D} = 0.4$ to 0.7.

Examples of measurements of steady-state surface pressures are given by Fage (6, 7, 8), Roshko (12, 15) and Bursnall and Loftin (16). The subcritical regime is characterized by flow separation at $\theta \approx 60^\circ$ yielding a wide wake ($\overline{C_{p_{base}}} \approx -1.0$) and consequently high drag coefficient. The supercritical range has flow separation at $\theta \approx 100^\circ$ with a narrow wake width ($\overline{C_{p_{base}}} \approx -0.2$) and low drag coefficient, and the transcritical regime shows a widening of the wake ($\overline{C_{p_{base}}} = -0.5$ to -0.8), and higher drag coefficient with separation at $\theta \approx 80^\circ$.

Investigations of the dynamic properties of cylinder flow began with measurements of vortex shedding and wake flow. Based on experimental evidence various wake regimes seem to exist: (1) laminar or Oseen flow in the Reynolds Number range less than 40, (2) stable range with vorticity pattern extending far downstream ($40 < Re < 150$), (3) transition ($150 < Re < 300$), and (4) an irregular range for $Re = 300$ to 10^5. In the irregular range the vortices are destroyed by turbulent diffusion as they travel downstream. Roshko's results (17) show that

wake periodicity begins at Strouhal number S = 0.12 at Re ≈ 50 and rises to S ≈ 0.2 at Re ≈ 300. Roshko, Kovasznay (18) and Relf and Simmons (19) as well as others (see Krzywoblocki (20))have verified that in the wake S ≈ 0.2 for $300 \leq Re \leq 10^5$.

After transition the character of the wake changes and no simple periodicity has been observed. Relf and Simmons (19) using a hot-wire with a vibration galvonometer recorded the most prominent disturbances in the range $10^5 \leq Re \leq 10^6$ as rising from S = 0.2 to S ≈ 0.3 with much scatter. Drescher's (21) measurements in water at $10^4 \leq Re \leq 1.13 \times 10^5$ show also that the dominant frequencies gave S = 0.2 to 0.3. Delany and Sorensen (11) measured wake fluctuations at S = 0.35 to 0.45 using a pressure transducer in a probe placed closely behind the cylinder for $Re \approx 2 \times 10^6$. Their results were determined by obtaining the dominant frequencies from an oscillograph trace of the transducer output signal. Roshko (12) used hot-wire techniques with a wave analyzer for a wake study in the range $2 \times 10^6 \leq Re \leq 8.4 \times 10^6$. Above $Re = 3.5 \times 10^6$ he found definite frequencies were discernible at S ≈ 0.27, while in the lower range no dominant frequencies could be found, contrary to Delany and Sorensen. However, Roshko's hot-wire was 7.3 diameters downstream and 0.7 diameters to the side which, according to Roshko, may have placed the hot-wire out of the narrow supercritical wake.

Measurements of the unsteady forces acting on the cylinder itself are the most recent of data with Fung (22) discussing the scope of published work to about 1959. For the higher subcritical regime, McGregor (23) (1957) measured oscillatory pressure distributions,

$\sqrt{\overline{C_p{}^2}}$ vs. θ, and estimated $\sqrt{\overline{C_L{}^2}}$ and $\sqrt{\overline{C_D{}^2}}$ for $4.5 \times 10^4 \leq Re \leq 1.3 \times 10^5$ using a microphone as a pressure transducer. Gerrard (24, 25) measured fluctuating surface pressures in the range $4 \times 10^3 < Re < 1.14 \times 10^5$ using a capacitance transducer and also estimated $\sqrt{\overline{C_L{}^2}}$ and $\sqrt{\overline{C_D{}^2}}$ from his pressure data. Two-point correlation coefficients for surface pressure fluctuations at $\theta = 90^\circ$ and 180° were measured by Prendergast (26) for $2.5 \times 10^4 \leq Re \leq 1.25 \times 10^5$, and el Baroudi (27) measured two-point correlations for velocities at $\theta = 90^\circ$ using hot-wires for $1.1 \times 10^4 \leq Re \leq 4.5 \times 10^4$. Humphreys (28) measured fluctuating lift and drag on a cylinder suspended in a wind tunnel for $4 \times 10^4 \leq Re \leq 6 \times 10^5$. Keefe (29) measured oscillatory lift and drag for $6 \times 10^3 \leq Re \leq 1.15 \times 10^5$ using a strain-gauge load cell in a one-diameter section of the cylinder model.

In general these experiments show that end-effects and three-dimensional aspects of the flow are quite important. Correlation lengths were found to be from 3 to 6 diameters by el Baroudi, whereas Prendergast obtained slightly lower values at $\theta = 90^\circ$ while correlation lengths at $\theta = 180^\circ$ were about one-fourth of values at $\theta = 90^\circ$. Humphreys estimated a correlation length of 1.56 dia. at $Re \approx 10^5$. At Reynolds Numbers approaching transition, the correlation lengths drop rapidly to about one diameter. Distributions of $\sqrt{\overline{C_p{}^2}}$ vs. θ show a rise to maximum values at $\theta \approx 90^\circ$ to 150° at $S \approx 0.2$ with the second harmonic becoming evident in the more rearward angular locations (120° to 180°). Gerrard found the pressure fluctuations to be 180° out-of-phase between cylinder sides. The values of $\sqrt{\overline{C_L{}^2}}$ vary between tests with most data lying between 0.3 and 0.8. Drag, $\sqrt{\overline{C_D{}^2}}$, tends to be

one-tenth of $\sqrt{\overline{C_L 2}}$ at twice the frequency.

Interest in the dynamics of large cylinders with application to missiles was stimulated by Ezra and Birnbaum (30) and by the analysis of Fung (31). In the supercritical regime, Fung (22) was the first to measure oscillatory lift and drag for $2 \times 10^5 \leq Re \leq 1.4 \times 10^6$ using a strain-gauge load cell in a 1.75 diameter section of the cylinder. Humphreys (28) also measured $\sqrt{\overline{C_L 2}}$ and $\sqrt{\overline{C_D 2}}$ in the supercritical range but discovered, as did Fung, that the three-dimensional character fo the flow and high sensitivity to test conditions (surface, end effects, etc.) brought out the need for more data in this range. Using statistical methods of power spectral densities, Fung found fluctuating lift and drag to be essentially random. However, questions remained to be answered about the effect of wind tunnel turbulence and testing techniques on the data.

As part of the program at the California Institute of Technology under Dr. Fung, L. V. Schmidt (13b, 32) designed and developed a pressure-transducer technique of measuring sectional loads on a very smooth cylinder exposed to the flow in a cantilevered, "smokestack" configuration. Schmidt's data resulted in power spectral densities also indicating randomness in lift and drag fluctuations for the range $3.8 \times 10^5 \leq Re \leq 7.5 \times 10^5$. Three-dimensionality became evident with correlation lengths of less than one diameter. Schmidt found $\sqrt{\overline{C_L 2}} \approx 0.04$ (about one-fourth of Fung's value) and $\sqrt{\overline{C_D 2}} \approx 0.03$ (about the same as Fung). Another significant effect was the extreme sensitivity of the data to model surface smoothness (also noted by Fung and by Buell (13c)). By blowing jets of air through 0.020-inch

orifices at $\theta = \pm 30^{\circ}$, Schmidt was able to change the character of lift and drag frequency spectra as $\sqrt{\overline{C_L 2}}$ rose to 0.115-0.135. Further tests by Blackiston (13d, 33) in the same Reynolds number range on the effects of cylinder tip shape showed significant changes in fluctuating lift and drag at the tip. Blackiston's cross-correlation data showed that tip-loading effects are not felt past approximately two diameters along the cylinder axis for the blunt-end, "smokestack" configuration. Tests by Buell (13c, 14) show general agreement with Blackiston at the transcritical Reynolds numbers.

It was decided that more information was needed to describe in greater detail the nature of the flow in the supercritical regime. As part of the continuing program under Dr. Fung, the test plan for this report was to map the fluctuating pressures over the surface of the cylinder, to scan the wake for frequency distributions and to learn more about the effect of surface disturbances, namely boundary layer tripping by blowing air from the cylinder surface.

The experimental arrangement is described in Section II with data reduction described in Section III. The experimental results are presented in Section IV, including pressure distributions, pressure power spectral densities, wake survey results and the effects of surface disturbance.

SECTION II

DATA ACQUISITION

The objectives of the wind tunnel test were to measure the following:

1. Fluctuating and steady pressures over the cylinder to determine their spatial distribution and frequency content in the supercritical range,
2. Lift fluctuations as a verification of repeatability of the results obtained by Schmidt,
3. Velocity distributions and fluctuations in the wake of the cylinder to determine dominate frequencies, and
4. Effects of boundary-layer tripping on the pressure distribution and wake by blowing jets of air from the cylinder surface.

Data were recorded for $2.5 \times 10^5 \leq Re \leq 7.5 \times 10^5$ in the GALCIT* Ten-Foot Wind Tunnel using the cylinder model of Schmidt (32) and Blackiston (33). A calibration was made of the tunnel flow, and the dynamic pressure was corrected to account for model blockage (2%). A plot of tunnel characteristics for this test is given in Figure 1. Approximately 85% of the area over the turning vanes in the low-velocity settling section was covered with cheese-cloth to lower turbulence and filter dust particles from the air (the entire tunnel was scrubbed before the test).

The model was a smooth cylinder (8.54-inch diameter) cantilevered 8.1 diameters from a flat floor in the tunnel. The model

---

* Graduate Aeronautical Laboratories, California Institute of Technology

passed through the tunnel floor to a four-foot diameter steel tank anchored on ten-inch steel channels to the building structure as shown in Figure 2. Figure 3 presents photographs of the model which was made of interchangeable aluminum sections, allowing the instrumen - tation packages to be placed in many different positions along the cylinder axis. Cylinder sections were made to fine tolerances yielding a high quality surface with very little discontinuity at the interface between sections. The gap around the model at the floor was sealed with tape. The top section of the cylinder contained 40 lbs. of lead shot for damping purposes. This was found by Schmidt and Blackiston to be sufficient to prevent aeroelastic feedback effects on the data. With the damping, the resonance frequency was about 10 cps (see Reference 32).

Fluctuating pressures were measured through a 0.025-inch orifice by a reluctance-type pressure transducer of the same design as developed by Schmidt. Angular position was determined by rotation of the model to align the orifices with a protractor to within one degree of the desired value. Proper back pressure was supplied to the trans- ducer by a second orifice placed 0.75-inch (0.088 diameter) below the transducer orifice at the same angular position. To assure a steady back pressure, a calibrated "dashpot" was placed in the system to dampen the fluctuations in pressure from the back-pressure orifice, and this steady-state surface pressure was measured using a fluid-in- glass manometer. The instrumented cylinder section is shown in Figure 4.

The transducers had sensitivities of about 2 volts/psi with

linearity to $\pm$ 0.75 psi., calibrated statically with a 100 kc carrier amplifier. The transducer and orifice system were calibrated dynamically, using an acoustical driver for sinusoidal pressure fluctuations up to 0.16 psi-RMS, by measuring the gain and phase shift caused by the orifice (see Reference 32 for details). The results agreed closely with Schmidt, showing the system to have flat response characteristics up to 200 cps. The pressure "dashpot" dynamic calibration showed complete damping in the range of the data.

Lift fluctuations were measured using the instrumentation sections built by Schmidt. Lift was determined by 18 pressure transducers, nine on each side of the section, spaced to cover equal portions of the cylinder chord. Electrical integration of each nine gave the loading on each side of the cylinder. A differential 100 kc carrier amplifier gave the amplified electrical difference between sides, i.e., fluctuating lift signal. Back pressure of $\overline{C}_p = -0.8$ was supplied to all lift transducers by a static pressure orifice on a two-inch diameter cylinder placed out from the tunnel wall (the orifice was out of the wall boundary-layer).

Data were recorded on one-inch magnetic tape using four frequency-modulated channels of a seven-channel Ampex FR-100 tape recorder. A schematic of the pressure and lift data acquisition system is given in Figure 5. In order to make use of the existing differential carrier amplifiers (which had operating noise levels of 0.4 mv RMS), a load-balancing transducer was required for each of the pressure measuring transducers. Care was taken to keep these "dummy" transducers from registering pressure changes. RMS values of

pressure and lift fluctuations were recorded using a Ballantine Type 320 True RMS Voltmeter with capactive damping to give a long time constant. A D. C. "bucking" voltage was applied to one side of the Epsco Differential D. C. Amplifiers to null out direct current voltages so as not to overdrive the $\pm$ 1. 4 volt D. C. (1. 0 volt RMS) range of the Ampex recorder.

Hot-wire data were taken using a 0. 0002-inch tungsten wire, approximately 0. 08-inch in length (time constant $\approx$ 0. 001 sec.), spot-welded to the tips of two needles. The axis of the hot-wire was parallel to the cylinder axis at all times during the test. A standard constant-current (50 ma. - maximum) circuit was used. The frequency response of the hot -wire was corrected using a compensating output amplifier which had variable-gain capability. Compensation was achieved by placing a 60 cps square-wave on the wire and adjusting the amplifier frequency compensation using an oscilloscope. Fluctuating output signal was measured by the damped Ballantine voltmeter before being recorded on magnetic tape.

After calibration in free-stream flow (model out of tunnel) the hot-wire was mounted on a probe which moved along a remotely-operated traverse to scan the wake behind the cylinder. The traverse could be positioned laterally to within 0. 0005 diameters and up to five diameters downstream of the model trailing edge. A sketch of the traverse is given in Figure 6 with a schematic of the hot-wire data acquisition system shown in Figure 7. The traverse was in the tunnel only for hot-wire data runs (which excluded most of the basic pressure-mapping runs).

Since Fung and Schmidt found the flow to be quite sensitive to boundary-layer tripping, it was decided to continue this type of study in the test. Using the system designed and developed for tests by Schmidt and Blackiston, the flow was disturbed at an axial location (near the end of a spacer section) by blowing air radially from the surface through 0.020-inch orifices at $\theta = \pm 30^{\circ}$. Air was supplied and regulated using parallel lines from a Fischer and Porter flow meter. Air could be supplied to one or both orifices as desired. The effects of blowing on lift, pressure distribution, and wake were measured.

Several precautions were taken during the test to assure accurate data. Before each data run the model was cleaned with solvent, and all nicks and scratches were rubbed smooth. Twice each day of the test a static pressure calibration was made on all of the transducer systems to check sensitivities. Noise levels were checked, and most signal-to-noise ratios were kept at ten or above. Before and after each data run, calibration voltages of zero and $\pm$ 1.4 volts D.C. were recorded on the magnetic tape to provide a proper reference for adjusting output amplifiers upon data playback. The linearity of the Ampex was checked each day to determine reliability. Frequency response of the tape recorder was not exceeded. Data signals were monitored by a Dumont Model 411 dual beam oscilloscope at various points going to the tape recorder and off the tape directly after recording. All other measuring and monitoring equipment were removed from the circuit during recording to reduce the possibility of interference. All data were recorded according to the coordinate system of Figure 8.

SECTION III

DATA REDUCTION

3.1 Mathematical Background

In the supercritical regime, the amount of turbulence present in the flow makes necessary the treatment of the data by statistical methods. Several texts deal with statistical techniques; see, for example, Chapter 8 of Fung (34) and Chapter 6 of James, Nichols, and Phillips (35).

Consider the signals from a random process to be given by the following:

$$P(x_i, t) = P_i(t) + \overline{P_i} \qquad (3.01a)$$

$$P(x_j, t+\tau) = P_j(t+\tau) + \overline{P_j} \qquad (3.01b)$$

where $\overline{P_i}$ and $\overline{P_j}$ are the mean values of $P(x_i, t)$ at x_i and $P(x_j, t+\tau)$ at x_j averaged over a long time interval while $P_i(t)$ and $P_j(t+\tau)$ are the fluctuating components of $P(x_i, t)$ and $P(x_j, t+\tau)$ respectively.

The auto-correlation function is defined, letting $x_i = x_j$, as

$$A^*(\tau) = \overline{P(x_i, t) \cdot P(x_i, t+\tau)} \qquad (3.02)$$

and gives an indication of how well a process correlates with itself in a time shift, τ. To emphasize the fluctuating part of the auto-correlation function one may remove the mean value $\overline{P_i}$ and define

$$A(\tau) = \overline{P_i(t) \cdot P_i(t+\tau)} \qquad (3.03)$$

Note that for zero time shift ($\tau=0$) the auto-correlation becomes the

mean square of $P_i(t)$ and is proportional to the energy represented by the signal.

The cross-correlation coefficient measures the spatial correlation of a process at two points, x_i and x_j. For zero time shift and normalizing with respect to the square root of the product of the sums of the mean square and squared mean of each signal, the cross-correlation coefficient is given by

$$R^{*}(x_i\, x_j) = \frac{\overline{P(x_i,\, t)\; P(x_j,\, t)}}{\sqrt{\overline{P(x_i,\, t)^2}}\sqrt{\overline{P(x_j,\, t)^2}}} \qquad (3.04)$$

A further simplification can be made with the assumption of mean average being zero, i.e., $\overline{P_i} = \overline{P_j} = 0$; therefore,

$$R(x_i\, x_j) = \frac{\overline{P_i(t) \cdot P_j(t)}}{\sqrt{\overline{P_i(t)^2}}\sqrt{\overline{P_j(t)^2}}} \qquad (3.05)$$

where $\overline{P_i(t) \cdot P_j(t)}$ is now the time average of the product of the fluctuating components of the signals. Cross-correlation coefficient values range over + 1.0 (complete in-phase correlation) to zero (no correlation) to - 1.0 (180° out-of-phase correlation).

The auto-correlation function is an even function. The Fourier transform of $A(\tau)$ is given by

$$\phi(f) = \int_0^{\infty} A(\tau)\; [\cos 2\pi f \tau]\, d\tau \qquad (3.06)$$

where

$$A(\tau) = \int_0^\infty \phi(f) \left[\cos 2\pi f \tau\right] df \qquad (3.07)$$

For $\tau=0$, the auto-correlation becomes the mean square of $P_i(t)$ i.e.,

$$A(0) = \overline{P_i(t)^2} = \int_0^\infty \phi(f)\, df \qquad (3.08)$$

and $\phi(f)$ is defined as the power spectral density. The power spectral density shows the distribution of energy in the signal as a function of frequency.

3.2 Analog Reduction

Cross-correlation coefficients were determined using analog techniques on 2.5-minute traces of the data played back from the magnetic tape. An averaging circuit and analog multiplier which could handle both fluctuating and steady voltages were used. A schematic of the system is shown in Figure 9. For the averaging circuit a Philbrick UP A-2 operational amplifier was used with capacitive feedback. The circuit time constant was 9 seconds with a gain of approximaetly -7.5. This choice of time constant was made to allow damping for fluct - uations of 1 cps and up.

Tape data played back through the system consisted of typical signals

$$e(x_1, t) = e_1(t) + \overline{e_1} \qquad (3.09a)$$

$$e(x_2, t) = e_2(t) + \overline{e_2} \qquad (3.09b)$$

where $e(x_1, t)$ and $e(x_2, t)$ corresponded to data recorded simul -

taneously on two channels from positions x_1 and x_2, and typically were either pressure or lift recordings. As explained below, five curves plotted with a Moseley 2D-2A, X-Y plotter were required to determine each cross-correlation coefficient. Data first plotted were the tape signals which passed through the averaging circuit; this yielded

$$\overline{e\,(x_1,\ t)} = \overline{(e_1\,(t) + \bar{e}_1)} = \bar{e}_1 \qquad (3.10a)$$

and

$$\overline{e\,(x_2,\ t)} = \overline{(e_2\,(t) + \bar{e}_2)} = \bar{e}_2 \qquad (3.10b)$$

The D. C. "bucking" voltages applied to the Epsco differential D. C. amplifiers were used to bias the output to make the means of both data signals approximately zero for a common period of time. "Bucking" was required to nullify any D. C. component from the tape.

Without changing any circuit settings, the tape signal was sent through the Philbrick K5M analog multiplier whose averaged output was plotted against time to yield

$$\overline{e\,(x_1,\ t)^2} = \overline{e_1\,(t)^2} + (\bar{e}_1)^2 \qquad (3.11a)$$

$$\overline{e\,(x_2,\ t)^2} = \overline{e_2\,(t)^2} + (\bar{e}_2)^2 \qquad (3.11b)$$

$$\overline{e\,(x_1,\ t)\ e\,(x_2,\ t)} = \overline{e_1\,(t)\cdot e_2\,(t)} + \bar{e}_1 \cdot \bar{e}_2 \qquad (3.11c)$$

For the period of time when $\overline{e\,(x_1,\ t)} = \overline{e\,(x_2,\ t)} = 0$, $\overline{e\,(x_1,\ t)^2}$, $\overline{e\,(x_2,\ t)^2}$, and $\overline{e\,(x_1,\ t)\cdot e\,(x_2,\ t)}$ reduce to $\overline{e_1\,(t)^2}$, $\overline{e_2\,(t)^2}$, and $\overline{e_1\,(t)\cdot e_2\,(t)}$. The correlation coefficient, $R\,(x_1\ x_2)$, was determined according to Equation (3.05). This method

has been checked against digital computer results by Schmidt (32) and has been found to be sufficiently accurate for data reduction. As an additional precaution, checks were made on the averaging circuit gain and time constant, and on the multiplier alignment for each set of plots.

3.3 Digital Reduction

Selected portions of the data were converted to digital form using the Biological Systems Mark II analog-digital conversion unit at the Booth Computing Center, at the California Institute of Technology. The conversion unit had the capability of digitizing at the rate of 10,000 numbers per second. For the following data analysis the rate of 1000 numbers per second was chosen. The analog signal from the tape was sampled each 0.001 second with the digitizing equipment determining the signal voltage in one microsecond.

Before digitizing, a 1000 cps clock signal was recorded for 10 seconds on an unused direct-reproduce channel of the tape to serve as the digitizing trigger pulse. The clock signal was generated by a Berkeley Universal Counter and Timer, Model 550I, which in turn commanded a square-wave Pulse (400 μsec width, 15 volt peak) from a Rutherford Pulse Generator, Model B7B. The signal saturated the direct-reproduce channel of the Ampex distorting the wave shape but gave a rapid-rise spike which sufficed for digitizing purposes. The digital results were printed on tape by the I. B. M. 7040 unit of the I. B. M. 7094 Computing System at Caltech. Care was taken throughout the digitizing to use sufficient checks to indicate the validity of the digitized values. A computer program converted the data

to the Fortran input tape used in the computation of power spectral densities.

Following the lead of Schmidt (32), an I. B. M. 7094 computer program based on techniques outlined by Press and Tukey (36) and Blackman and Tukey (37) was used to estimate auto-correlation and power spectral density. Obtaining the power spectra of the digital record assumes that $y_1, y_2, \ldots, y_n$ represents a series of data points at times $t_1, t_2, \ldots, t_n$ where all time intervals are equal. To conform to the basic equations, the first step of the program adjusted the input data to satisfy that the mean average of a complete sampling of data (i. e., 10 second digital trace) be zero;

$$\sum_{i=1}^{n} y_i = 0 \qquad (3.12)$$

Auto-correlation was estimated next for values of the index L from 0, 1, 2, ..., M to be the following; (3.13)

$$A(L) = \frac{1}{(n-L)} \sum_{i=L+1}^{n} y_{i-L}\, y_i - \frac{1}{(n-L)^2} \sum_{i=L+1}^{n} y_{i-L} \sum_{i=L+1}^{n} y_i$$

A Fourier Cosine Transformation applied to the auto-correlation for values of K from 0, 1, 2, ..., M gives the power spectral density estimate (3.14)

$$X(K) = \frac{\delta_K}{M} \left[A(0) + \sum_{L=1}^{M-1} e(L) \left\{ \cos \frac{L\pi K}{M} \right\} A(L) \right]$$

where

$$\delta_K = \begin{cases} 0.5 & \text{for } K = 0 \text{ or } M \\ 1.0 & \text{for all other values of } K \end{cases} \qquad (3.14)$$

$$e(L) = 1 + \cos \frac{L\pi}{M} = \text{Hanning factor.}$$

Details on the use of such a factor in calculations with discrete data points may be found in Reference 37, and discussion of a similiar, but more involved, program may be found in Reference 32. Estimates were made at intervals of one cycle per second with a band-pass filter width of 2 cps. In the program it was possible to set the computation cutoff frequency by choosing to work with digital points representing more than 0.001 second spacings. This was accomplished by proper choice of the index, M, and the time shift (i.e., choice of data point spacing) $\Delta \tau$ in the program format.

Checks were made on the program by computing the power spectral density estimate for a sine-wave of known frequency. The result was a spike at that frequency. Cutting the number of samples to two to three samples per wave cycle did not hinder the program's ability to point out the frequency.

The total energy of the signal, A (0), was computed, as was the energy in the range for the computation of power spectral density. Because of computing time, the upper frequency for the power spectral density estimate was determined by containing over 99% of the energy of the signal within the limits. This cutoff frequency was about 125 cps; hence, the power spectral density was normalized by

the energy in the frequency range, satisfying the equation:

$$\int_{o}^{125} \phi_n (f)\ d f = 1 \qquad (3.15)$$

Thus, plots of $\phi_n (f)$ vs. frequency for different data could be compared directly.

SECTION IV

RESULTS

The objective of this study was to gain some insight into the details of the flow over a cylinder in the supercritical Reynolds number range. In order to compare the results with those of Schmidt (32) and Blackiston (33), most data presented were obtained along the cylinder axis from $x/d = 4.86$ to 5.87 (cylinder length was 8.1 diameters). The determining factor in keeping the majority of measurements below $x/d = 6$ was the effect of the blunt tip whose region of influence was found by Blackiston to extend approximately two diameters down the cylinder.

It was possible to estimate data accuracy in most instances. The tunnel operating parameter, dynamic pressure (q), could be set to within $\pm$ 1%, except for q = 5 psf which was held to within $\pm$ 5%. Steady-state pressure coefficient, $\overline{C_p}$, was determined using a fluid-in-glass manometer to within $\pm$ 6% for data taken at q = 5 psf, dropping to less than $\pm$ 1% for q = 40 psf. Error estimates of the fluctuating pressure and fluctuating lift data were based upon the following; transducer sensitivities were about 2 volts/psi, operating noise levels were approximately 0.4 mv, and the signal-to-noise ratio was never less than five. The root-mean-square (RMS) value of fluctuating pressure coefficient, $\sqrt{\overline{C_p{}^2}}$, could be determined to within $\pm$ 20 % for the lowest signal levels; these were recorded at angular positions near the leading edge for data taken at q = 5 and 10 psf. In general, however, the value of $\sqrt{\overline{C_p{}^2}}$ was determined more accurately, ranging, for example, from $\pm$ 10% at $\theta = 90^\circ$, q = 5psf to $\pm$ 3% at $\theta = 90^\circ$,

q = 40 psf. The root-mean-square value of fluctuating lift coefficient, $\sqrt{\overline{C_L 2}}$, varied in accuracy depending on signal strength from $\pm$ 20% at q = 5 psf to $\pm$ 6% at q = 40 psf. It should be noted that further amplification of all fluctuating signals provided by the Epsco amplifiers brought the levels well into the optimum range of the tape recorder. The hot-wire system signal exceeded noise level by a minimum factor of seven in the outer fringes of the wake, whereas the higher velocity fluctuations near the wake center yielded signal-to-noise ratios of approximately one-hundred.

The RMS voltage readings corresponding to $\sqrt{\overline{C_p 2}}$, $\sqrt{\overline{C_L 2}}$, and $\sqrt{\overline{V^2}}$ were obtained from the capacitance-damped Ballantine True RMS Voltmeter. The inherently unsteady character of the signal initially created a problem in data recording until capacitive damping was added to the voltmeter to increase the time constant. The RMS results presented are felt to be the mean values of the signal fluct - uations recorded from the Ballantine voltmeter.

To demonstrate that data were obtained in the supercritical regime, static drag coefficient, $\overline{C_D}$, is plotted versus test Reynolds number in Figure 10 together with data from several references. Values of $\overline{C_D}$ were determined by integrating cylinder static pressure distributions according to the equation:

$$\overline{C_D} = \int_0^{\pi} \overline{C_p} \cos\theta \, d\theta \qquad (4.01)$$

Figure 11 presents steady-state pressure distributions about the cylinder, $\overline{C_p}$ vs. θ, for each of the five test Reynolds numbers (i.e.,

$Re = 2.5 \times 10^5$, 3.8×10^5, 5.3×10^5, 6.5×10^5, and 7.5×10^5). The shift in the separation point from $\theta \approx 60^\circ$ to $\theta \approx 110^\circ$ comes between $Re = 2.5 \times 10^5$ and $Re = 3.8 \times 10^5$ resulting in the drop in drag coefficient indicative of the supercritical regime.

Fluctuating pressures over the cylinder were obtained by recording data at each of the angular positions during separate data runs. The resulting distributions of RMS pressure coefficient, $\sqrt{\overline{C_p 2}}$, plotted with respect to angular position, θ, are presented in Figure 12 for each test Reynolds number. Prior to transition, at $Re = 2.5 \times 10^5$, there is an increase in RMS pressure coefficient associated with the flow separation point aft of $\theta = 60^\circ$. With the separation point shift to $\theta \approx 110^\circ$, i.e., for $Re \geq 3.8 \times 10^5$, the nature of the distribution of $\sqrt{\overline{C_p 2}}$ changes, showing maximum values occurring near $\theta = 110^\circ$. The magnitude of $\sqrt{\overline{C_p 2}}$ remains approximately the same for $Re = 2.5 \times 10^5$ and $Re = 3.8 \times 10^5$ on the portions of the cylinder ahead of the separation points. At Reynolds number of 5.3×10^5 the magnitudes of $\sqrt{\overline{C_p 2}}$ ahead of the separation point and on the aft portions of the cylinder attain a distribution pattern which remains constant through $Re = 7.5 \times 10^5$. The magnitudes of pressure fluctuations at $\theta \approx 110^\circ$ decrease with Reynolds number increase from $Re = 3.8 \times 10^5$ to 7.5×10^5. Data repeatability was found to be quite good with consistently repeatable values of $\sqrt{\overline{C_p 2}}$ at most angular positions. The exception was found at $\theta = 110^\circ$ for $Re = 3.8 \times 10^5$ to $Re = 7.5 \times 10^5$. At $\theta = 110^\circ$, the values of $\sqrt{\overline{C_p 2}}$ obtained from repeated measurements are shown in Figure 12 (flagged symbols) to indicate the amount of scatter.

Axial cross-correlation coefficients of pressure fluctuations, $R(x_1\ x_2)$, recorded at the same angular position but axially separated by 0.32 diameter ($^{x_1}/_{d} = 5.49$ and $^{x_2}/_{d} = 5.17$) were determined. Results are plotted versus angular position in Figure 13 for each of the test Reynolds numbers. A drop in the axial cross-correlation coefficient, $R(x_1\ x_2)$, occurs at the flow separation point for $Re \geq 3.8 \times 10^5$ with a small dip prior to $\theta = 100^\circ$ becoming more evident with increasing Reynolds number. The drop in correlation coefficient becomes more acute with increasing Reynolds number while the degree of correlation ahead of flow separation tends to remain quite high. At every test Reynolds number the correlation coefficient between fluctuating pressures recovers in the rearward portion of the cylinder.

Pressure-to-pressure axial cross-correlation coefficients were determined for varying axial separation distances at $\theta = 110^\circ$, the position of highest pressure fluctuation for $Re \geq 3.8 \times 10^5$. Figure 14 presents plots of cross-correlation coefficient, $R(x_1\ x_2)$, versus axial spacing ($^{x_2}/_{d} = 5.17$, $^{x_1}/_{d}$ ~varied) for $\theta = 110^\circ$ and $\theta = 80^\circ$. The spacing for effectively complete loss of correlation at $\theta = 110^\circ$ drops from approximately 0.8 diameter at $Re = 2.5 \times 10^5$ to 0.4 diameter for $Re \geq 5.3 \times 10^5$. Values of correlation coefficient at $\theta = 80^\circ$, shown for comparison, indicate higher axial correlation in the attached flow regions. Correlation lengths defined by

$$\chi_i = \int_0^\infty R(x_i\ \Delta x)\ d\left(\frac{\Delta x}{d}\right) \qquad (4.02)$$

are on the order of 0.1 diameter for $\theta = 110^{\circ}$ and an estimated 0.5 diameter at $\theta = 80^{\circ}$ for $Re \geq 5.3 \times 10^5$.

Normalized power spectral densities of the pressure fluctuations at $^{x}/_{d} = 5.17$ were computed according to the procedures described in Section III. Results are presented at 30° intervals around the cylinder according to the test Reynolds number in Figures 15 through 19. Since data points were computed at frequency intervals of one cycle per second, only the faired curves are shown in any of the power spectra plots. Definite periodicity is seen to exist at some locations on the cylinder for each of the test Reynolds numbers. The periodic nature of the pressure fluctuations was found to essentially disappear at the point of flow separation ($\theta = 60^{\circ}$, $Re = 2.5 \times 10^5$ and $\theta \approx 110^{\circ}$ to 120°, $Re \geq 3.8 \times 10^5$). The amount of random energy appears to increase with increasing values of Reynolds number, causing a corresponding decrease in the strength of the periodic portions of the signal. Periodicity is evident in the pressure fluctuations on the rearward portions of the cylinder except at $Re = 7.5 \times 10^5$, where definite periodic frequencies are not discernible.

The dominant frequency found in the pressure fluctuations for Reynolds numbers from $Re = 2.5 \times 10^5$ through $Re = 3.5 \times 10^5$ occurs at a Strouhal number $S = 0.12$. The relative amount of periodic signal progressively weakens (note the scale change at $Re = 6.5 \times 10^5$ in Figure 18); the first indication of harmonics occurs at $\theta = 0$, $Re = 5.3 \times 10^5$, where some hint of $S = 0.24$ is evident. Power spectral densities of the pressure fluctuations at $Re = 6.5 \times 10^5$ (Figure 18) indicate multiple harmonics of the basic frequency,

S = 0.12, with the largest portion of periodic energy occurring at S = 0.24. Several computations to frequencies above 125 cps were also made; frequency spikes were found for S = 0.12, 0.24, 0.36, and 0.48 for $Re = 6.5 \times 10^5$. Harmonics are again indicated on the forward pressure fluctuations at $Re = 7.5 \times 10^5$, but the increased proportion of random energy largely overwhelms any periodic fluctuations at this Reynolds numbers.

Measurements of fluctuating li t were made during each data run; for 95 recordings taken at $^x/_d = 4.86$, including all five test Reynolds numbers, the mean value of RMS lift coefficient, $\sqrt{\overline{C_L 2}}$, was found to be 0.041, with maximum and minimum values being 0.067 and 0.028 respectively. Additional measurements obtained at $^x/_d = 6.3$ showed similar values except at $Re = 2.5 \times 10^5$ where the mean value of $\sqrt{\overline{C_L 2}}$ was 0.146.

Lift fluctuations were recorded with fluctuating pressures, and cross-correlation coefficients were determined between the lift and pressure fluctuations recorded simultaneously at an axial spacing of 0.32 diameter. Values of the correlation coefficient, R (p, ℓ), are plotted versus the angular position of the pressure orifice in Figure 20. Even though the axial spacing was the same for the results of pressure-to-pressure correlation shown in Figure 13, the general degree of correlation is smaller. At $Re = 2.5 \times 10^5$ the highest value of correlation coefficient (0.30) was found at $\theta = 60^\circ$. With transition, the amount of pressure-to-lift correlation drops to very small values, indicating little correlation between lift and pressure fluctuations, for $Re = 3.8 \times 10^5$. For Reynolds numbers from $Re = 5.3 \times 10^5$ to

$Re = 7.5 \times 10^5$, the angular distribution of correlation coefficient is generally the same with magnitudes increasing with Reynolds number (highest value at 0.46).

Normalized power spectral densities of fluctuating lift recorded at $^x/_d = 4.86$ were computed at each Reynolds number; results for $Re = 2.5 \times 10^5$ and 5.3×10^5 are presented in Figure 21. Only at $Re = 2.5 \times 10^5$ did a discernible frequency ($S = 0.12$) become evident. Note the indication of a 60 cps frequency at $Re = 2.5 \times 10^5$ caused by the low signal levels at $q = 5$ psf. Power spectra of lift fluctuations for $Re = 3.8 \times 10^5$ to $Re = 7.5 \times 10^5$ show essentially random energy content; however, in a few instances (i.e., for $Re \leq 5.3 \times 10^5$) evidence of some dominance at $S \approx 0.4$ could be found. More will be said about fluctuating lift in Section V.

As the second aspect of this study, hot-wire data were recorded in the wake and reduced according to the methods described by Kovasznay (38). The wire was calibrated at constant current in the clear tunnel (i.e., no model) to measure resistance change with air velocity. In the cylinder wake sufficient measurements were made to determine the mean-velocity profiles. At one diameter behind the model, $^z/_d = 1.0$, all centerline velocities came within $\pm$ 10 % of being $0.43\ \overline{V}_\infty$ with profile shapes similar to developed wakes described by Goldstein (9). At three diameters downstream the centerline velocities were within $\pm$ 3 % of $0.93\ \overline{V}_\infty$ except for $Re = 2.5 \times 10^5$ which exhibited a lower velocity ($0.5\ \overline{V}_\infty$). The voltage fluctuations were reduced to root-mean-square (RMS) velocity fluctuations, $\sqrt{\overline{V^2}}$, and referenced to free stream velocity, $\overline{V}_\infty$, by the following equation:

$$\frac{\sqrt{\overline{v^2}}}{\overline{V_\infty}} = \frac{-2}{\bar{a}} \cdot \frac{\sqrt{\overline{e^2}}}{\bar{e}} \cdot \frac{\overline{V_{Local}}}{\overline{V_\infty}} \qquad (4.03)$$

where

$\sqrt{\overline{e^2}}$ = RMS hot-wire signal corresponding to wake velocity fluctuations,

$\bar{e}$ = steady-state hot-wire voltage corresponding to mean flow velocity $(\overline{V_{Local}})$,

$\bar{a}$ = normalized wire resistance change due to the local flow velocity.

Since only a single wire was used, with axis parallel to the cylinder, it should be noted that velocity measurements were effected by flow components in both the stream direction and transverse to the stream direction.

Within the limitations of measuring velocity components, the level of free-stream turbulence was found to be approximately 0.35% of $\overline{V_\infty}$. Power spectral densities of the free stream indicated mostly random energy content in the flow. Normalized wake profiles for RMS velocity fluctuations, $\sqrt{\overline{v^2}}$, determined for Re = 2.5×10^5 at $x/d = 5.17$ are shown in Figure 22. The wake width (about 2 diameters at $z/d = 1.0$) corroborates with the cylinder data which indicate flow separation at $\theta \approx 60^\circ$. The purpose of the wake profiles is to provide a reference for the power spectral densities computed from hot-wire data recordings. Figure 23 presents several samples of the normalized power spectral densities for wake velocity fluctuations at Re = 2.5×10^5. Essentially turbulent or random distributions were

found in the center of the wake at $^{z}/_{d}$ = 1.0 with perhaps some indication of lower frequency dominance near the edge of the wake. Downstream at $^{z}/_{d}$ = 3.0 dominance is seen at S = 0.12 near the edge of the wake.

After transition, the wake width and velocity profiles became quite similar for Re = 3.8×10^5 to Re = 7.5×10^5. Corresponding to the change in the point of flow separation, the wake width at $^{z}/_{d}$ = 1.0 narrowed to approximately 0.8 diameter. Root-mean-square velocity fluctuations for Re = 5.3×10^5 and Re = 7.5×10^5 are shown in Figure 24. Power spectral densities were computed for wake velocity fluctuations at each test Reynolds number from Re = 3.8×10^5 to 7.5×10^5; examples of the results are shown in Figure 25 ($^{z}/_{d}$ = 1.0) and Figure 26 ($^{z}/_{d}$ = 3.0). At one diameter downstream there is some indication of frequency dominance at S $\approx$ 0.4 near the edge of the wake as seen at Re = 3.8×10^5 shown in Figure 25. Some of the data at Re = 5.3×10^5 also seemed to have indicated dominant frequencies near S = 0.4; however, it was found that most power spectra of the wake velocity fluctuations showed random energy content with no perceptible frequency dominance. This fact was especially true of spectra of the hot-wire data obtained from the center portions of the wake. Velocity fluctuations downstream at $^{z}/_{d}$ = 3.0 (Figure 26) indicate randomness also.

The third portion of this program was to investigate the effects of boundary-layer tripping on pressure distributions near the point of separation. Tripping was accomplished by blowing jets of air through orifices at $\theta = \pm 30^{\circ}$. In order to provide a basis for this study, the

effects of blowing on lift were again measured. Figure 27 shows typical results found at Re = 5.3×10^5; the dashed line represents the results obtained by Schmidt (32). Boundary-layer tripping induced steady-state lift as high as $\overline{C_L} = 0.3$, and the fluctuating lift rose considerably from the normal RMS lift coefficient, $\sqrt{\overline{C_L 2}}$, value of 0.040 to about 0.110. Effects of blowing below Re = 5.3×10^5 could not be felt.

In the following results blowing was established through both orifices at $0.3\ \overline{V_\infty}$; this rate was chosen as the lowest value which would clearly change the flow pattern. Figure 28 presents normalized power spectral densities of fluctuating lift at Re = 5.3×10^5 and 7.5×10^5 with and without blowing. With blowing the spectra indicate that the energy content becomes more pronounced in the frequencies at or below S = 0.12. Normalization hides the fact that lift fluctuations with blowing also were approximately three times stronger than those without blowing. Attention should also be given to the slight frequency dominance seen at $S \approx 0.4$ in the lift spectra without blowing.

Boundary-layer tripping had definite effects on the cylinder static pressure distribution, $\overline{C_p}$ vs. θ, near the point of flow separation as seen in Figure 29. The data appear to indicate earlier flow separation and higher drag coefficient (estimations of $\overline{C_D}$ with blowing are shown in Figure 10). Blowing changed the levels of fluctuating pressure as shown in Figure 30 which presents the distribution of $\sqrt{\overline{C_p 2}}$ for the angular positions of $\theta = 80^\circ$ to 120° for Re = Re = 5.3×10^5 and 7.5×10^5. Data are presented for two axial separation distances ($\Delta x/d = 0.19$ and 0.82) from the location of the

blowing orifices ($^{x}/_{d} = 5.68$). Blowing effects on $\sqrt{\overline{C_p 2}}$ at $^{\Delta x}/_{d} = 0.82$ are seen to be some what less that at the 0.19 diameter spacing. Also, it was found that the static pressure distribution changed very little with blowing for the larger spacing.

Cross-correlation coefficients between the fluctuating pressures ($^{\Delta x}/_{d} = 1.01$) as affected by blowing are shown in Figure 31 for Re = 5.3×10^5 and 7.5×10^5. The correlation coefficient is higher in magnitude with blowing, and evidence is also seen of the earlier flow separation point. Qualitatively, the correlation pattern without blowing conforms with the correlation coefficients presented for closer spacing in Figure 13. Power spectral densities of pressure fluctu - ations at $\theta = 95^{\circ}$ and 0.19 diameter from the blowing orifices are presented in Figure 32 with and without blowing for Re = 5.3×10^5 and Re = 7.5×10^5. Note the recovery of periodicity with blowing at Re = 5.3×10^5 and the apparent loss of periodicity at Re = 7.5×10^5. Comments about flow separation characteristics will be made in Section V.

Effects of blowing were felt in the wake in that the region of highest velocity fluctuations shifted from the center in the direction corresponding to a downwash corroborating with the steady-state lift coefficient. Several power spectral densities of wake velocity fluctuations in region of highest activity were computed and are presented in Figure 33. Without blowing the wake at Re = 5.3×10^5 seems to indicate frequency dominance near S = 0.4. Blowing shifts the emphasis of frequency dominance to the lower frequencies at Re = 5.3×10^5 while the data at Re = 7.5×10^5 indicate randomness.

SECTION V

DISCUSSION

5.1 Test Results Compared With Other Experiments

The shift in separation point to the rearward position on the cylinder and the accompanying decrease in drag coefficient (for $Re \geq 3.8 \times 10^5$) demonstrate that measurements were indeed made in the supercritical flow regime. Values of cylinder drag coefficient shown in Figure 10 are seen to be somewhat less than corresponding data from the references. Bursnall and Loftin (16), for example, obtained higher values of $\overline{C}_D$ using the same pressure-integration technique defined in Equation (4.01). The distributions of static pressure coefficient around the cylinder, $\overline{C}_p$ vs. θ, shown in Figure 11 compare quite favorably with those of Bursnall and Loftin except for the values of base pressure coefficient (which account for the differences in value of drag coefficient). The higher base pressure with corresponding lower drag coefficient as measured in this investigation has been found by McKinney (39) to be attributable to differences in fineness ratio coupled with free-end effects. The cylinder used by Bursnall and Loftin extended completely across the tunnel with a fineness ratio of 18, whereas the model used in this test had a free-end and a fineness ratio of 8.1. Delany and Sorensen (11) noted that for the portion of their measurements in the subcritical regime, values of drag coefficient were lowered with open gaps around the model where it passed through the tunnel walls. Their conclusion was that an inflow of air at pressures approximately equal to free-stream static caused a rise in the base pressure. This type of phenomena may also account

for the drag difference found in the transcritical range between the results of Roshko (12) and those of Bohne (13a) and Buell, et. al.,(14). Roshko's cylinder extended completely across the tunnel with no gaps at the walls ($\overline{C_D} \approx 0.7$), and the models of both Bohne and Buell were three-dimensional missile configurations ($\overline{C_D} \approx 0.5$).

The distribution of fluctuating pressures about the cylinder had not been measured (to the author's knowledge) in the supercritical range prior to this test. Considerable difference is found between the test data shown in Figure 12 and the results of McGregor (23) and Gerrard (24, 25) for the subcritical regime. Both experimenters present only RMS pressure coefficients for pressure fluctuations at the fundamental frequency ($S \approx 0.2$) and at the "second" harmonic ($S \approx 0.4$). McGregor's distribution of RMS pressure coefficient at $S \approx 0.2$ rises from quite low values ($\sqrt{\overline{C_p 2}} \approx 0.003$) at $\theta = 0^\circ$ to a relatively constant maximum level ($\sqrt{\overline{C_p 2}} \approx 0.3$) for $\theta = 90^\circ$ to 150° dropping to low values again in the rearward portion of the cylinder. Gerrard found similar pressure distributions at the fundamental frequency only with the maximum value of $\sqrt{\overline{C_p 2}}$ given as 0.5. Supercritical flow data from this study show that the values of RMS pressure coefficient (all frequencies included) remain fairly constant at low levels, near $\sqrt{\overline{C_p 2}} = 0.04$, except in the vicinity of the point of flow separation where $\sqrt{\overline{C_p 2}} \approx 0.2$.

Axial cross-correlation coefficients determined between two fluctuating-pressure signals are also not found elsewhere. Gerrard (25) plots pressure-to-pressure cross-correlation coefficients for an axial spacing of one-third diameter where one transducer was kept

at $\theta = 90^{\circ}$ and the second transducer was rotated to various angular positions. Gerrard's goal was to determine angular phase relation - ships, whereas data presented in this report intend to show the vari - ation of axial correlation with angular position. Nevertheless, Gerrard shows correlation coefficients at the one-third diameter spacing with $\theta = 90^{\circ}$ (both transducers) to be approximately 0.60 for $Re = 8.5 \times 10^{4}$ and 0.85 for $Re = 1.14 \times 10^{5}$. Prendergast (26) presents pressure-to-pressure axial cross-correlation coefficients for varying separation distances at $\theta = 90^{\circ}$ and 180° showing $R(x_1 x_2) \approx 0.9$ at approximately one diameter spacing for subcritical Reynolds numbers. Both authors indicate a relatively high degree of correlation between pressure fluctuations, similar to the results found in this investigation for the attached flow regions of the cylinder. Correlation lengths estimated from Figure 14 are of the same order of magnitude as the more extensive results presented by Schmidt (32) for supercritical lift (and drag) fluctuations. Supercritical correlation lengths (0.5 diam - eter or less) are much shorter than those found by Prendergast (26) and el Baroudi (27) for subcritical Reynolds numbers.

Periodic pressure fluctuations in the subcritical regime were found by McGregor and Gerrard at frequencies corresponding to $S \approx 0.2$ with dominance shifting to $S \approx 0.4$ on the rearward portions of the cylinder. Periodicity found in this study occurred at $S = 0.12$ (or har - monics thereof) over the entire cylinder with no apparent shift to higher frequencies at the aft angular positions. Buell (14) shows some fluctuating-pressure power spectra (at $\theta = 45^{\circ}$, 75°, 105°, and 135°) for the transcritical range from $Re = 2.2 \times 10^{6}$ to $Re = 6.2 \times 10^{6}$.

Buell's data from a smooth cylinder (missile configuration) indicate random pressure fluctuations with maximum levels occurring at $\theta = 105^{o}$. However, his spectra for pressure fluctuations near the model tip or for the models with boundary-layer tripping (using tape along the forward portions of the cylinder) show periodic effects at Strouhal numbers near S = 0.09.

The randomness of the lift (and drag) fluctuations for $Re = 3.8 \times 10^{5}$ to $Re = 7.5 \times 10^{5}$ were also found by Fung (22) and Schmidt (32). Fung's fluctuating lift power spectra for his lowest range of Reynolds numbers ($Re = 3.3 \times 10^{5}$ to 5.7×10^{5}) seem to show peak energy at $S \approx 0.12$; however, the majority of the data presented in Reference 22 indicate only randomness. Schmidt found lift power spectra to contain some indication of energy concentration near S = 0.32 close to the model tip. Similar energy dominance was found occasionally in this investigation at $S \approx 0.4$ in the lift fluctuations recorded at $^{x}/_{d} = 4.86$ for $Re = 3.8 \times 10^{5}$ and at $^{x}/_{d} = 5.87$ for Reynolds numbers to 7.5×10^{5}. Schmidt attributed this phenomena to a tip effect since evidence of such frequency content was more pronounced closer to the tip. Subcritical load data from Keefe (29) show that lift fluctuated at $S \approx 0.2$ while the drag periodicity appeared at $S \approx 0.4$ in contrast to lift fluctuations measured at $Re = 2.5 \times 10^{5}$ indicating periodic dominance at S = 0.12.

The hot-wire wake surveys for velocity fluctuations shown in Figures 22 and 24 are similar in shape to those seen in Reference 17 except that the magnitudes of the RMS velocity fluctuations are quite high owing to the close proximity to the cylinder. The appearance of

dominant frequency at S = 0.12 for Re = 2.5×10^5 differs from the data of Drescher (21) and Roshko (17) who found S = 0.2 for wake velocity fluctuations in the upper subcritical range. Power spectral densities showing frequency dominance at S ≈ 0.4 presented in Figure 25 (Re = 3.8×10^5) and Figure 34 (Re = 5.3×10^5, no blowing) agree somewhat with the findings of Relf and Simmons (19) at Re ≈ 5×10^5 to 10^6 and Delany and Sorensen (11) at Re ≈ 2×10^6. The absence of definite periodicity in the wake for supercritical Reynolds numbers was also noted by Relf and Simmons (who took measurements at two diameters downstream) and by Delany and Sorensen (who took measurements between one and two diameters downstream). Neither reference presents any distribution of frequency across the wake, whereas results of this study show that periodic effects were seen only near the edges of the wake. The increasing amount of randomness found in the velocity fluctuations with increasing Reynolds number agrees with results of hot-wire investigation of the wake at supercritical Reynolds numbers by Tani (40). Roshko's (12) findings of randomness below Re = 3.5×10^6 in the wake seven diameters downstream are seemingly confirmed by the spectra found at three diameters downstream. Also in the transcritical range, using the model which gave periodic pressure fluctuations, Buell (14) recorded both fluctuating static and total-pressure fluctuations. The tunnel free-stream static pressure was found to fluctuate at S = 0.09 comparable to the cylinder surface pressures, while total-head pressure fluctuations (e.g., velocity fluctuations) were found to oscillate at S ≈ 0.18.

The effects of boundary-layer tripping caused by orifice

blowing again show that the flow is quite sensitive to disturbances as noted by Fung (22), Schmidt (32), Blackiston (33), and Buell (13c) among others. Blowing effects on lift fluctuations were found to be somewhat different from the results presented by Schmidt (see Figure 27); however, the blowing rates required to initiate a change in the flow pattern were found to be quite close to the values used by Schmidt. The shifts in fluctuating lift power spectra with blowing compare well with lift spectra presented by Schmidt whose data showed definite frequency dominance near S = 0.12. Also, the increased axial correlation between fluctuating pressures is similar to higher correl - ation coefficients found for lift and drag data with blowing by Schmidt.

5.2 Discussion of the Results

The data acquired in this investigation provide some insight into the flow over a cylinder at supercritical Reynolds numbers but also raise new questions to be answered. The primary purpose of obtaining steady-state data was to confirm that measurements were made in the desired testing regime. Measurement of fluctuating pressures around the cylinder, along with fluctuating lift, was one of the key objectives in the program. The mapping of unsteady pressure fluctuations showed that values of $\sqrt{\overline{C_p{}^2}}$ were rather low in the super - critical regime except in the region of flow separation where levels rose by a factor of five or more. At all test Reynolds numbers axial correlation between pressure measurements remains high on the portions of the cylinder where flow is attached, but much correlation is lost at the points of flow separation. Axial correlation data indicate the high degree of three-dimensionality in the flow field. Power

spectral densities computed from records of the fluctuating pressures show definite periodicity at frequencies corresponding to S = 0.12 or harmonics thereof except at points of flow separation. The amount of random energy was found to increase until periodic pressure fluct - uations fail to recover on the rearward portions of the cylinder at $Re = 7.5 \times 10^5$. The amount of correlation between pressure and lift fluctuations was quite small at transition to supercritical flow. Power spectra of the lift fluctuations corroborate with the correlation data by showing essentially random loading except for $Re = 2.5 \times 10^5$ where a discernible frequency appears at S = 0.12.

Wake widths and profiles determined from hot-wire measure - ments verified the transition to the supercritical flow. Power spectra of the wake velocity fluctuations were determined; a large portion of the energy in the wake is random in character. At $Re = 2.5 \times 10^5$ the indication of wake periodicity at $S \approx 0.12$ seemed to reveal vortex shedding. Near the edges of the wake some evidence of dominant frequencies near $S \approx 0.4$ was found; however, the majority of power spectra showed only turbulent velocity fluctuations.

Boundary-layer tripping by orifice blowing showed that super - critical flow is quite sensitive to small disturbances. Tripping was achieved only from $Re = 5.3 \times 10^5$ to $Re = 7.5 \times 10^5$ which seems significant after studying the RMS pressure coefficient distributions (Figure 12). There may be some evidence concerning flow stability found in the uniformity of the distribution of $\sqrt{\overline{C_p}^2}$ for $Re \geq 5.3 \times 10^5$. Results of blowing indicated earlier flow separation, higher steady-state drag, flow inclination and accompanying steady-state lift, much

higher amplitudes of $\sqrt{\overline{C_p{}^2}}$ and $\sqrt{\overline{C_L{}^2}}$, axial correlations of increased magnitude, and a shift in power spectra toward S = 0.12.

The existence of periodicity at S = 0.12 instead of the familiar subcritical value, S = 0.2, appears to be related to the higher base pressure associated with the free-ended model. Roshko (15) postulates that vortex shedding frequency is dependent upon wake parameters (width, d_w, and velocity, $\overline{V_w}$) and that there exists a universal Strouhal number, S^*, independent of the body producing the wake. Roshko relates the actual Strouhal number to the universal value by the following equation:

$$\frac{S}{S^*} = \frac{d}{d_w} \cdot \frac{\overline{V_w}}{\overline{V_\infty}} = \frac{d}{d_w} \left(1 - \overline{C_{p_w}}\right)^{1/2} \qquad (5.01)$$

where

d_w = wake width defined as the distance between the free shear layers, and

$\overline{C_{p_w}}$ = wake static pressure coefficient which is equal to the cylinder base pressure, $\overline{C_{p_{base}}}$.

In reference 12, Roshko shows that the value of d_w is calculated from the following;

$$d_w = -d \left(\frac{\overline{C_D}}{\overline{C_{p_{base}}}} \right) \qquad (5.02)$$

Thus, the Strouhal number can be determined simply by using static measurements as seen in the following;

$$S = -S^* \left(\frac{\overline{C_{p_{base}}}}{\overline{C_D}} \right) \left(1 - \overline{C_{p_{base}}} \right)^{1/2} \qquad (5.03)$$

On the basis of experimental data for cylinders of various cross-sections, Roshko found that the value of universal Strouhal number was $S^* = 0.16$. This value corroborated with wake velocity fluctuations measured in the subcritical regime (see Reference 15) and in the trans-critical range (see Reference 12). The measurements made in this test, prior to the shift in separation point, at $Re = 2.5 \times 10^5$ show that $\overline{C_D} = 0.74$ and $\overline{C_{p_{base}}} = -0.49$; Equation (5.03) gives $S = 0.13$ which is quite close to the measured frequency of $S. = 0.12$. Also, the cal-culated wake width, $d_w = 1,5d$, is seen to be in fair agreement with the wake profile at $^z/_d = 1.0$ in Figure 22. Subcritical fluctuating lift was found by Keefe (29) to occur at the same frequency ($S \approx 0.2$) measured in the wake velocity fluctuations by other experimenters. Similar results were found in this study at $Re = 2.5 \times 10^5$ in that wake velocity fluctuations seemed to occur at the same frequency ($S = 0.12$) as the pressure and lift fluctuations. Thus, subcritical data indicate that vortex shedding does occur.

After transition to the supercritical flow regime fluctuating pressure periodicity continued at $S = 0.12$ until the appearance of harmonics at $Re = 6.5 \times 10^5$. For data taken from $Re = 3.8 \times 10^5$ to 7.5×10^5 the base pressure coefficient averaged at -0.17 and the mean value of drag coefficient was about 0.15. Equation (5.03) then shows that the Strouhal number should be $S = 0.196$ which hardly agrees with the measured values at $S = 0.12$. The calculated wake width, $d_w = 0.87d$, is in good agreement with test data at $^z/_d = 1.0$ presented in Figure 24. Roshko (12), using data from many experiments, was also unsuccessful in establishing a proper Strouhal number in the

supercritical range.

For supercritical data a seeming contradiction exists between the lift and pressure power spectra. A complete explanation of the dichotomy between periodic pressures and random lift has not been found. Some insight on the problem may be gained by considering the distribution of $\sqrt{\overline{C_p 2}}$ vs. 0 in conjunction with the pressure power spectra. It was found that slightly over one-half of the energy input to lift comes from the region of essentially random pressure fluctuations occurring about the flow separation point. However, this fact does not completely solve the problem since each side of the lift package electrically integrated all transducer signals (taken for each 11.1% of the chord), some of which would sense periodic pressure fluctuations (for instance, those transducers located ahead of the separation region). The absence of any definite indication of periodicity in the lift spectra (and drag also) for supercritical Reynolds numbers may possibly be attributed to pressure fluctuations of differing phase around the cylinder. The high degree of periodicity in the pressure fluctuations at $Re = 3.8 \times 10^5$, the randomness found in the corresponding lift fluctuations, and the accompanying low correlation between pressures and lift indicate that some cancelling effect exists in supercritical flow. Alternate shedding of vortices appears not to occur in the fashion found in the subcritical regime. One of the possible reasons for the failure of Equation (5.03) in the supercritical range lies in the assumption of the free-streamline flow model and its accompanying vortex shedding phenomena.

Perhaps some further insight into the problem may be gained

by considering another aspect of the flow field. Consider Figure 34 which summarizes the results of pressure mapping around the cylinder for Re = 5.3×10^5. There is some evidence of a small separated region ahead of the point of full flow separation, i.e., a separation "bubble" similar to that found by Bursnall and Loftin (16, 41). The slight rise in $\overline{C_p}$ aft of $\theta = 95^\circ$ has been known for some time, being shown by Flachsbart (5) and Fage (8) among many others. This steady-state effect is corroborated by the slight rise in $\sqrt{\overline{C_p 2}}$ at $\theta = 95^\circ$ and the corresponding drop in axial cross-correlation coefficient. Figure 35 shows power spectra of pressure fluctuations measured in this region; note the absence of periodicity at $\theta = 95^\circ$ as well as at $\theta = 110^\circ$ and 120° (the region of complete flow separation). Fage (8) measured the boundary-layer velocity profiles over this portion of the cylinder finding initial flow separation beginning close to $\theta = 95^\circ$ with seemingly reversed flow prior to complete separation at $\theta \approx 110^\circ$. These profiles are sketched in Figure 35 along with the change in boundary-layer thickness.

Several authors have discussed the existence of the separation bubble. Bursnall and Loftin (16) based their comments on this bubble in part upon previous experience with laminar separation bubbles on an airfoil as described in Reference 41. Roshko discusses the super - critical flow separation bubble in Reference 12. Lately, Tani (40) has conducted an investigation which seemingly shows the definite exist - ence of the bubble. A simple description of the flow field is proposed using ideas from the above references combined with the results of this test.

With increasing Reynolds number in the subcritical range the point of transition from laminar to turbulent flow seems to move forward through the wake until at the "critical" Reynolds number this transition occurs on the cylinder itself. The flow, which up to this point had been subject to laminar separation on the forward portion of the cylinder, becomes influenced by the transition and reattaches to the surface. The final flow separation point then shifts quite abruptly to the rearward position on the cylinder wtih the flow pattern apparently consisting of a laminar separation, transition, reattachment, and final turbulent separation. The angular position of transition seems seems to move forward around the cylinder as Reynolds number increases, and the separation bubble narrows until it finally disappears at the onset of transcritical flow.

At both subcritical and transcritical Reynolds numbers definite periodic vortex shedding has been measured. Both regimes seem to exhibit somewhat similar separation phenomena (i.e., separation simply caused by adverse pressure gradient) except that the turbulent boundary-layer causes the transcritical separation to occur further back on the cylinder. Perhaps the supercritical flow does attempt to separate simply, but the reattachment and almost immediate turb - ulent separation cancels any simple vortex shedding. The discovery of periodic pressure fluctuations for the early supercritical Reynolds numbers indicate that the cylinder flow attempts to shed a periodic vortex which is effectively obliterated by the second separation as is quite evident at $Re = 3.8 \times 10^5$; however, some indication of period - icity in the wake at $S \approx 0.4$ shows that the problem is not simple. With

increasing Reynolds number to Re = 7.5×10^5 even the periodic pressure fluctuations degenerate as the amount of turbulence increases.

Orifice blowing as a boundary-layer tripping technique indicated the general return of periodicity. Possibly blowing caused a local increase in Reynolds number which shortened the separation bubble and brought on the earlier flow separation point. It appears that even though the separation bubble existed in a subdued form a change in the character of the flow allowed some periodic vortex shedding. The periodicity in the pressure fluctuations on the cylinder to the point of final flow separation is corroborated by Figure 31 where the dip in the axial correlation coefficient prior to separation no longer is found with blowing. At Re = 7.5×10^5 the earlier flow separation point effectively cancelled the pressure periodicity at $\theta = 95^o$ as shown in Figure 32. Apparently simple periodic vortex shedding will occur where final flow separation is not effected by a laminar separation bubble. Thus, the supercritical regime is the Reynolds number range where transition to turbulence and vortex shedding interact quite dramatically.

5.3 Future Investigations

To learn more about the supercritical separation phenomena and the related vortex shedding problem, more testing needs to be done. One of the first priorities of such a test would be to determine the phase relationships in the pressure fluctuations around the cylinder. This could be accomplished by constructing an instrumentation package consisting of individual pressure transducers located at various angular position on both sides of the cylinder. By the use of a switching circuit it would be possible to relate the phase of pressure fluctuations to that

at same point, say $\theta = 0^{o}$. The answer to the question about random lift and periodic pressures could be found. By testing at both sub - critical and supercritical Reynolds numbers some knowledge of the stability of the location of the separation points could be gained which might indicate something about the nature of vortex formation.

A second aspect of any future test would be to make a detailed study of the region close to the supercritical separation point. This would include not only measuring the magnitudes and phase of pressure fluctuations, but the boundary-layer would have to be surveyed as well. Some time history of the flow pattern is desirable. The hot-wire technique and the power spectral density computer program are important tools in such a study. Perhaps some answers about the existence of periodicity at $S \approx 0.4$ in the wake can be found. The flow field appears quite complex, and earlier studies of this problem lacked the improved instrumentation and digital computer techniques available today.

SECTION VI

CONCLUDING REMARKS

The study of supercritical flow over a cylinder has been a subject of interest for almost one-half century, chiefly for the reason that abrupt and curious changes in the flow pattern are found. Many investigations and tests have been made, and gradually a picture of the flow field is being pieced together. This study was an attempt to add more pieces to that picture.

To some extent a certain amount of new knowledge about the problem has been gained. Subcritical flow, with its periodic vortices, is characterized on the cylinder by periodic pressure and lift fluct - uations, lift fluctuations caused by the alternately shedding vortices. With transition, supercritical flow is characterized by an apparent separation bubble followed by turbulent separation, with pressure fluctuations of greatly increased magnitude at this point. As can be seen from the test results the large random pressure fluctuations near the separation point appear to be responsible for the shortening of the axial correlation length from the comparatively large values found in subcritical data. Periodic pressure fluctuations ($S = 0.12$ for this test) on the surface remain but are attenuated as the Reynolds number increases beyond the initial transition values. Without the simple vortex shedding, lift fluctuations become random in nature and much smaller than subcritical values. At the "early" supercritical Reynolds numbers, there seems to be some indication of lift and wake velocity fluctuations near $S = 0.4$ which is unexplained. It may be that a complicated shedding takes place, perhaps a double shedding, which

is eventually overcome as the point of turbulent transition moves forward. With the forward movement of the transition point, the separation bubble disappears and transcritical vortex shedding begins.

Much of the preceding description of supercritical flow needs to be verified by a careful study of the dynamics of flow separation. With the testing equipment available it seems but a matter ot time until a detailed flow picture can be drawn. Perhaps then the phenomenon of vortex shedding can be more fully understood.

REFERENCES

1. Strouhal, V., "Uber eine besondere Art det Tonerregung", Wied. Ann. Physik U. Chem., Neue Folge, Band V, pp. 216 - 251 (1878).

2. Strutt, J. W. (Lord Rayleigh), "Theory of Sound", Vol. II, Dover Publications, pp. 412 - 414 (1945).

3. von Karman, Th. and Rubach, H., "Uber den Mechanisums des Flussigkeits und Luftwiderstandes", Physikalische Zeitschrift, Band 13, Heft 2, pp. 49 - 59 (January, 1912).

4. Relf, E. F., "Measurements of the Resistance of Wires, With Some Additional Tests on the Resistance of Wires of Small Diameter", British A. R. C., R. and M. 102 (March, 1914).

5. Flachsbart, Von O., "Neue Untersuchungen uber den Luftwiderstand von Kugeln", Physikalische Zeitschrift, Band 28, Heft 13, pp. 461 - 469 (July, 1927).

6. Fage, A. and Falkner, V. M., "The Flow around a Circular Cylinder", British A. R. C., R. and M. 1369 (February, 1931).

7. Fage, A., "Drag of Circular Cylinders and Spheres", British A. R. C., R. and M. 1370 (May, 1930).

8. Fage, A., "The Air Flow around a Circular Cylinder in the Region where the Boundary Layer Separates from the Surface", British A. R. C., R. and M. 1179 (August, 1928).

9. Goldstein, S. (editor), "Modern Developments in Fluid Mechanics", Vol. II, Oxford Press (1938).

10. Stack, John, "Compressibility Effects in Aeronautical Engineering", NACA A. C. R. 218 (August, 1941).

11. Delany, Noel K. and Sorensen, Norman E., "Low-Speed Drag of Cylinders of Various Shapes", NACA TN 3038 (November, 1953).

12. Roshko, Anatol, "Experiments on the Flow Past a Circular Cylinder at Very High Reynolds Number", Journal of Fluid Mechanics, Vol. 10, Part 3, pp. 345 - 356 (1961)

13. A. I. A. A. Fifth Annual Structures and Materials Conference, A. I. A. A. Publication CP-8, Palm Springs, Calif. April 1-3, (1964).
    a) Bohne, Quentin R., "Ground Wind Induced Loads on Axisymmetric Launch Vehicles", Boeing Co., pp. 282 - 293.

b) Schmidt, Louis V., "Measurements of Fluctuating Air Loads on a Circular Cylinder", Calif. Inst. of Tech., pp. 155 - 162.

c) Buell, Donald A., "Some Sources of Ground-Wind Loads on Launch Vehicles", NASA Ames Research Center, pp. 178 - 183.

d) Blackiston, H.S., Jr., "Tip Effects on Fluct - uating Air Loads on a Circular Cylinder", Hughes Aircraft Co., pp. 146 - 154.

14. Buell, Donald A., McCullough, George B., and Steinmetz, William J., "A Wind-Tunnel Investigation of Ground-Wind Loads on Axisymmetric Launch Vehicles", NASA TND-1893 (October, 1963).

15. Roshko, Anatol, "On the Drag and Shedding Frequency of Two-Dimensional Bluff Bodies", NACA TN 3169 (July, 1954).

16. Bursnall, William J. and Loftin, Laurence K., Jr., "Experimental Investigation of the Pressure Distribution about a Yawed Circular Cylinder in the Critical Reynolds Number Range", NACA TN 2463 (September, 1951).

17. Roshko, Anatol, "On the Development of Turbulent Wakes fron Vortex Streets", NACA Rep. 1191 (1954).

18. Kovasznay, L.S.G., "Hot-Wire Investigation of the Wake Behind Cylinders at Low Reynolds Numbers", Proc. Roy. Soc. (London), series A, Vol. 198, No. 1053, pp. 174 - 190 (August, 1949).

19. Relf, E.F. and Simmons, L.F.G., "The Frequency of the Eddies Generated by the Motion of Circular Cylinders Through a Fluid", British A.R.C., R. and M. 917 (June, 1924).

20. V. Krzywoblocki, M.S., "Vortex Streets in Incompressible Media, Review of the Literature", U.S. Naval Ordnance Test Station Tech. Memo. No. 1552 (June, 1953).

21. Drescher, H., "Messung der auf Querangestromte Zylinder Ausgeubten Zeitlich Veranderten Drucke:, Zeit. f. Flugwiss., Band 4, Heft 1/2, pp. 17 - 21 (1956).

22. Fung, Y.C., "Fluctuating Lift and Drag Acting on a Cylinder in a Flow at Supercritical Reynolds Numbers", Journal of Aerospace Sciences, Vol. 27, No. 11, pp. 801 - 814 (November, 1960).

23. McGregor, D.M., "Experimental Investigation of the Oscillating Pressures on a Circular Cylinder in a Fluid Stream", University of Toronto Institute of Aerophysics, U.T.I.A. Tech. Note No. 14 (June, 1957).

24. Gerrard, J.H., "Measurements of the Fluctuating Pressure on the surface of a Circular Cylinder - Part I: Cylinder of 1" Diameter", British A.R.C. Report 19, 844 (January, 1958).

25. Gerrard, J.H., "An Experimental Investigation of the Oscillating Lift and Drag of a Circular Cylinder Shedding Turbulent Vortices", Journal of Fluid Mechanics, Vol. 11, Part 2, pp. 244 - 256 (September, 1961).

26. Prendergast, V., "Measurement of Two-Point Correlations of the Surface Pressure on a Circular Cylinder", University of Toronto Institute of Aerophysics, U.T.I.A. Tech. Note No. 23 (July, 1958).

27. el Baroudi, M.Y., "Measurement of Two-Point Correlations of Velocity Near a Circular Cylinder Shedding a Karman Vortex Street", University of Toronto Institute of Aerophysics, U.T.I.A. Tech. Note No. 31 (January, 1960).

28. Humphreys, J.S., "On a Circular Cylinder in a Steady Wind at Transition Reynolds Numbers", Journal of Fluid Mechanics, Vol. 9, Part 4, pp. 603 - 612 (December, 1960).

29. Keefe, R.T., "An Investigation of the Fluctuating Forces Acting on a Stationary Circular Cylinder in a Subsonic Stream and of the Associated Sound Field", University of Toronto Institute of Aerophysics, U.T.I.A. Rep. No. 76 (September, 1961).

30. Ezra, A.A. and Birnbaum, S., "Design Criteria for Space Vehicles to Resist Wind Induced Oscillations", American Rocket Society Paper 1081 - 60, Structural Design of Space Vehicles Conference, Santa Barbara, Calif. (April 6-8, 1960).

31. Fung, Y.C., "The Analysis of Wind-Induced Oscillations at Large and Tall Cylindrical Structures", Space Technology Laboratories, Inc., STL/TR - 60 - 0000 - 09134, EM 10 - 3 (June, 1960).

32. Schmidt, Louis V., "Measurement of Fluctuating Air Loads on a Circular Cylinder", PhD. Thesis, California Institute of Technology (1963).

33. Blackiston, H.S., Jr., "Tip Effects on Fluctuating Lift and Drag Forces Acting on a Circular Cylinder Perpendicular to an Air Flow", Aeronautical Engineer Thesis, California Institute of Technology (1963).

34. Fung, Y.C., "The Theory of Aeroelasticity", John Wiley and Sons, Inc., New York, N.Y. (1955).

35. James, Hubert M., Nichols, Nathaniel B. and Phillips, Ralph S., "Theory of Servomechanisms", McGraw-Hill Book Company, Inc., New York, N.Y. (1947).

36. Press, H., and Tukey, J.W., "Power Spectral Methods of Analysis and Their Application to Problems in Airplane Dynamics", AGARD Flight Test Manual, Vol IV, Part IV-C (1957).

37. Blackman, R.B., and Tukey, J.W., "The Measurement of Power Spectra", Dover Publications, New York, N.Y. (1958).

38. Kovasznay, Laszlo, "Calibration and Measurement in Turbulence Research by the Hot-Wire Method", NACA TM 1130 (June, 1947).

39. McKinney, Linwood W., "Effects of Fineness Ratio and Reynolds Number on the Low-Speed Crosswind Drag Characteristics of Circular and Modified-Square Cylinders", NASA TN D-540 (October, 1960).

40. Tani, Itiro, "On the Periodic Shedding of Vortices from a Circular Cylinder at High Reynolds Numbers", IUTAM Symposium on Concentrated Vortex Motions in Fluids (paper presented by Prof. H. Sato), Ann Arbor, Michigan (July 6 - 11, 1964).

41. Bursnall, William J. and Loftin, Laurence K., Jr., "Experimental Investigation of Localized Regions of Laminar-Boundayr-Layer Separation"; NACA TN 2338 (April, 1951).

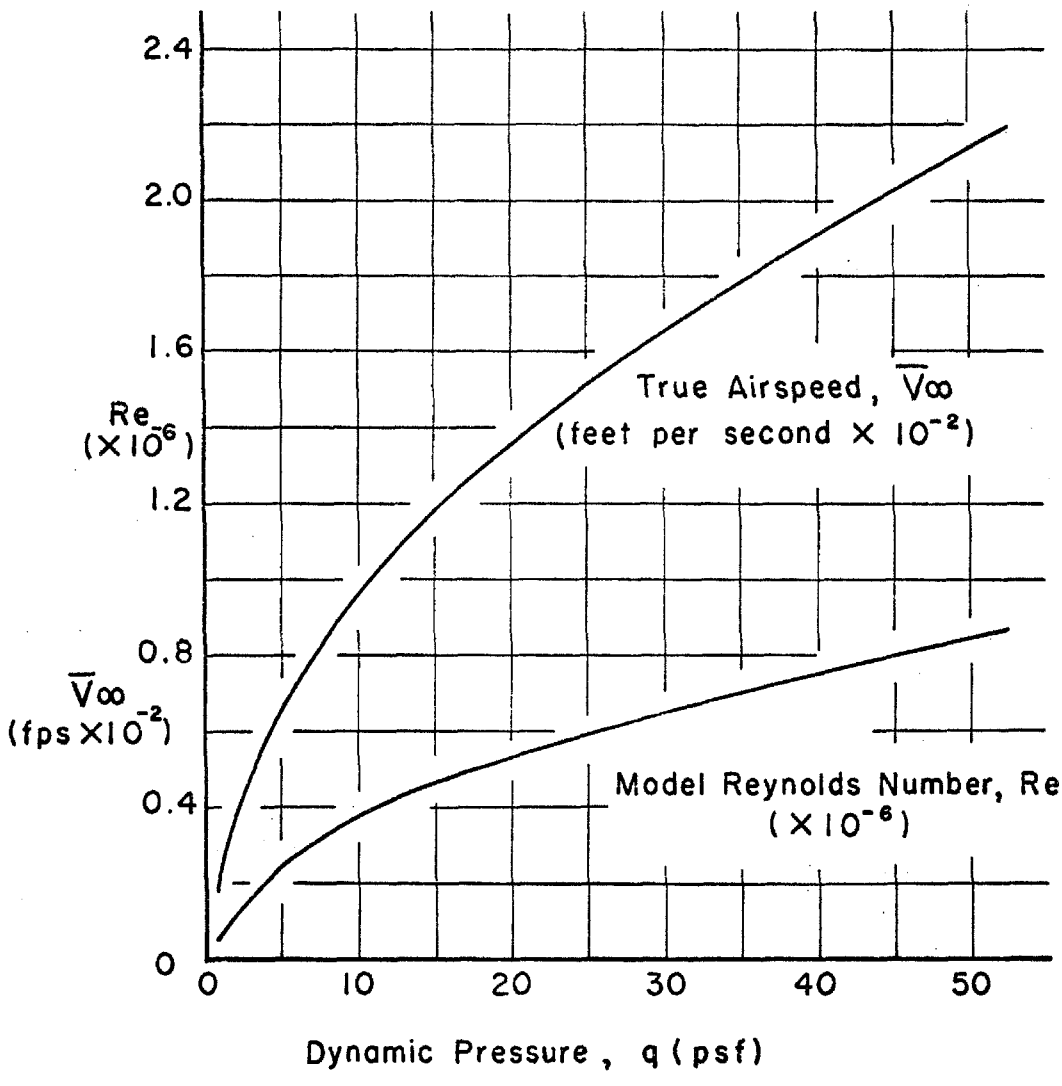

FIG. 1 AVERAGE WIND TUNNEL CHARACTERISTICS

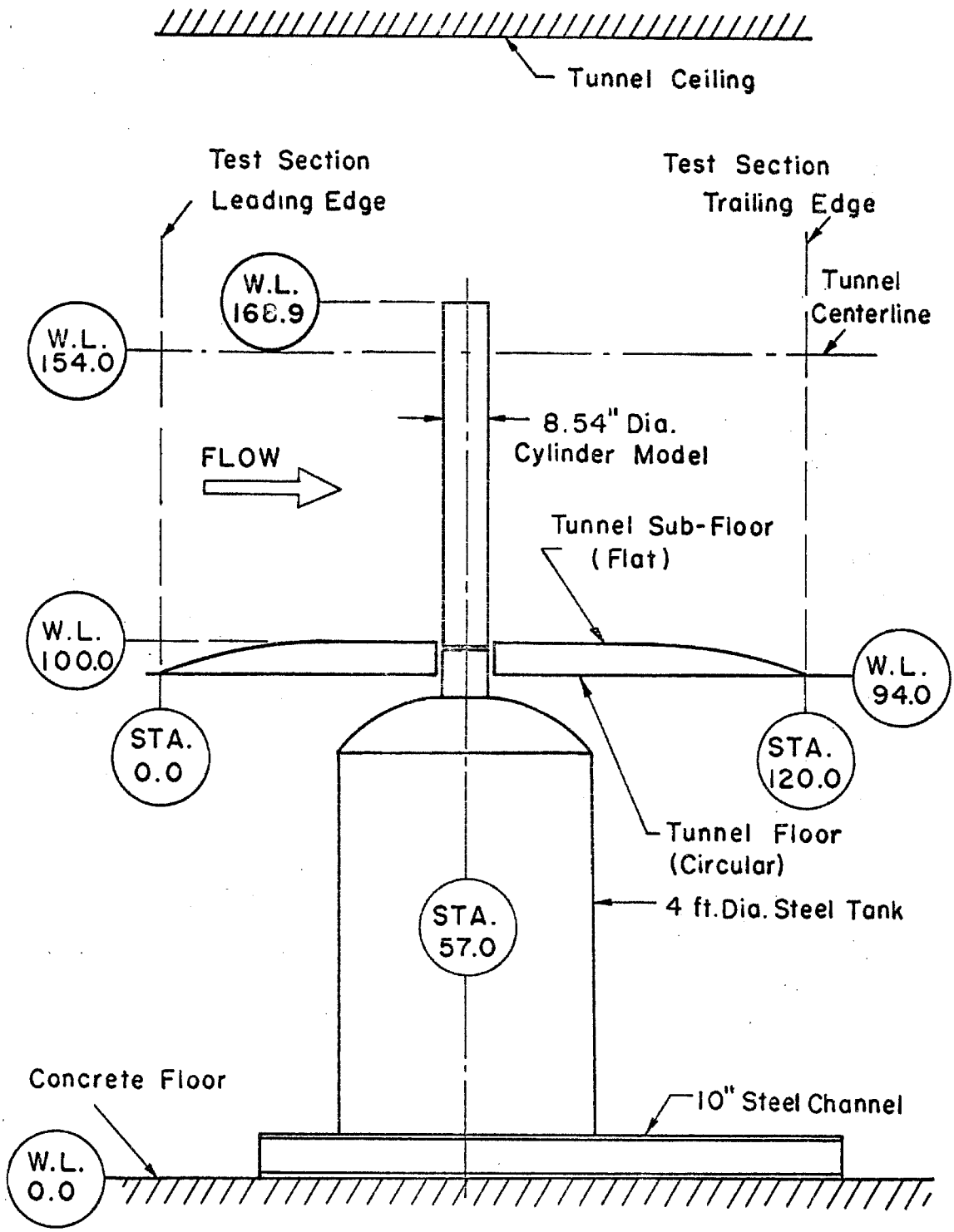

FIG. 2 MODEL INSTALLATION IN THE GALCIT 10-FOOT WIND TUNNEL

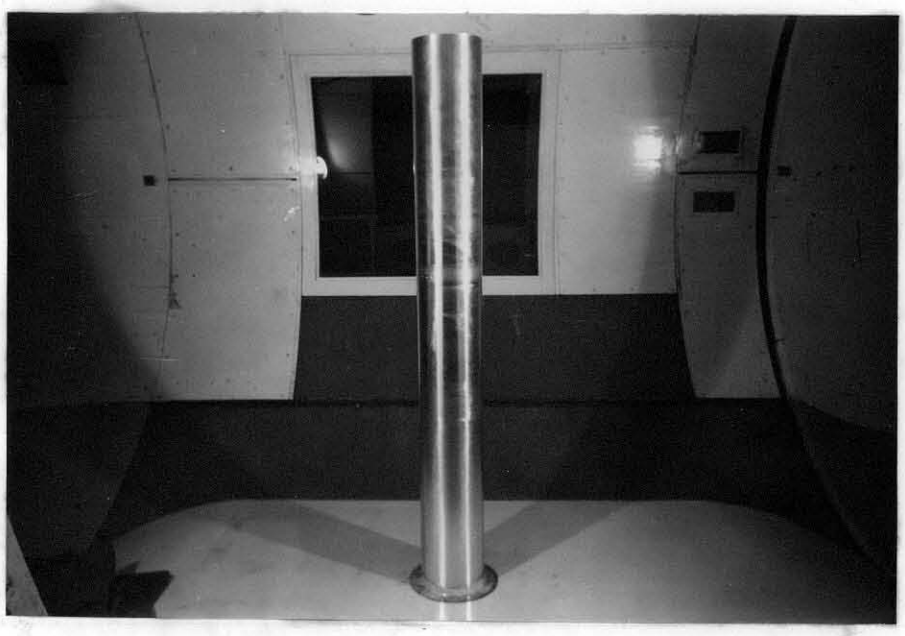

a. Side View

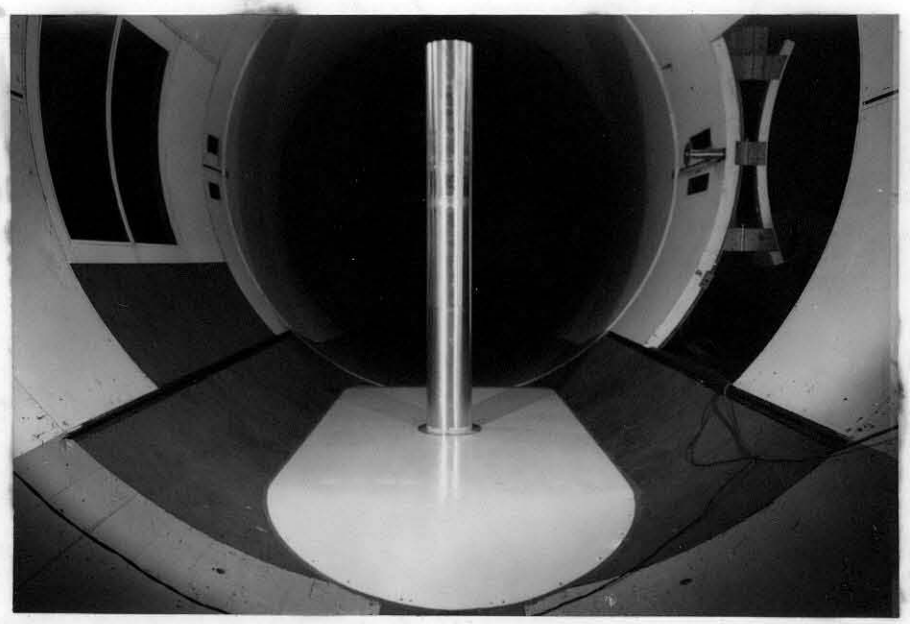

b. Front View

FIG. 3 CANTILEVERED CYLINDER MODEL

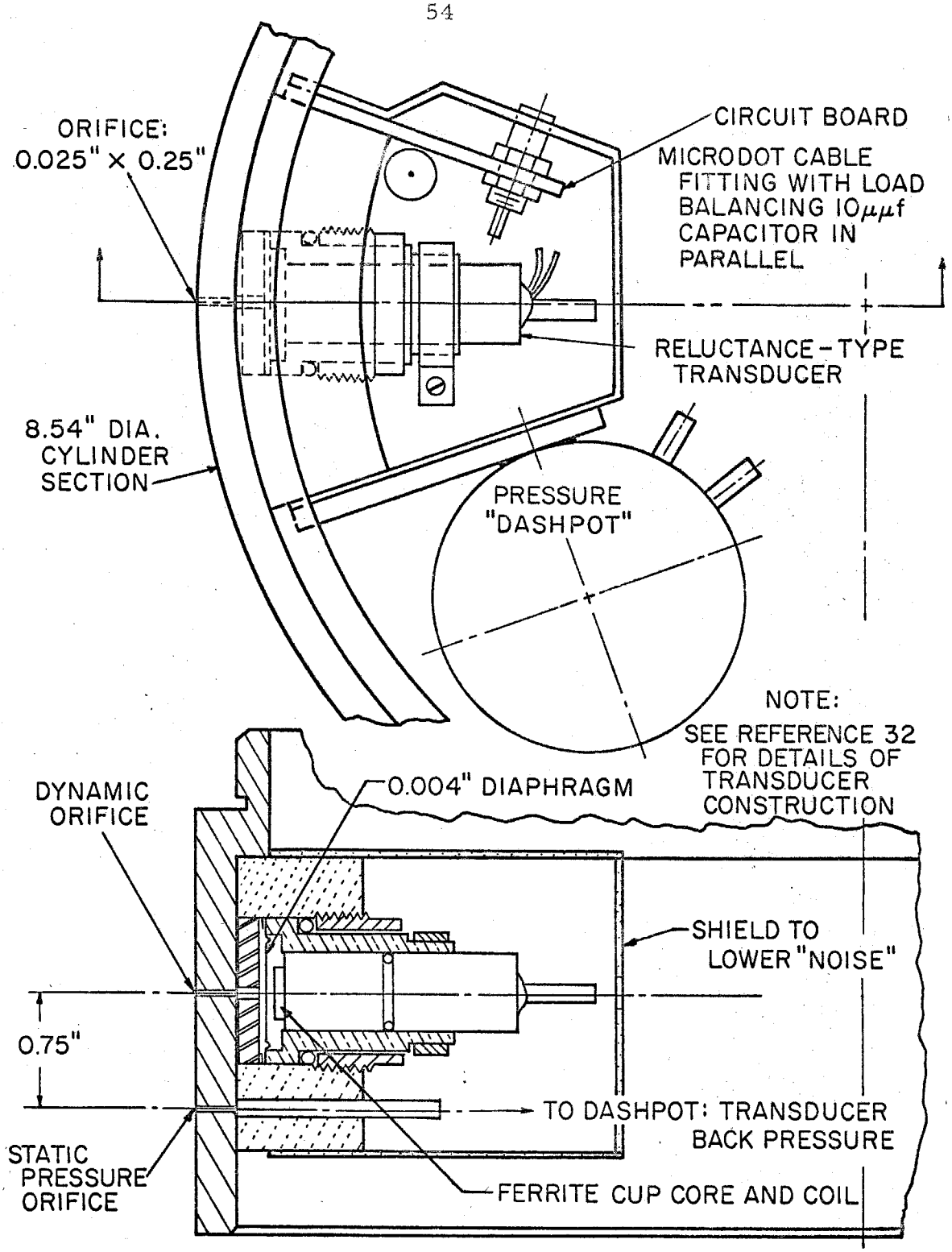

FIG. 4 PRESSURE MEASURING UNIT

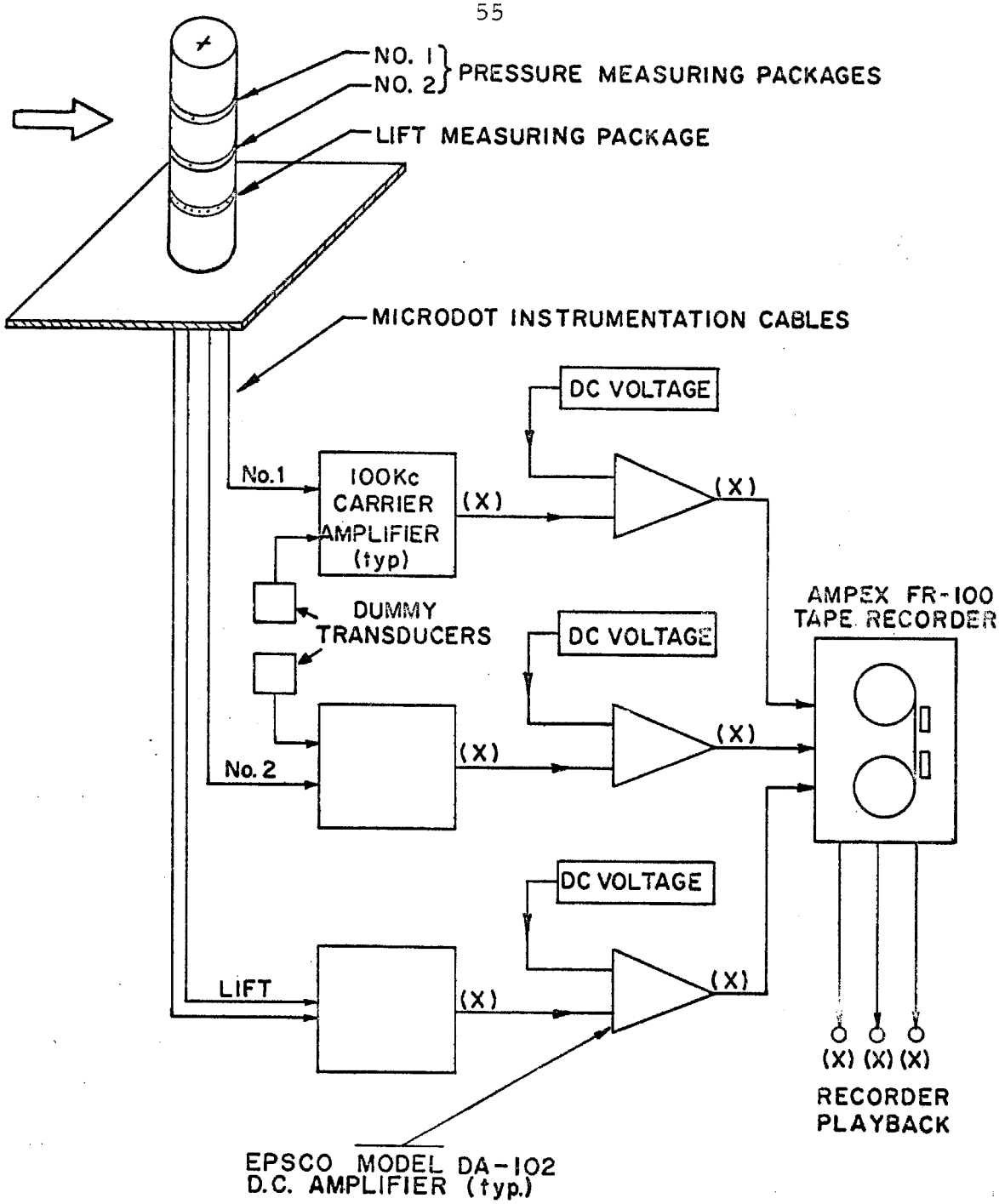

NOTE: MONITORING POINTS DENOTED BY (X).
SWITCH PANEL ALLOWED MONITORING AT ALL POINTS BY
1. BALLANTINE TYPE 320 TRUE RMS VOLTMETER
2. L. AND N. SPEEDOMAX D. C. VOLTMETER
3. DUMONT MODEL 411 DUAL BEAM OSCILLOSCOPE

FIG. 5 PRESSURE AND LIFT DATA RECORDING SCHEMATIC

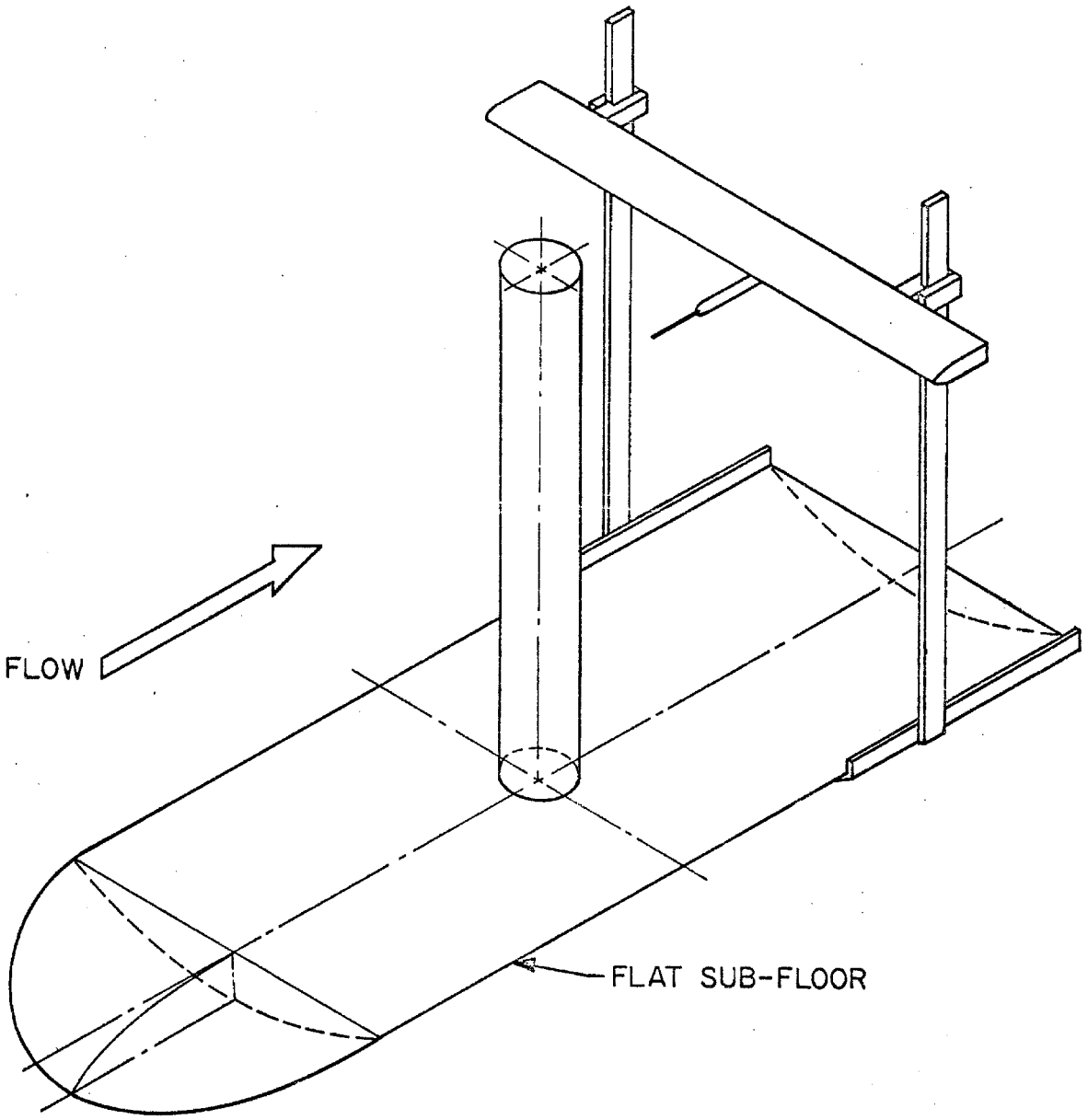

NOTE:

1. HOT-WIRE LOCATION WAS 11" AHEAD OF TRAVERSE FAIRING
2. TRAVERSE WAS HELD RIGID BY GUY-WIRES

FIG. 6 HOT-WIRE TRAVERSE ARRANGEMENT

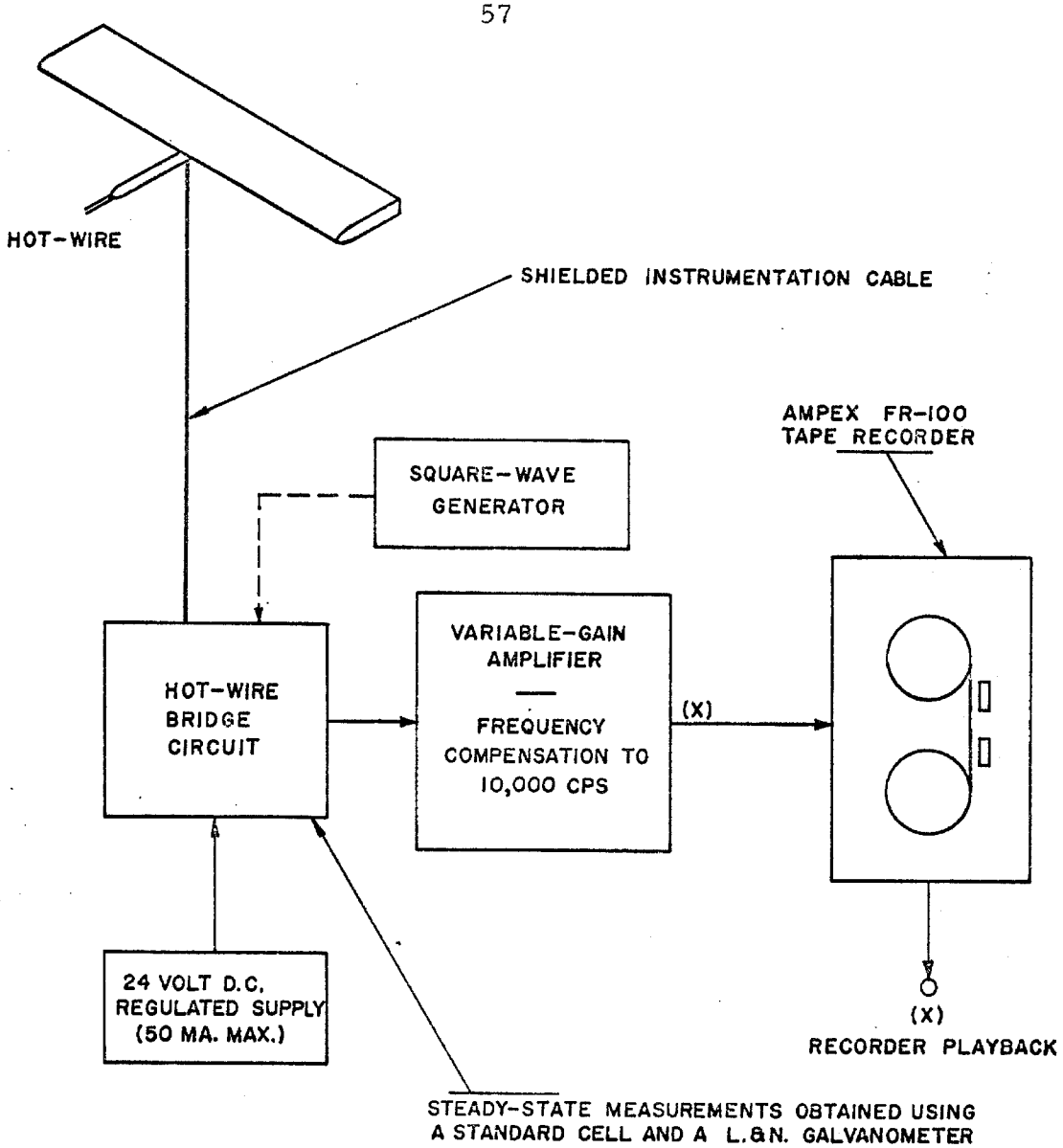

NOTE: MONITORING AT POINTS DENOTED BY (X) DONE WITH
1. BALLANTINE TYPE 320 TRUE RMS VOLTMETER
2. DUMONT MODEL 411 DUAL BEAM OSCILLOSCOPE

FIG. 7 HOT-WIRE DATA RECORDING SCHEMATIC

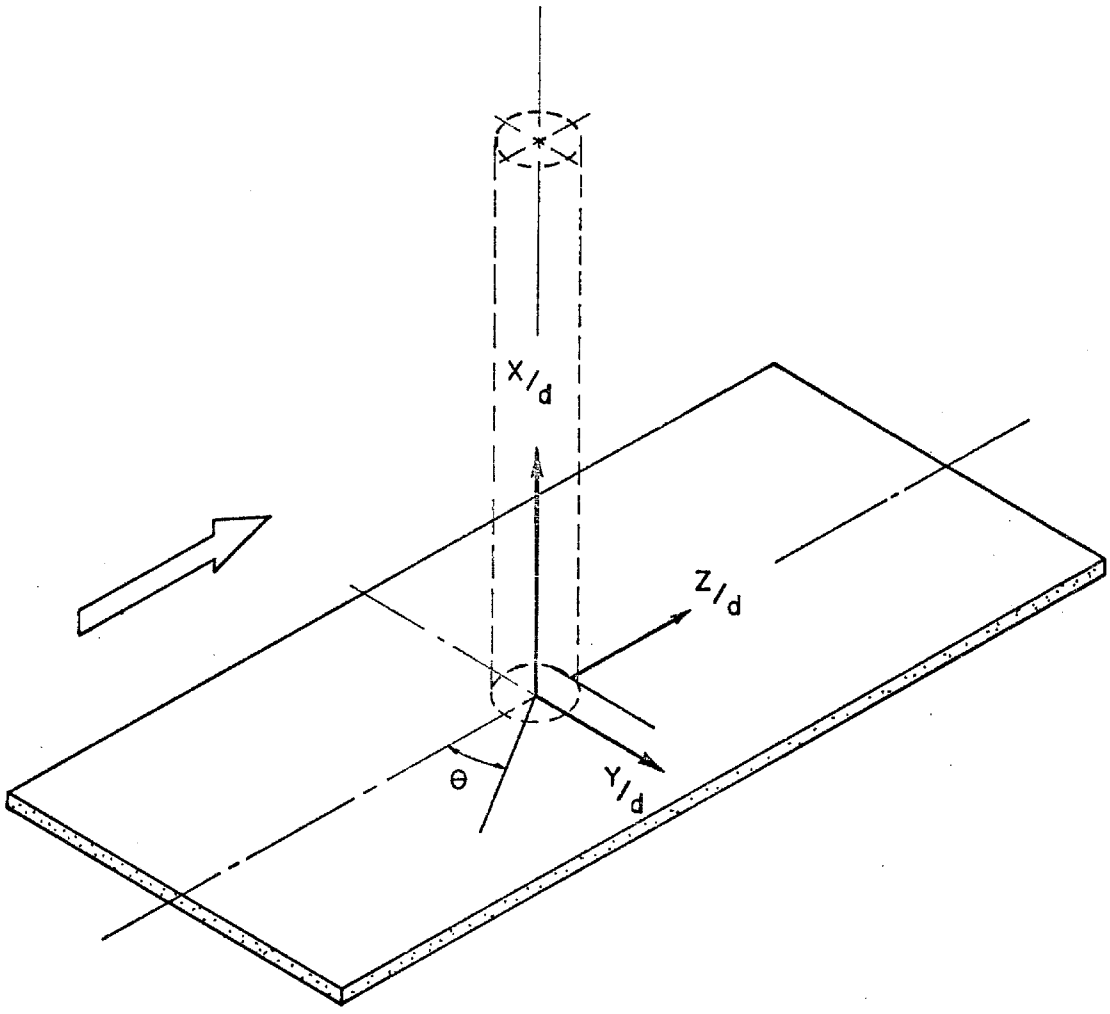

$Z/_d$ – MEASURED FROM TRAILING EDGE

FIG. 8 TEST COORDINATE SYSTEM

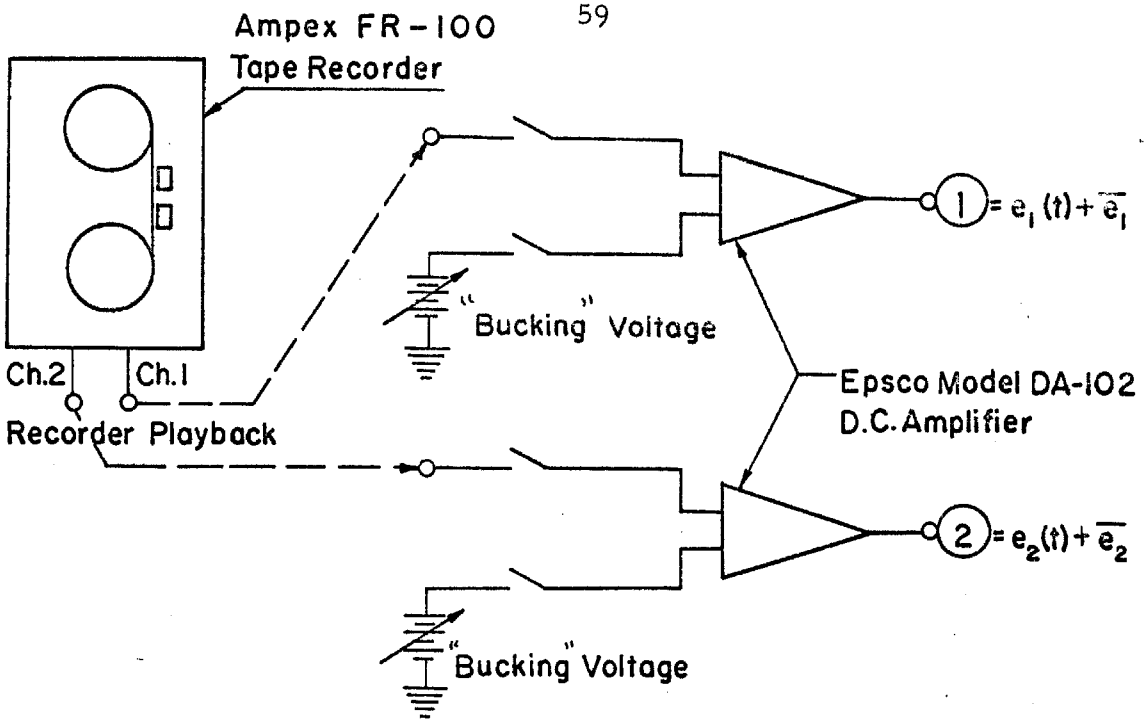

A. Amplifying Circuits

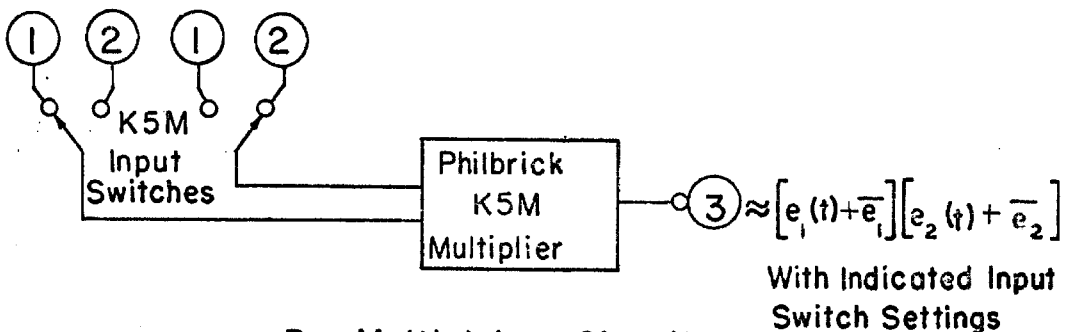

B. Multiplying Circuits

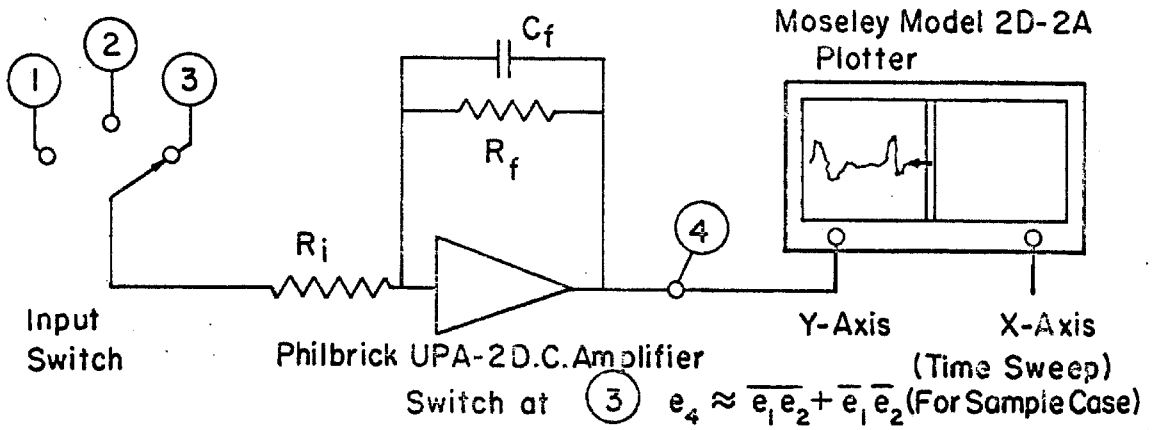

C. Time Averaging Circuit

FIG. 9 SCHEMATIC OF ANALOG CIRCUITRY

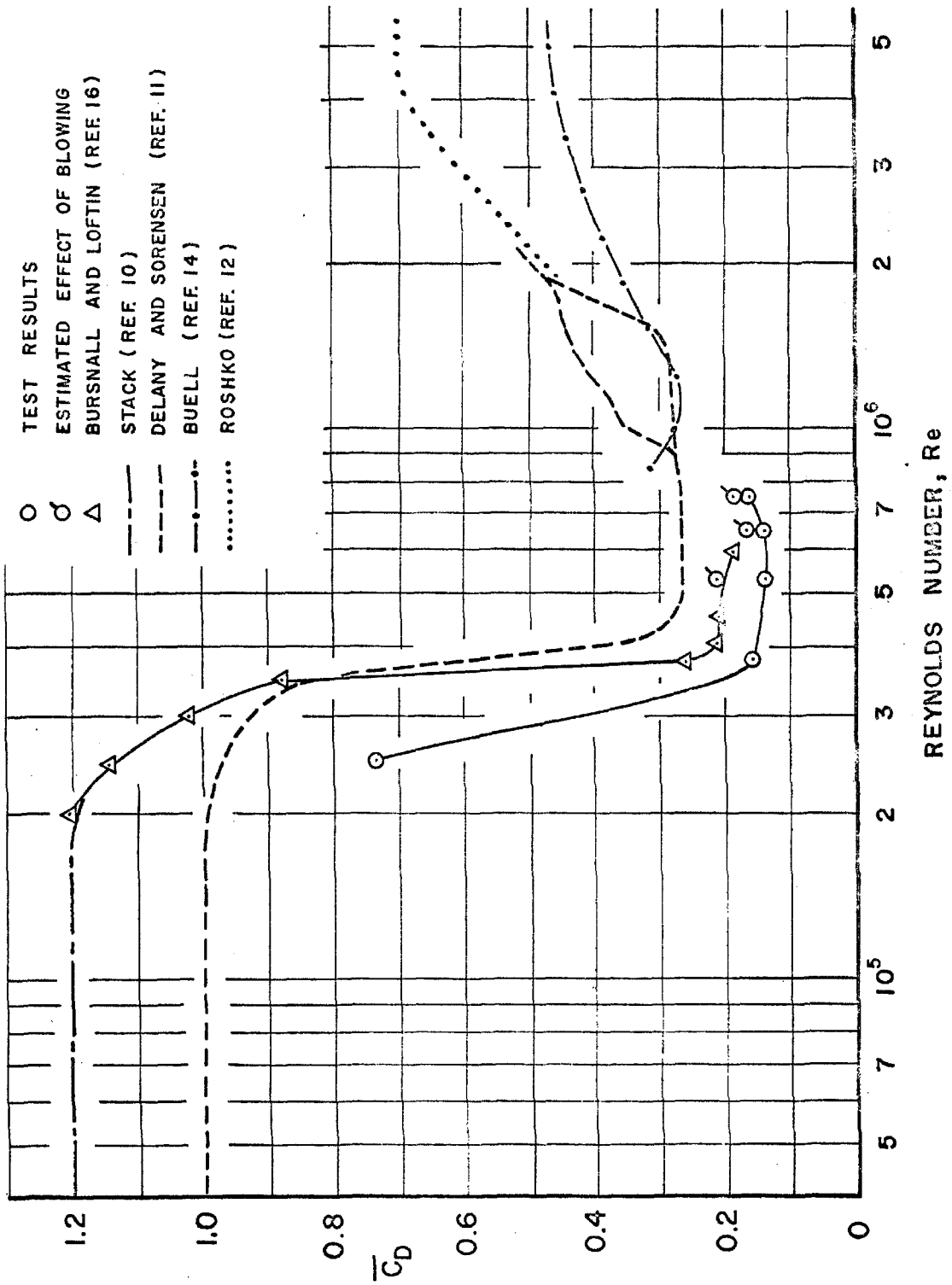

FIG. 10 DRAG COEFFICIENT VS. REYNOLDS NUMBER

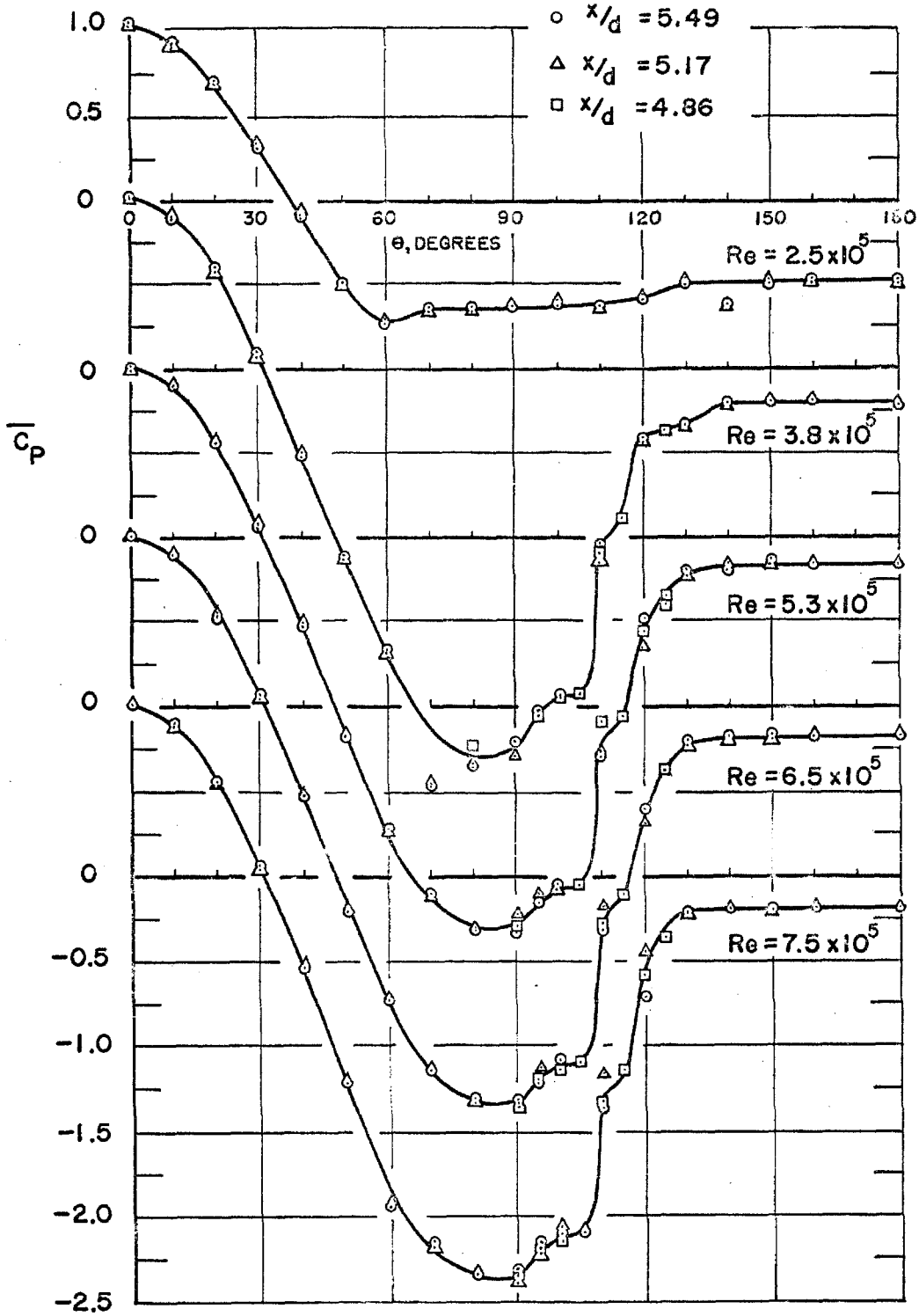

FIG. 11 CYLINDER STATIC PRESSURE DISTRIBUTIONS

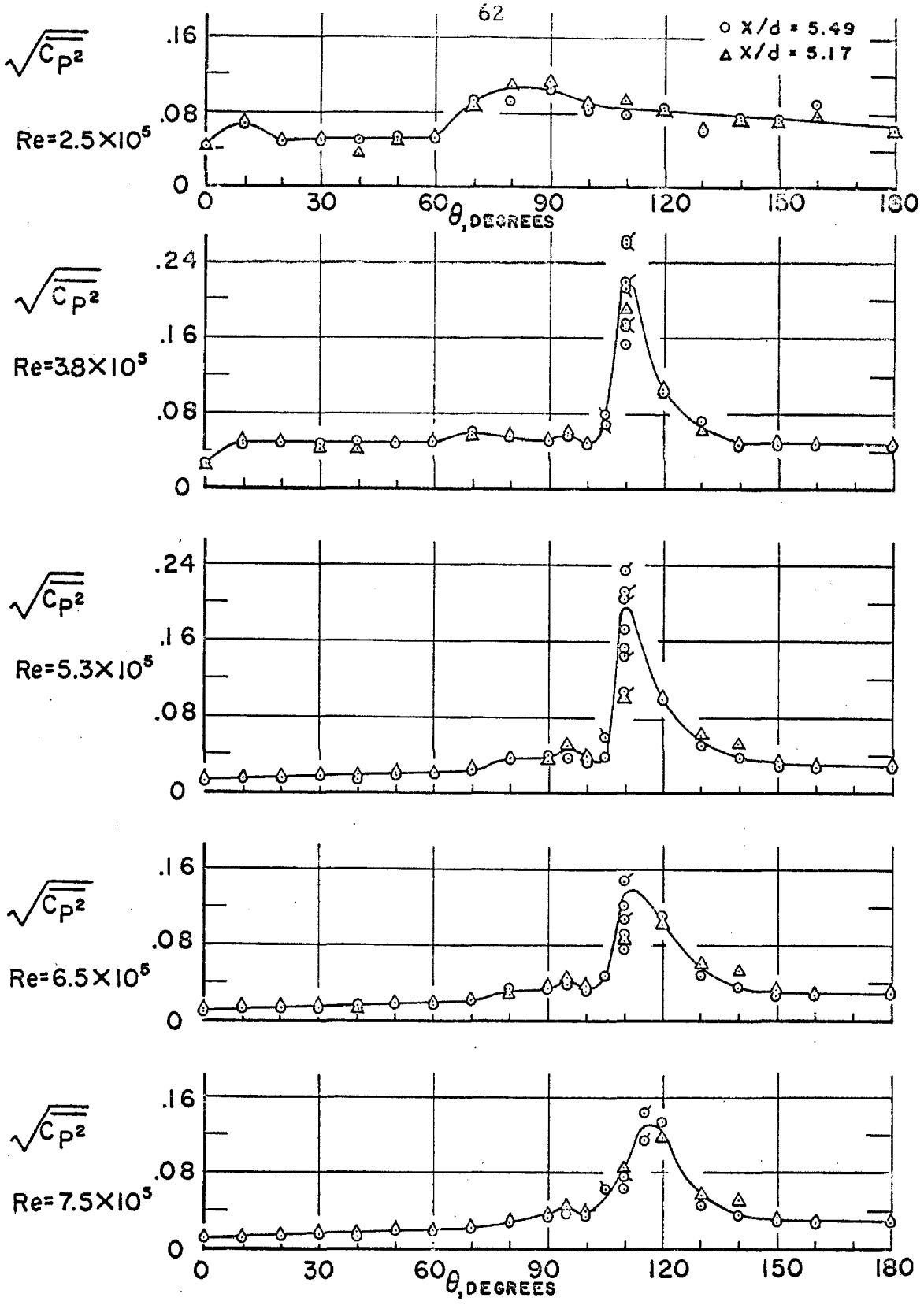

FIG.12 RMS PRESSURE FLUCTUATIONS OVER THE CYLINDER

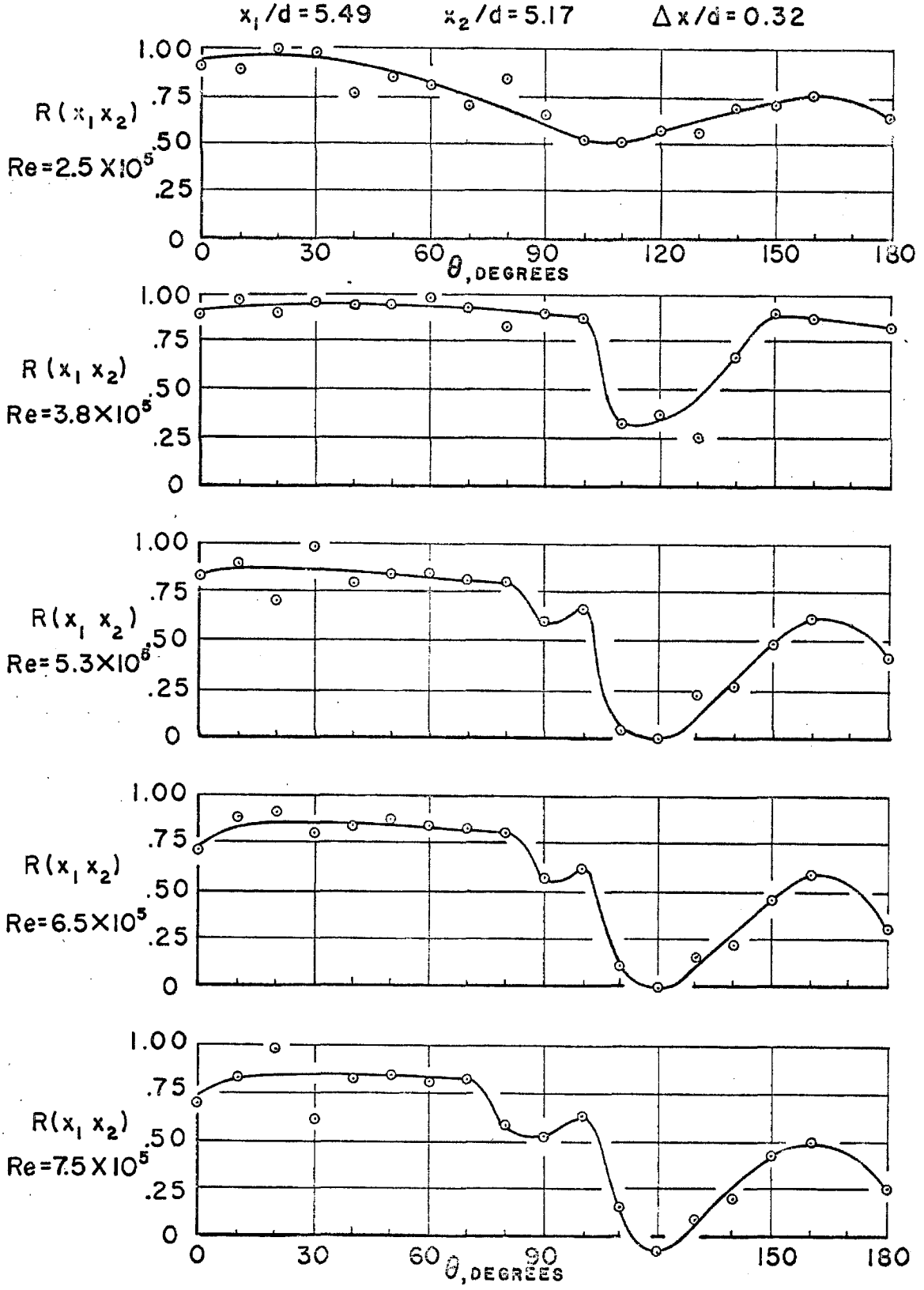

FIG.13 CORRELATION COEFFICIENT FOR PRESSURE FLUCTUATIONS AT $\Delta x/d = 0.32$

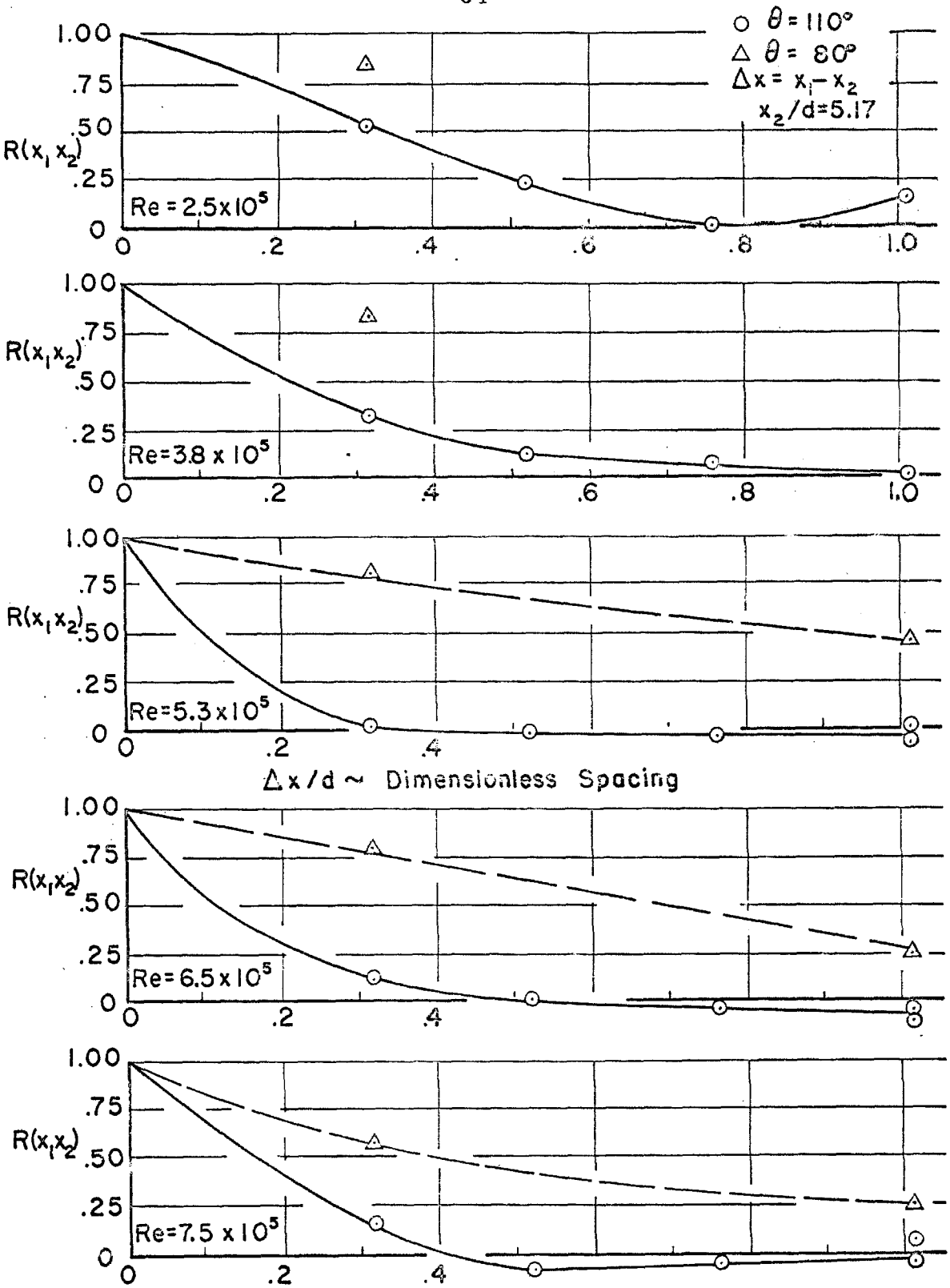

FIG. 14 CORRELATION COEFFICIENT FOR PRESSURE FLUCTUATIONS AT $\theta = 80°$ AND $110°$

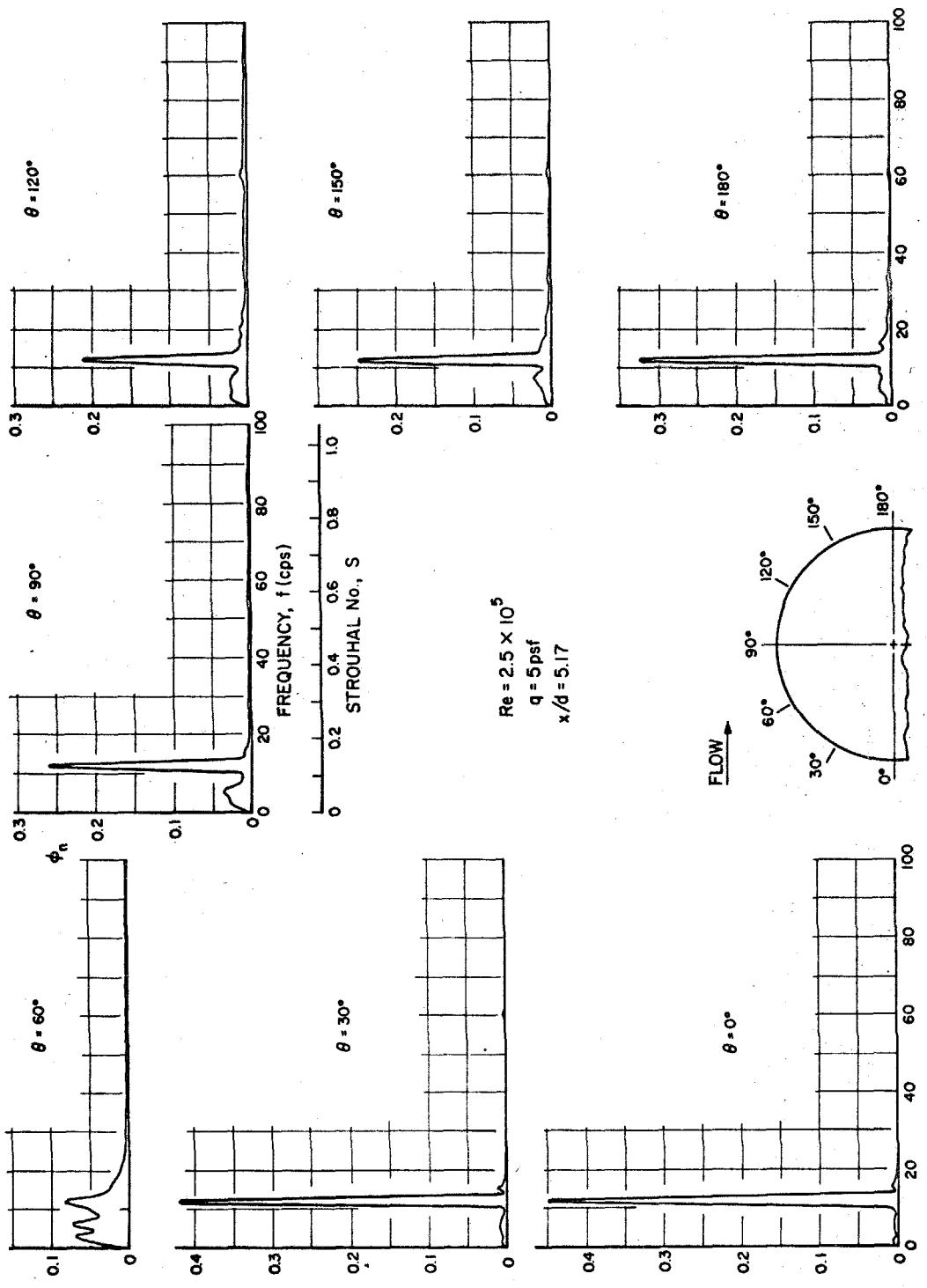

FIG. 15 POWER SPECTRA FOR FLUCTUATING PRESSURES

Re = 2.5×10^5

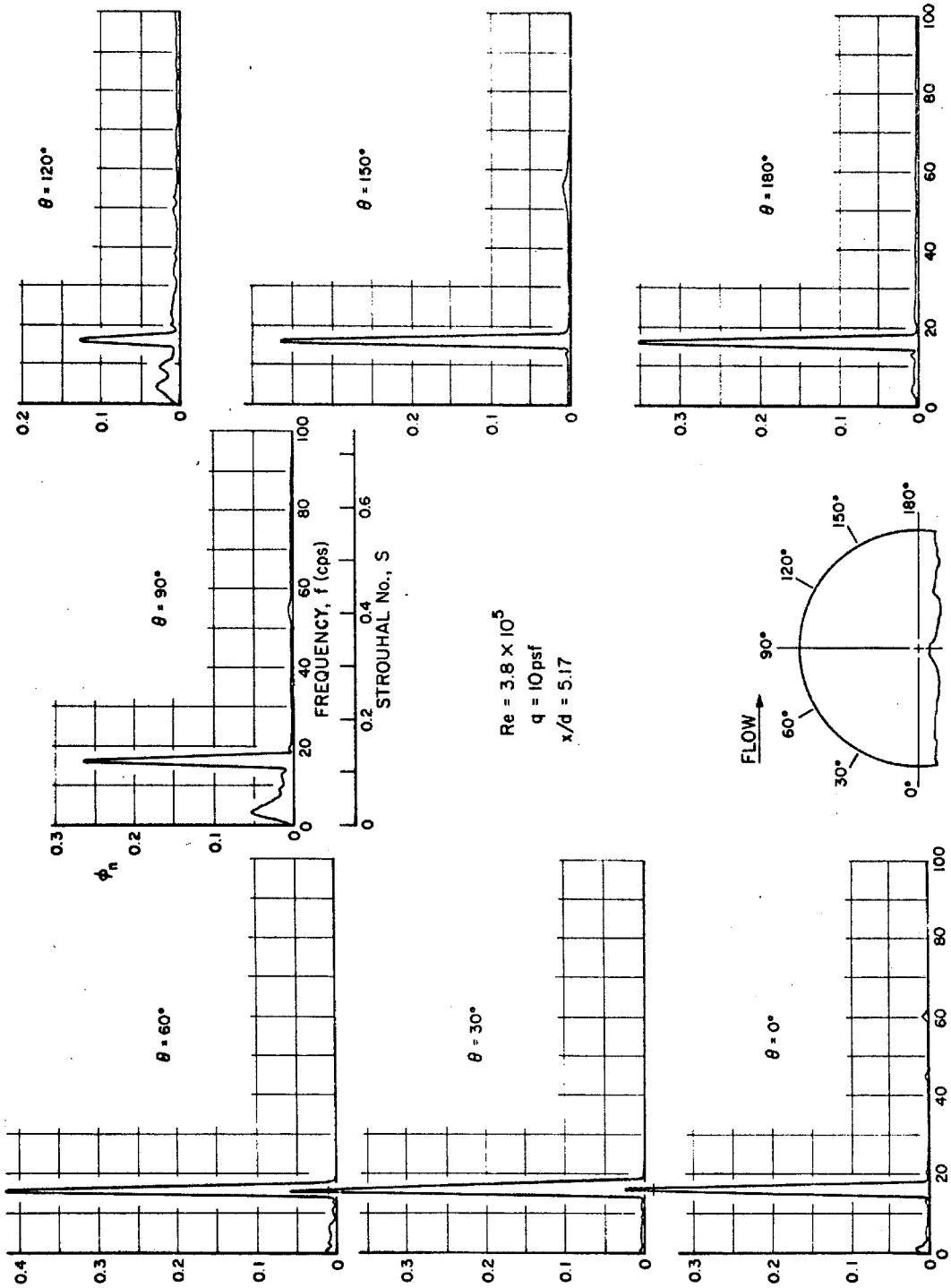

FIG. 16 POWER SPECTRA FOR FLUCTUATING PRESSURES

$Re = 3.8 \times 10^5$

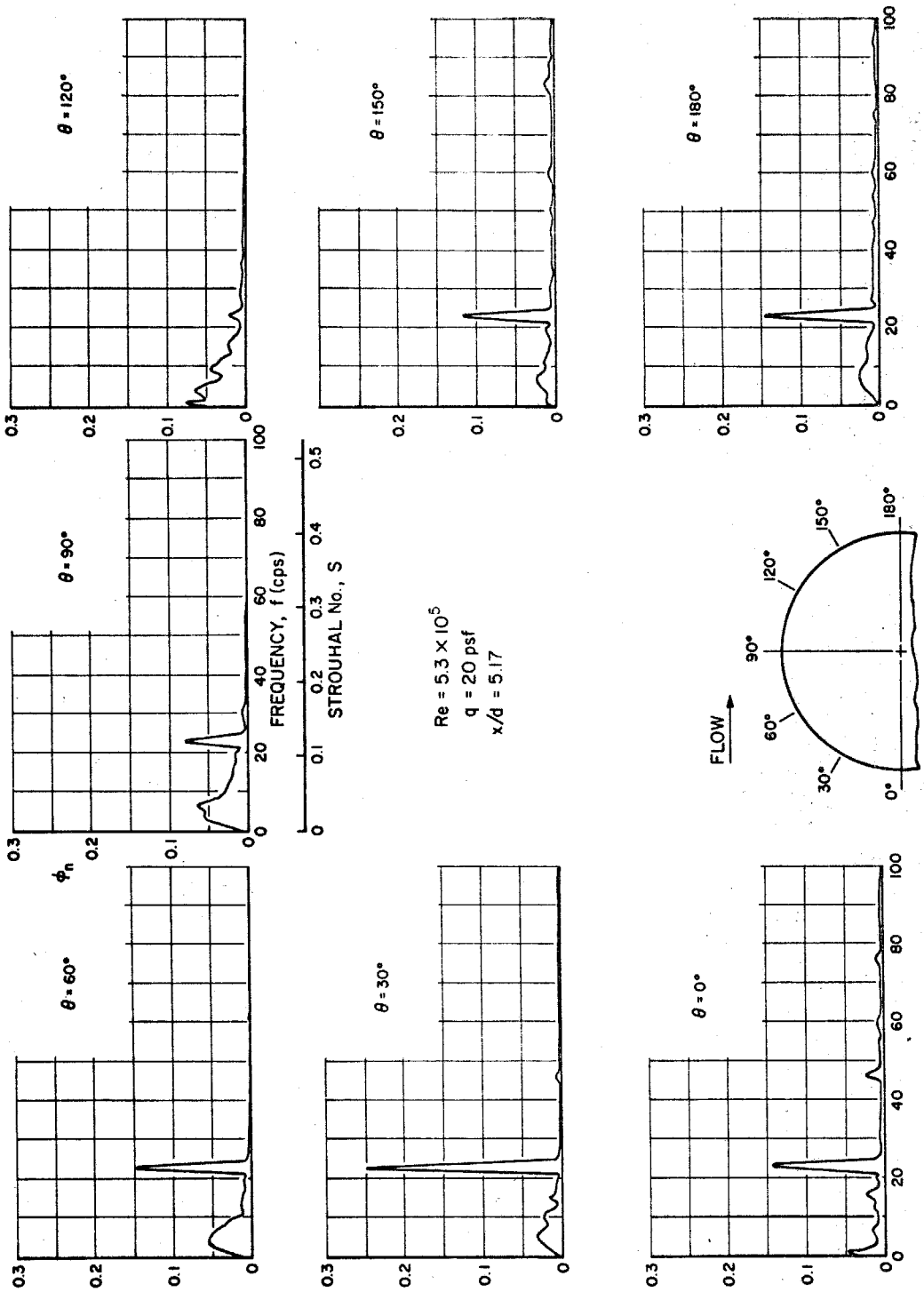

FIG. 17 POWER SPECTRA FOR FLUCTUATING PRESSURES

$Re = 5.3 \times 10^5$

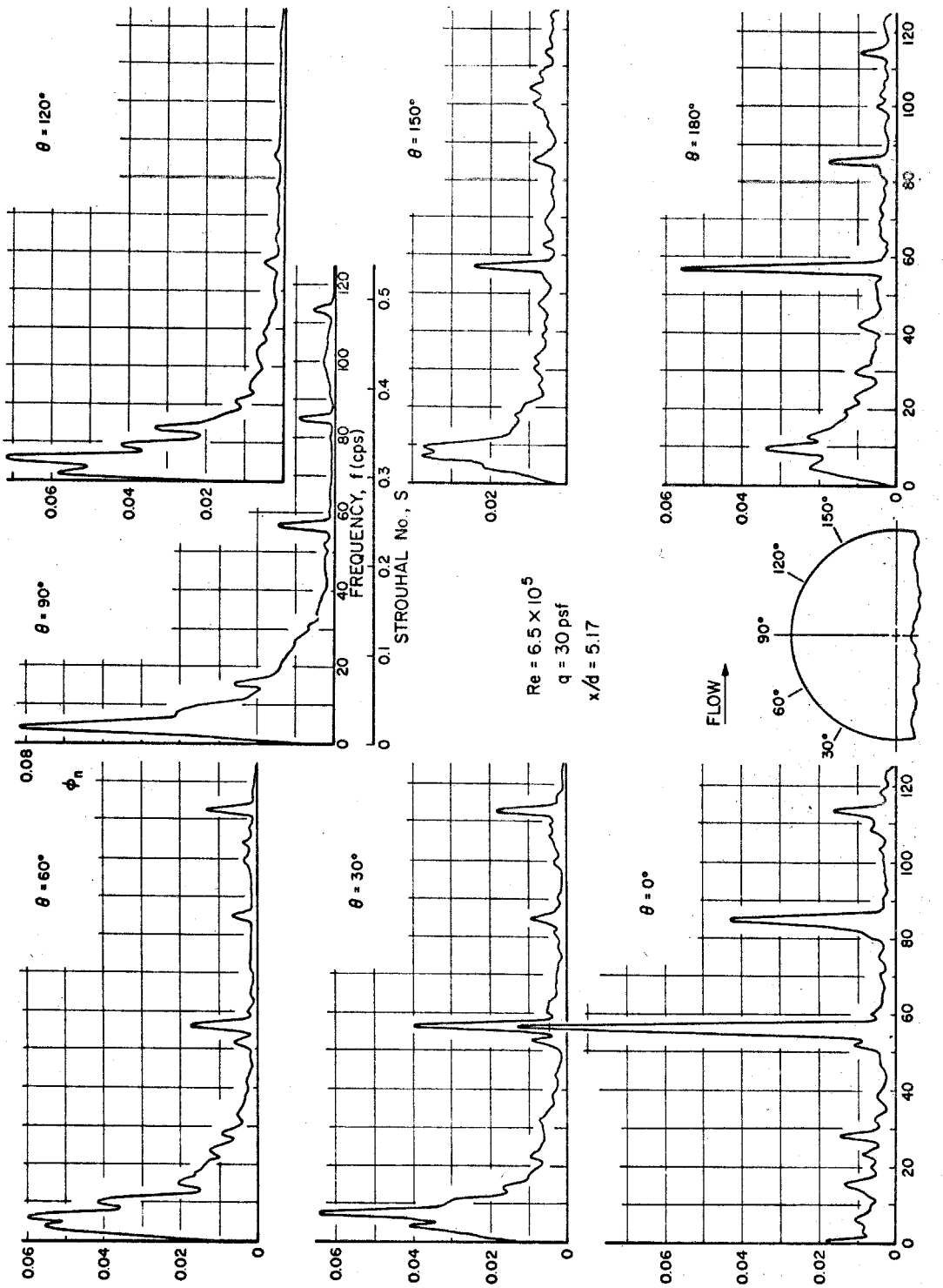

FIG. 18 POWER SPECTRA FOR FLUCTUATING PRESSURES

$Re = 6.5 \times 10^5$

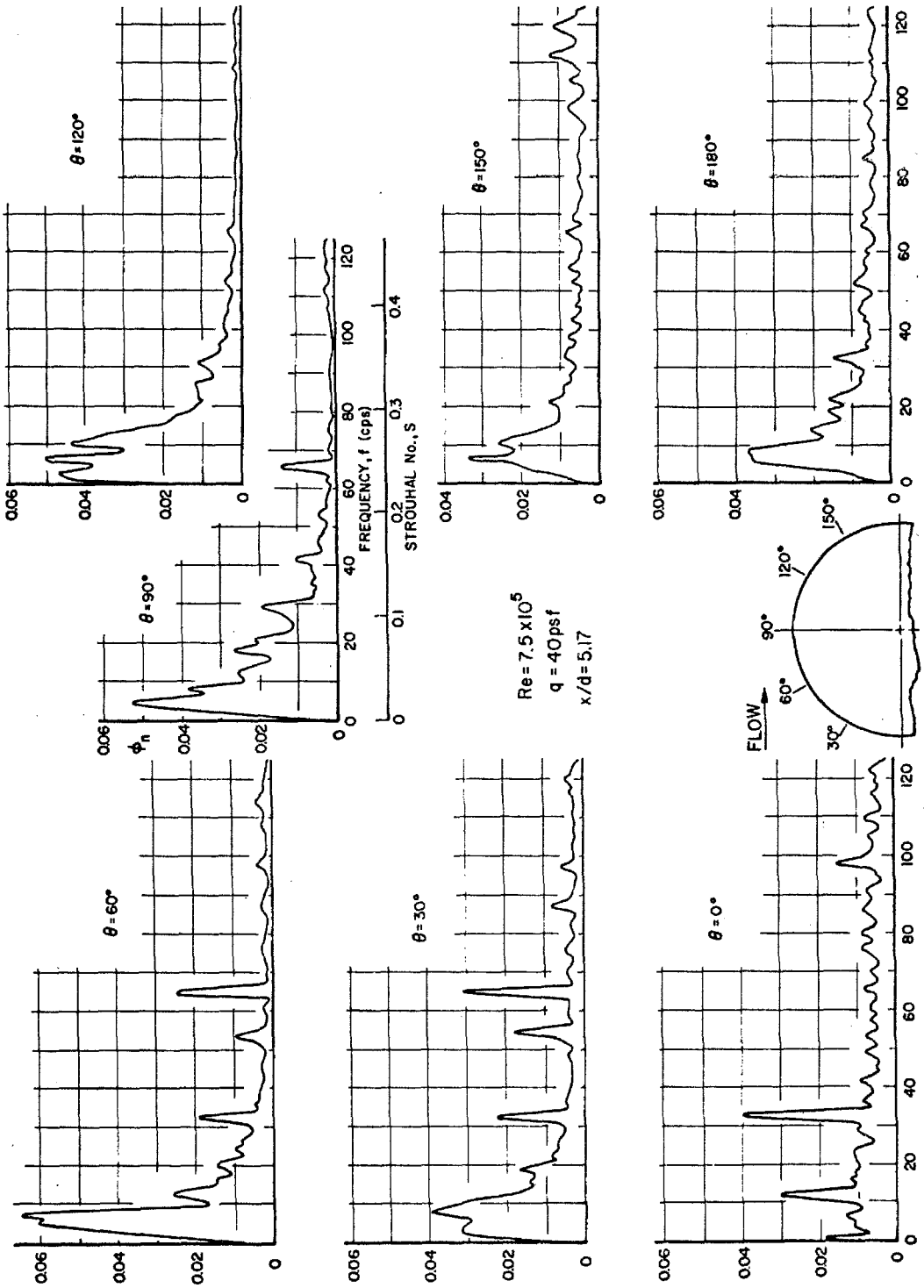

FIG. 19 POWER SPECTRA FOR FLUCTUATING PRESSURES

$Re = 7.5 \times 10^5$

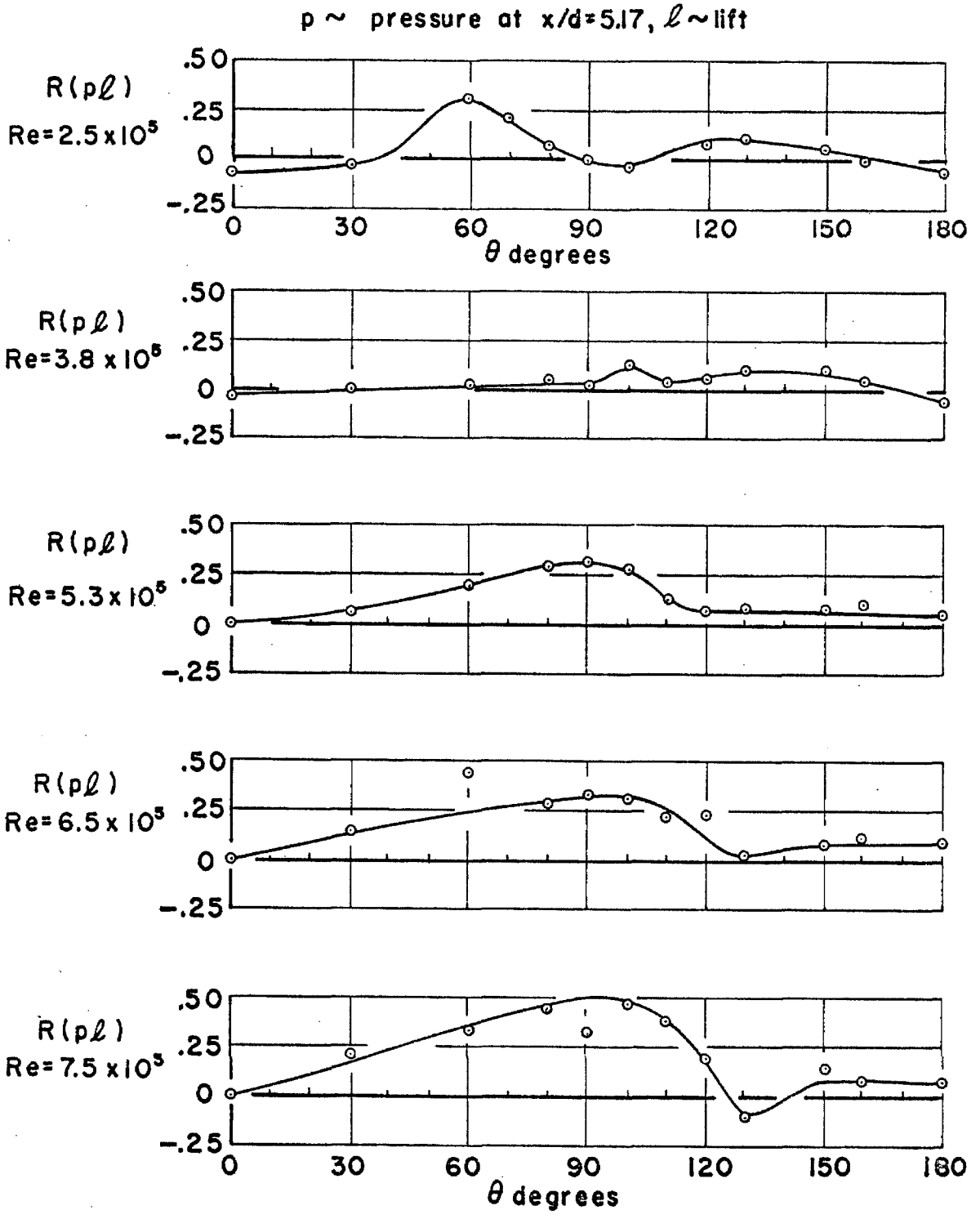

FIG. 20 CORRELATION COEFFICIENT BETWEEN FLUCTUATING LIFT AND FLUCTUATING PRESSURES AT $\Delta x/d = 0.32$

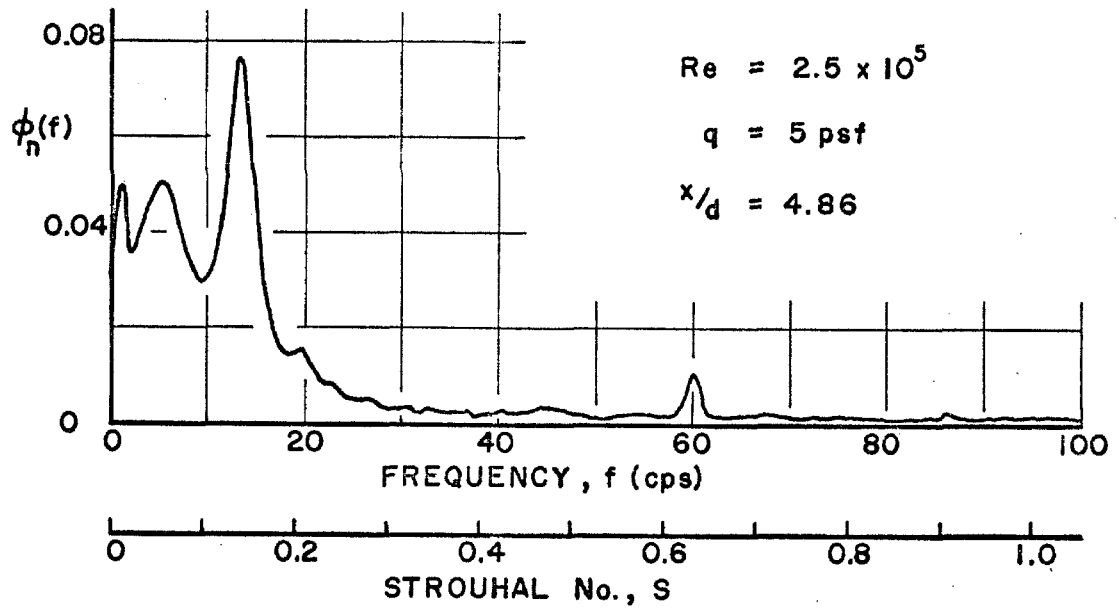

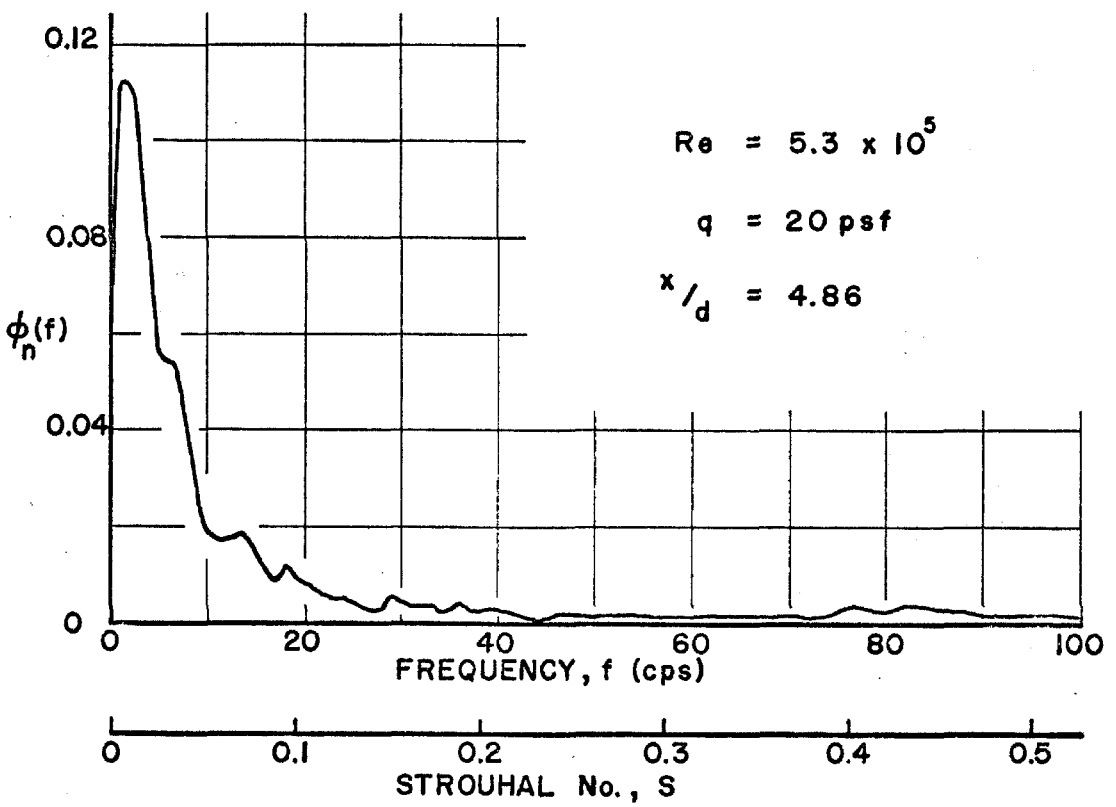

FIG. 21 POWER SPECTRA FOR FLUCTUATING LIFT
Re = 2.5 x 10^5 and 5.3 x 10^5

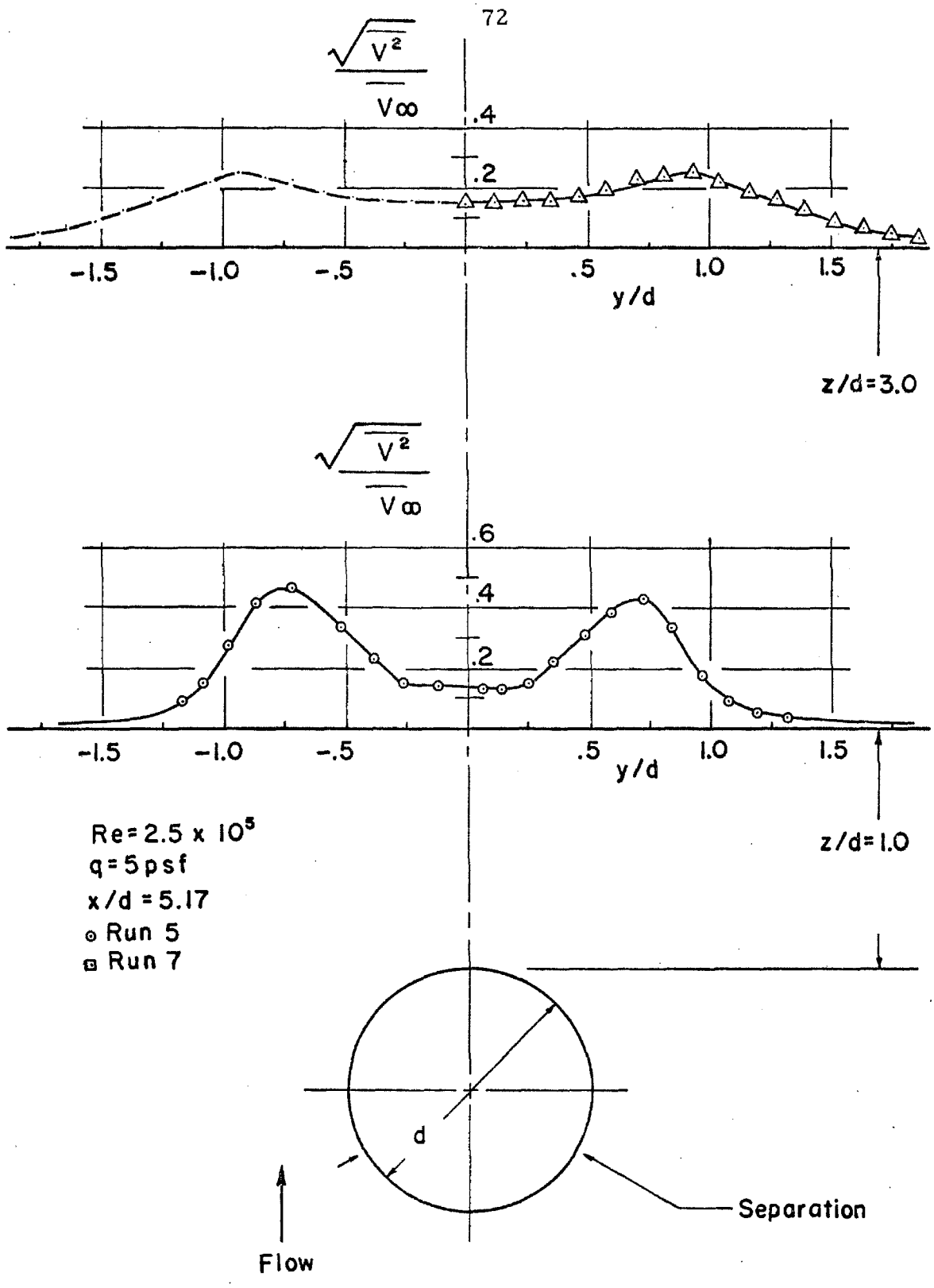

FIG. 22 RMS VELOCITY FLUCTUATIONS IN THE WAKE BEFORE TRANSITION

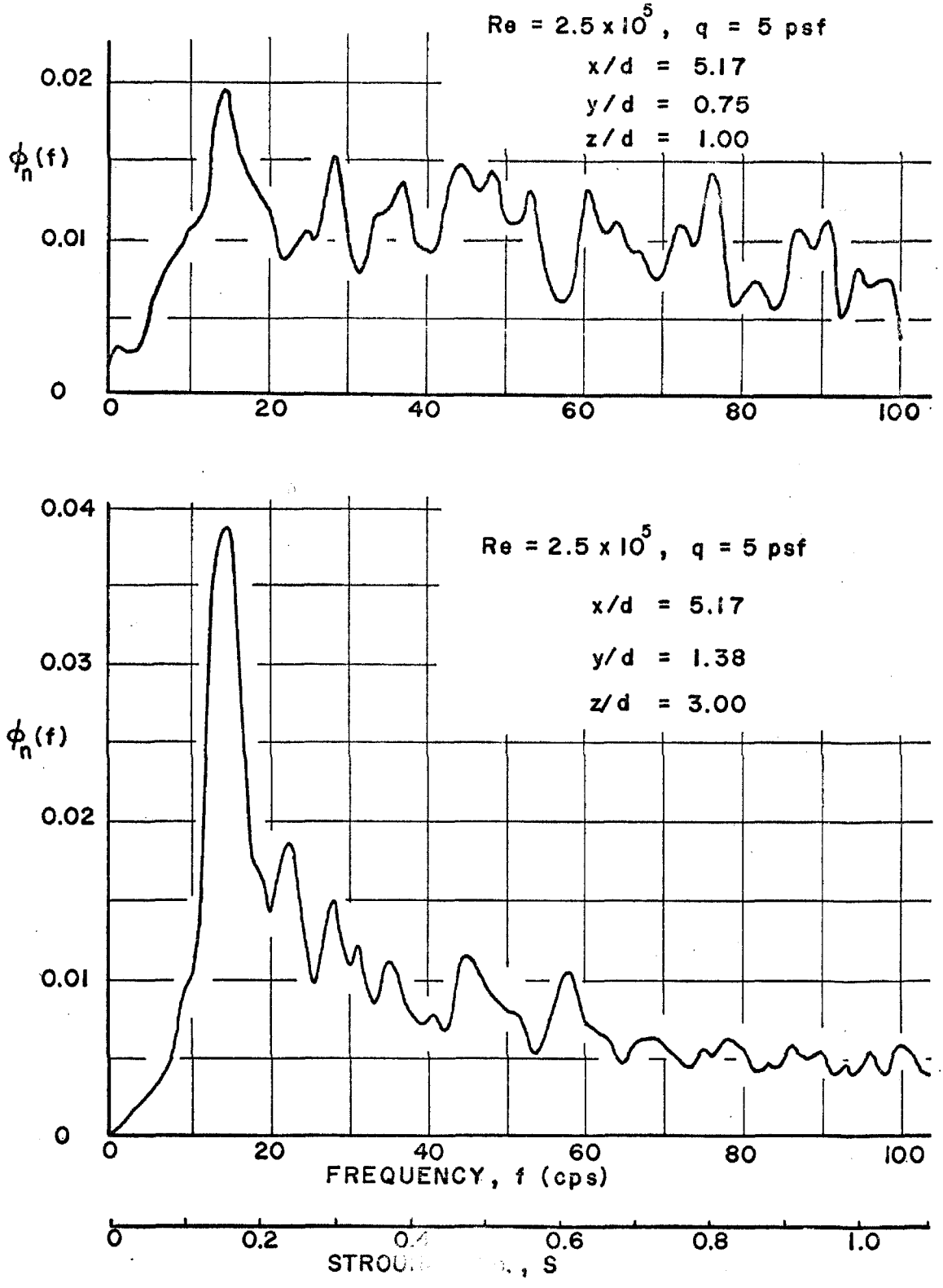

FIG. 23 POWER SPECTRA FOR WAKE VELOCITY FLUCTUATIONS BEFORE TRANSITION

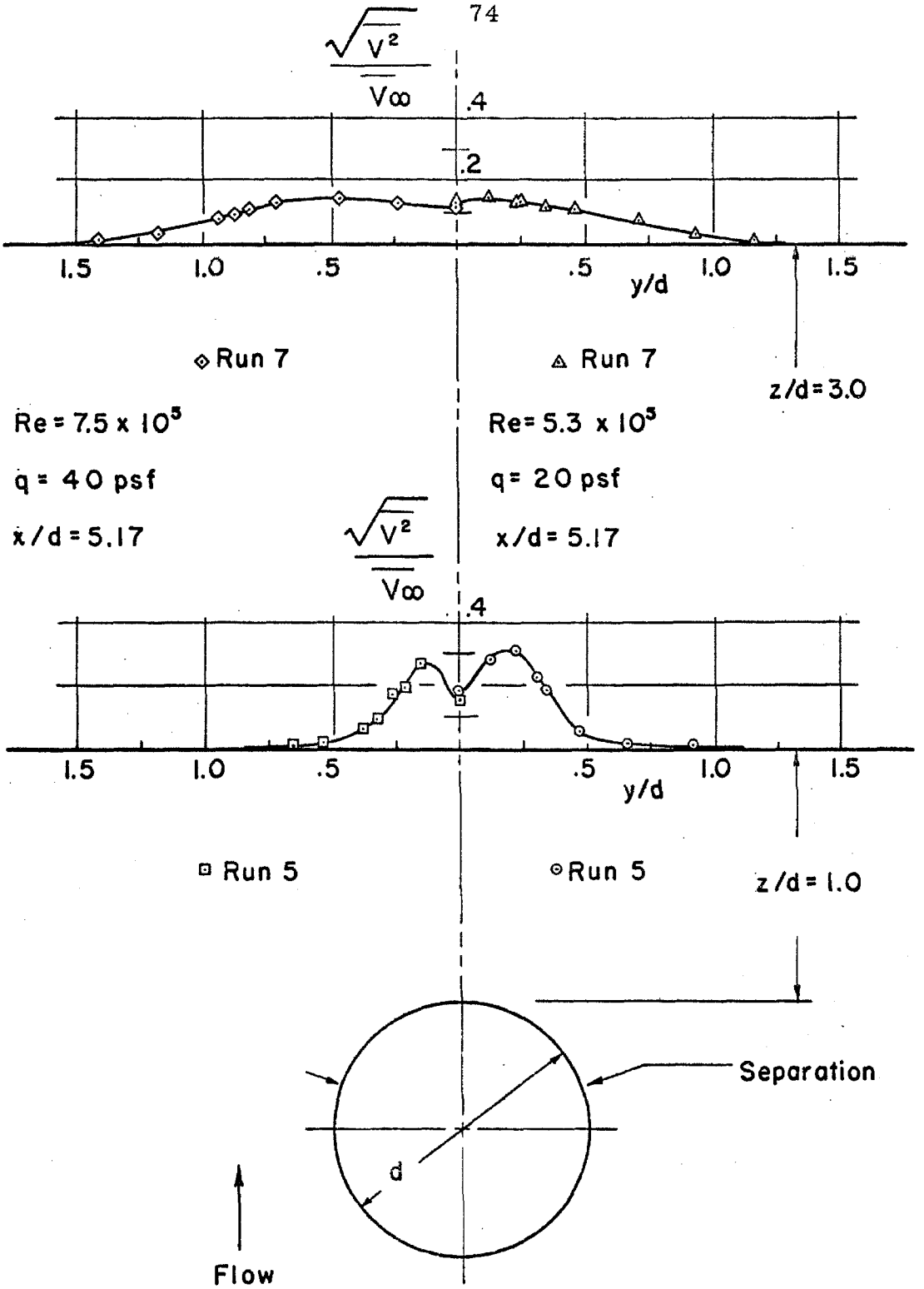

FIG. 24 RMS VELOCITY FLUCTUATIONS IN THE WAKE AFTER TRANSITION

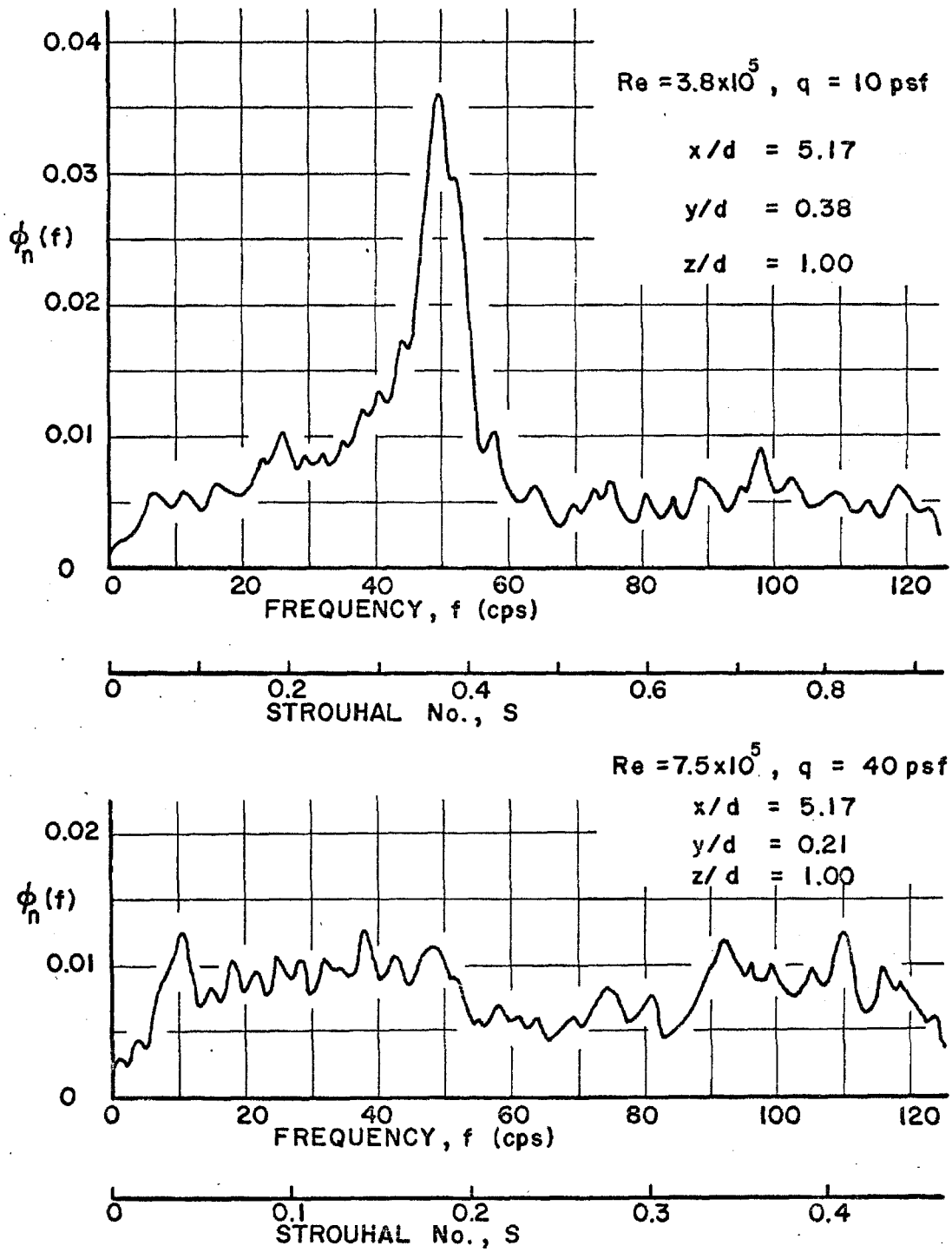

FIG. 25 POWER SPECTRA FOR WAKE VELOCITY FLUCTUATIONS AFTER TRANSITION (z/d=1.0)

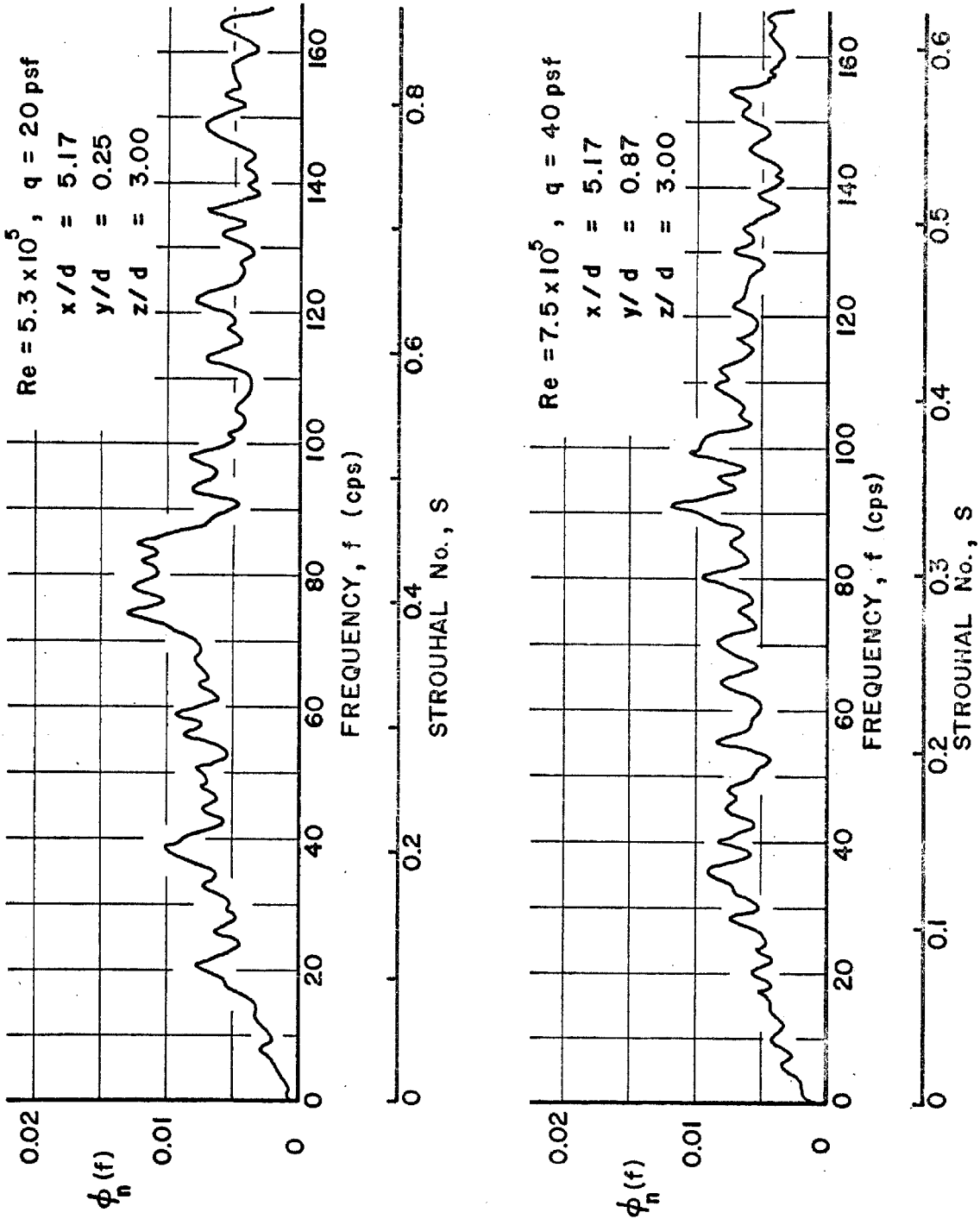

FIG. 26 POWER SPECTRA FOR WAKE VELOCITY FLUCTUATIONS AFTER TRANSITION (z/d=3.0)

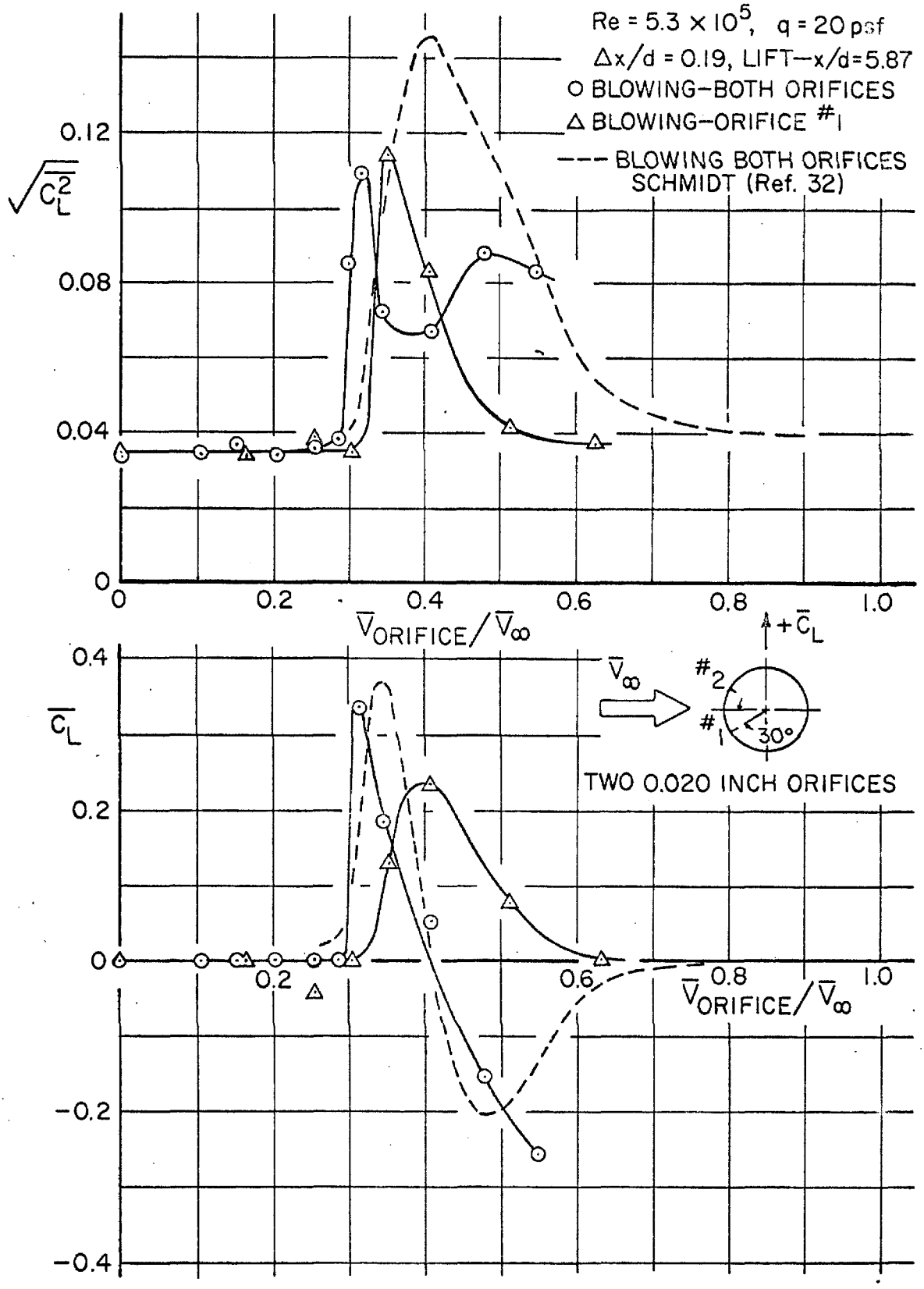

FIG. 27 EFFECTS OF ORIFICE BLOWING ON LIFT

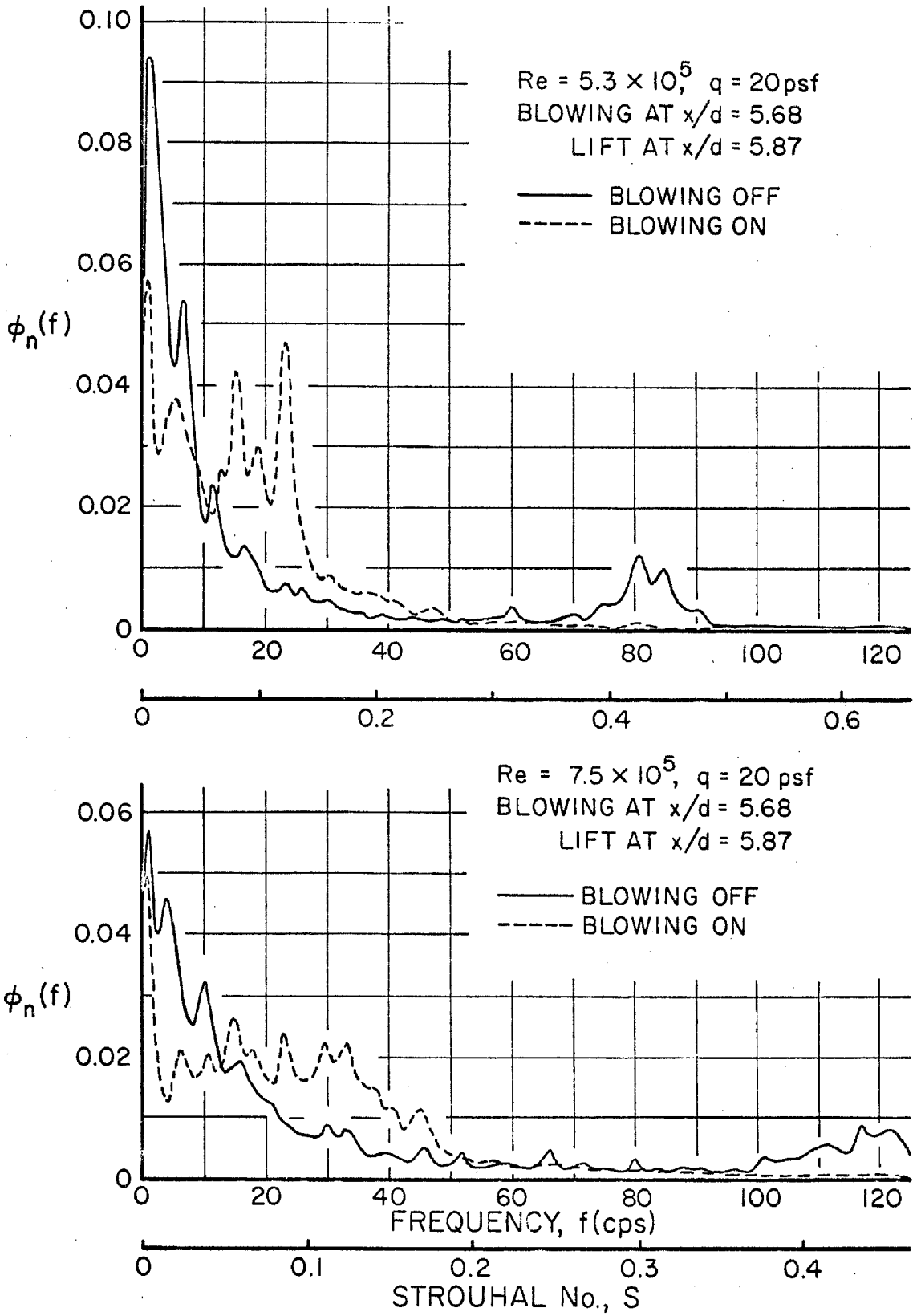

FIG. 28 EFFECTS OF ORIFICE BLOWING ON LIFT POWER SPECTRA

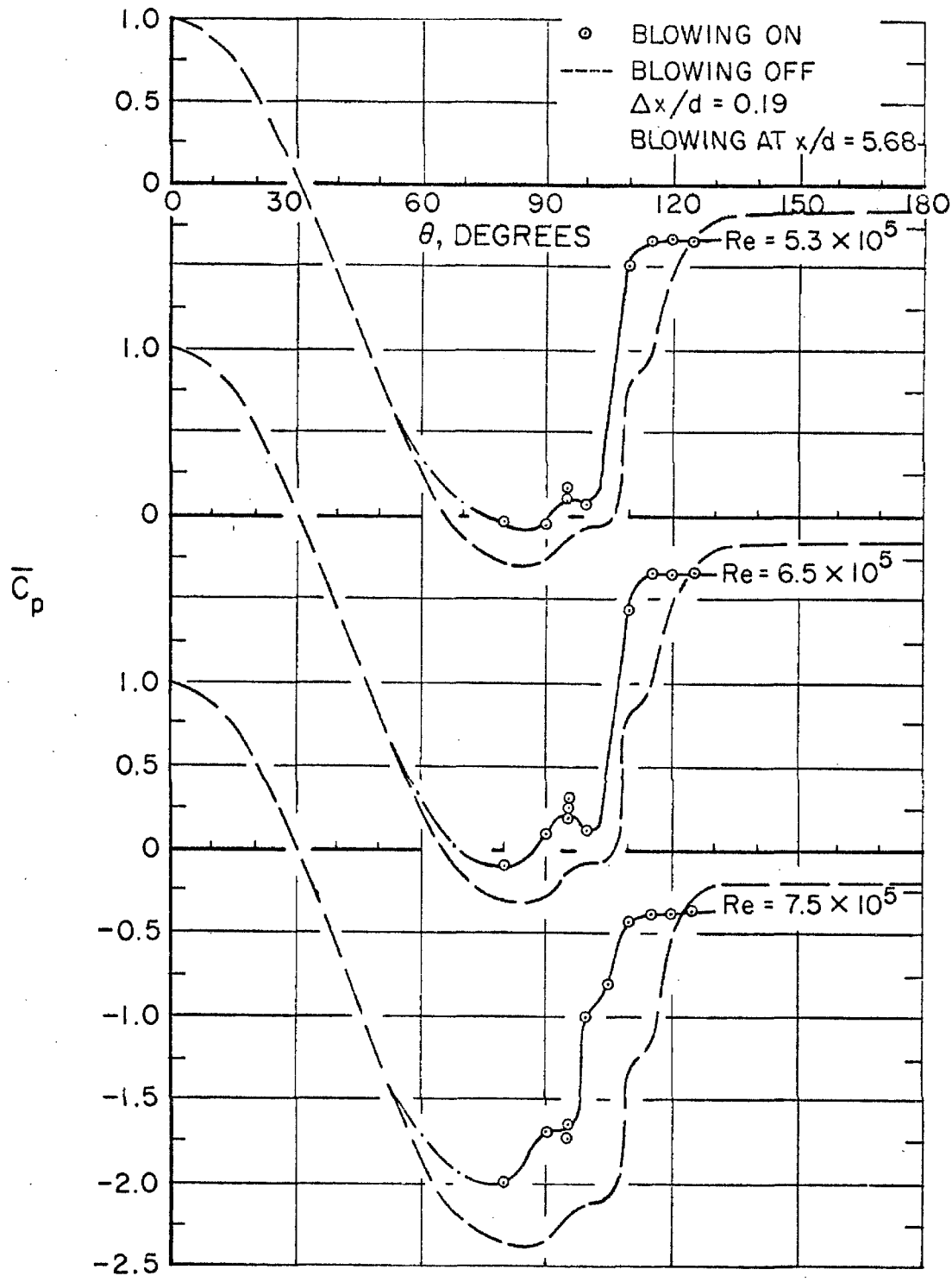

FIG. 29 EFFECTS OF ORIFICE BLOWING ON STATIC PRESSURE DISTRIBUTION

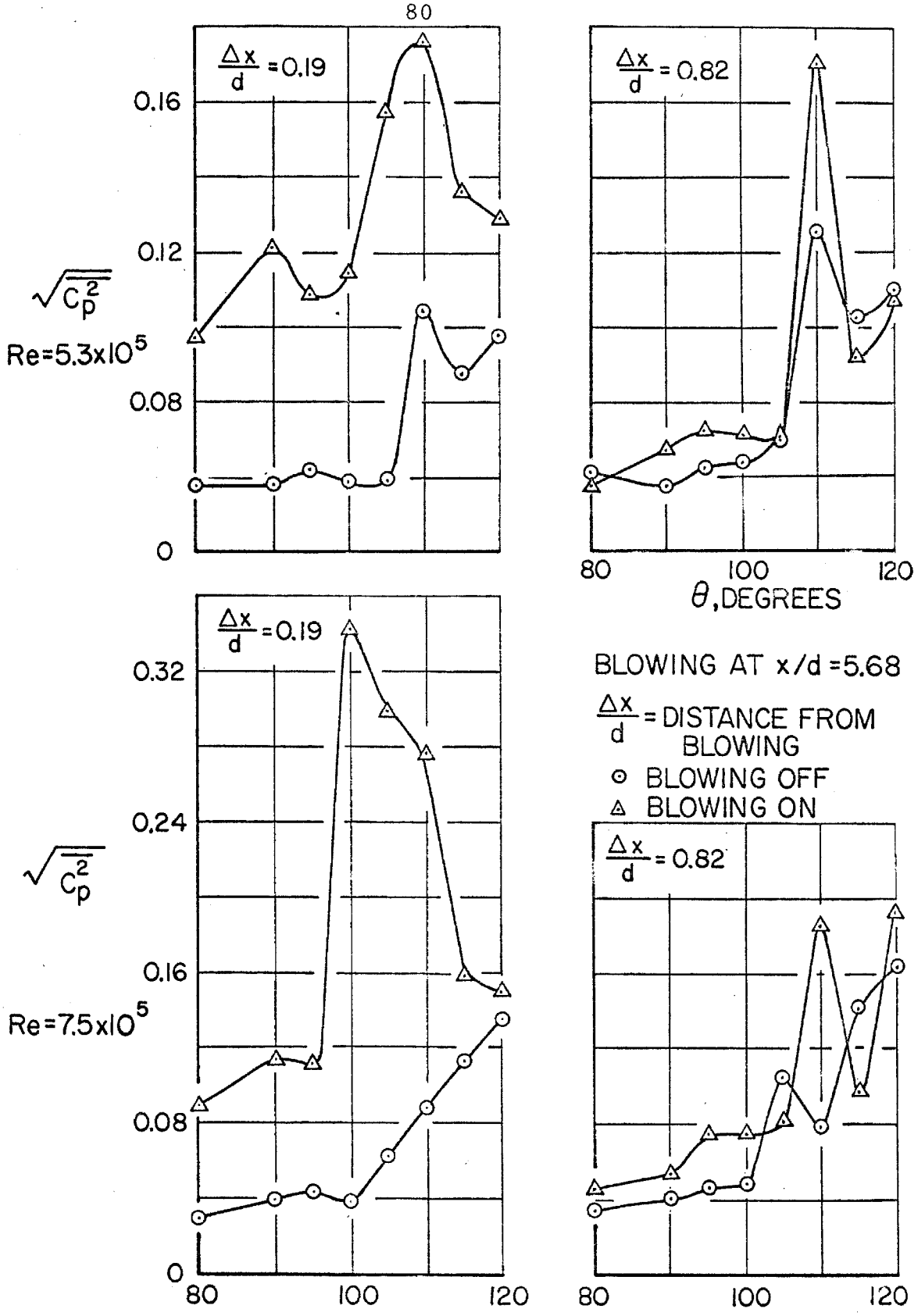

FIG. 30 EFFECTS OF ORIFICE BLOWING ON FLUCTUATING PRESSURE

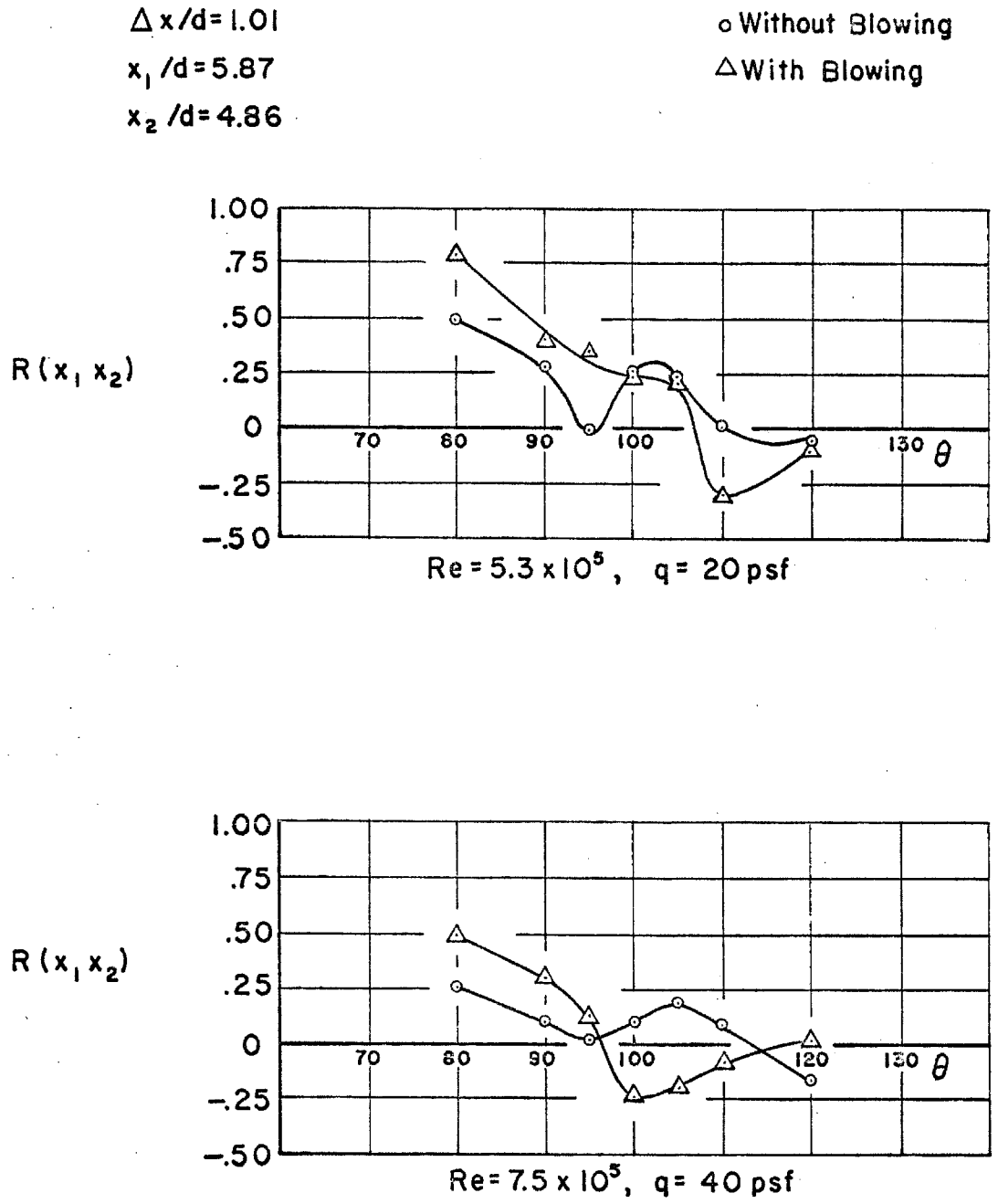

FIG. 31 CORRELATION COEFFICIENT FOR PRESSURE FLUCTUATIONS AS AFFECTED BY BLOWING

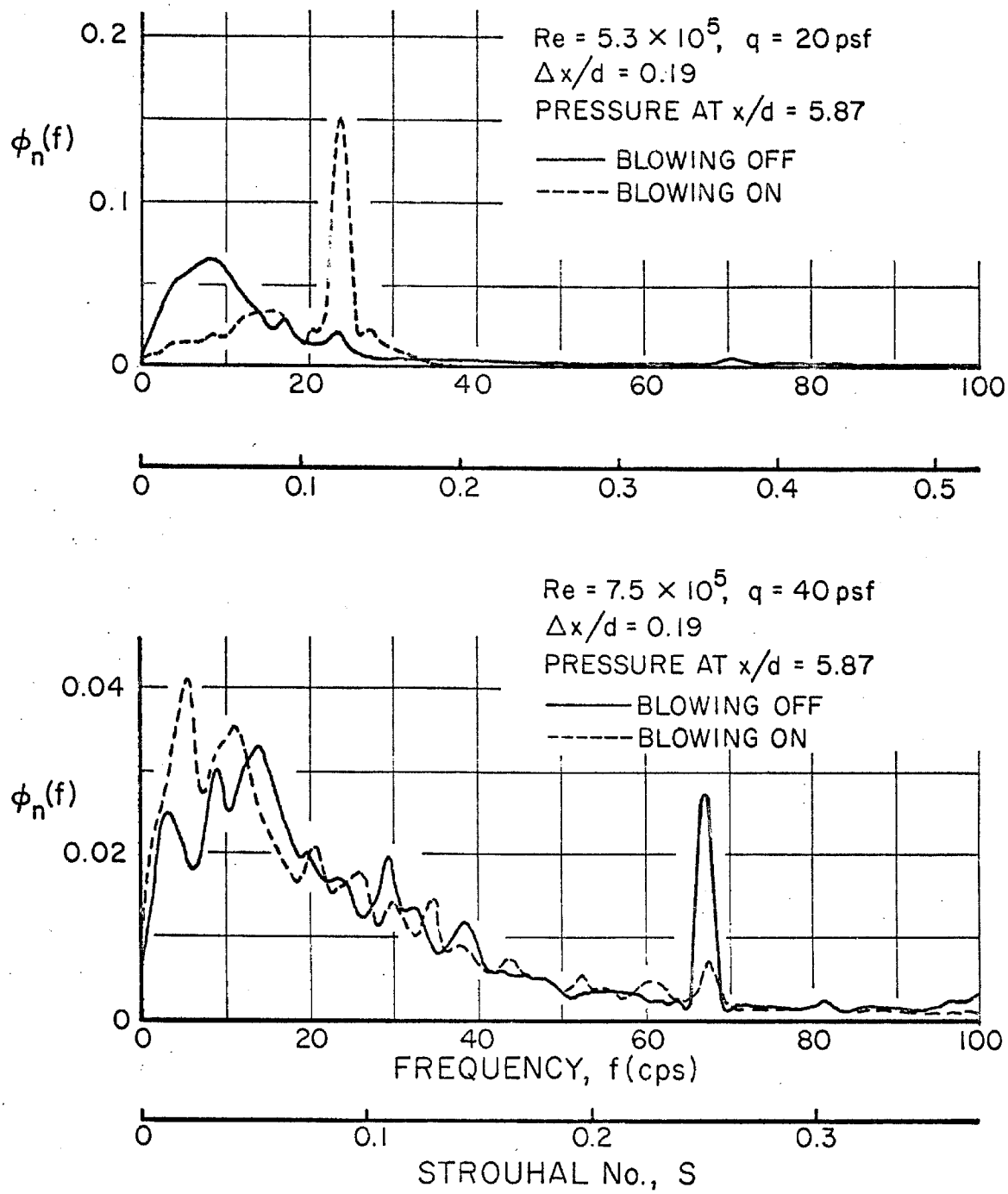

FIG. 32 EFFECTS OF ORIFICE BLOWING ON FLUCTUATING PRESSURE POWER SPECTRA AT $\Theta = 95^{\circ}$

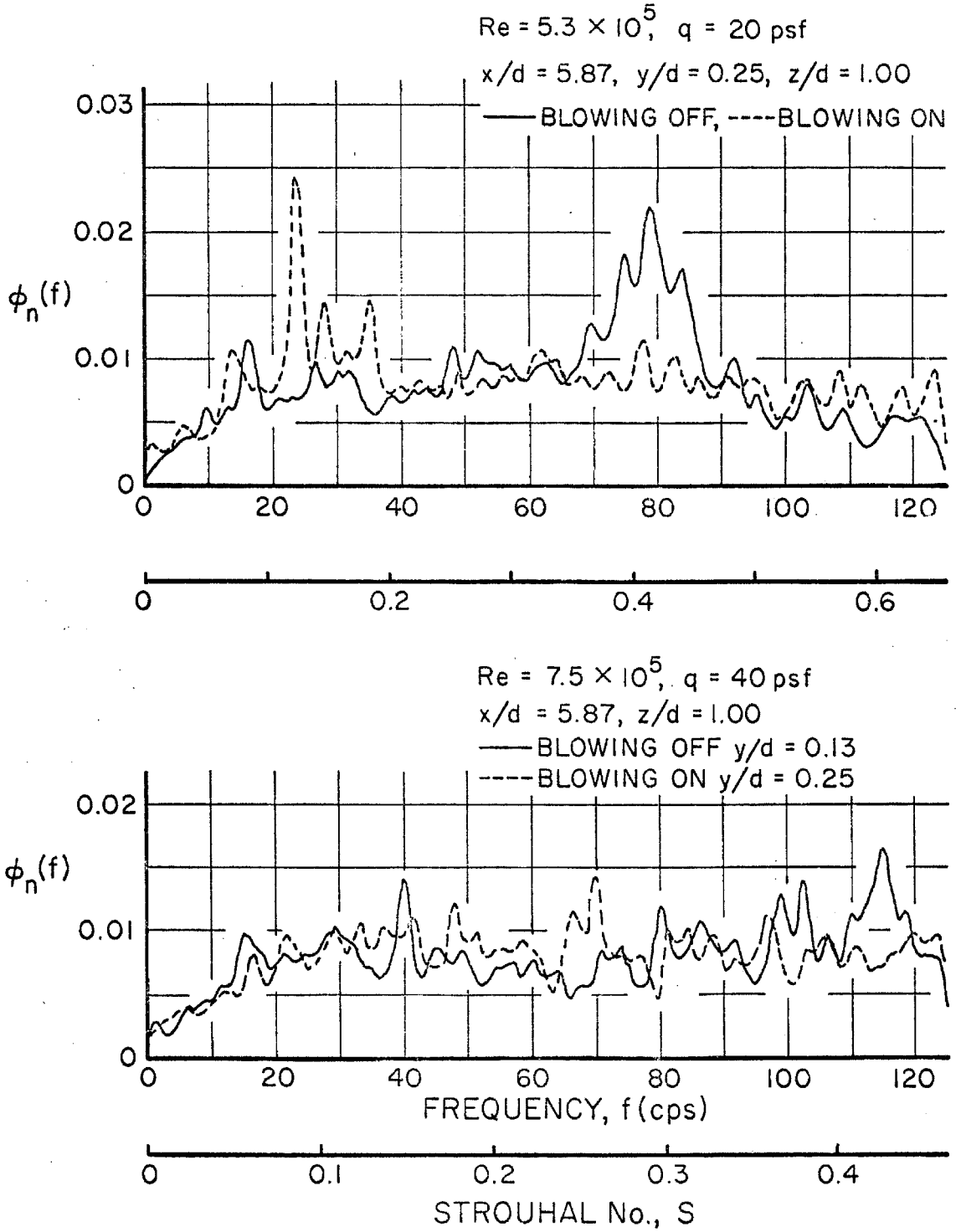

FIG. 33 EFFECTS OF ORIFICE BLOWING ON POWER SPECTRA OF WAKE VELOCITY FLUCTUATIONS

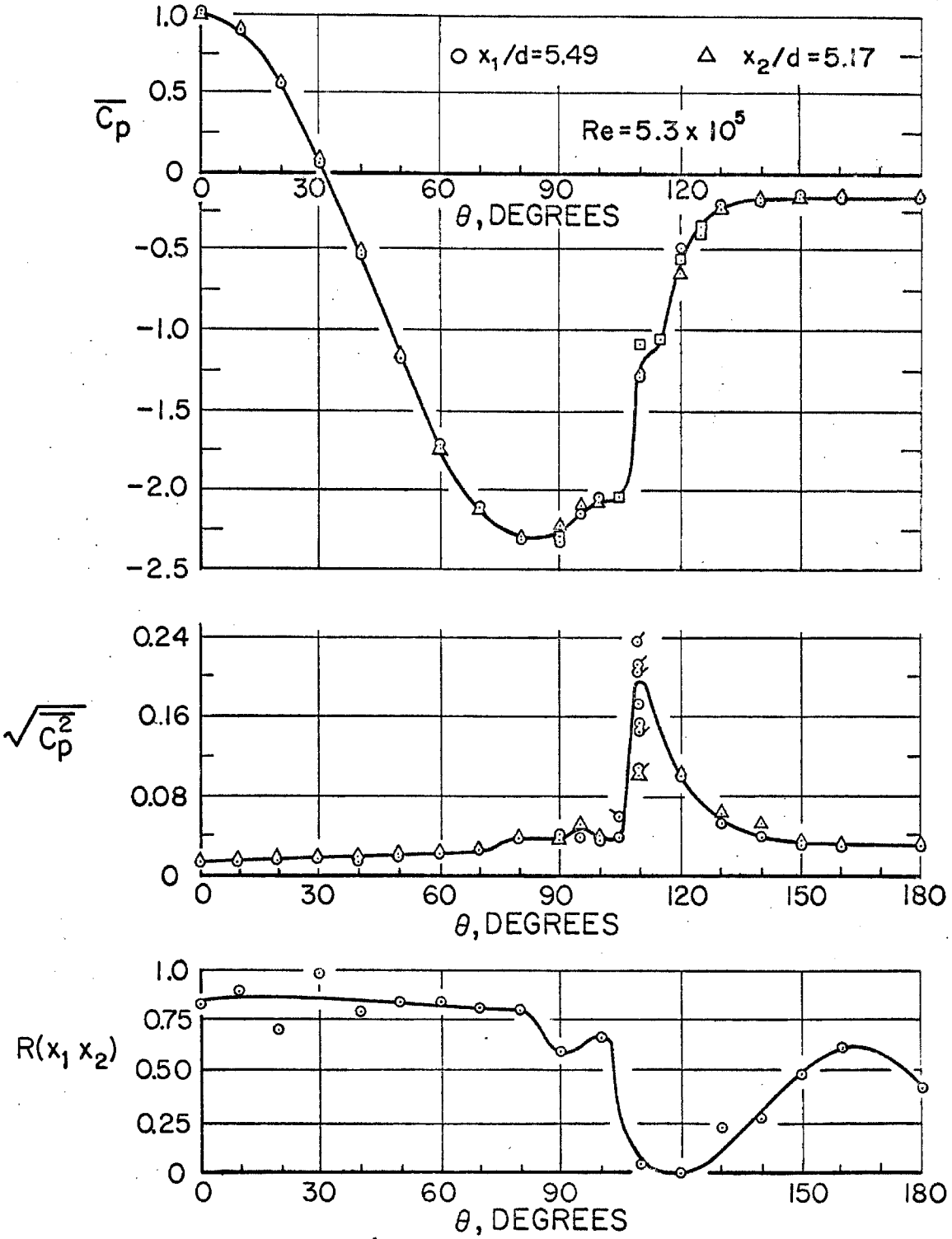

FIG. 34 SUMMARY OF PRESSURE MAPPING OVER THE CYLINDER

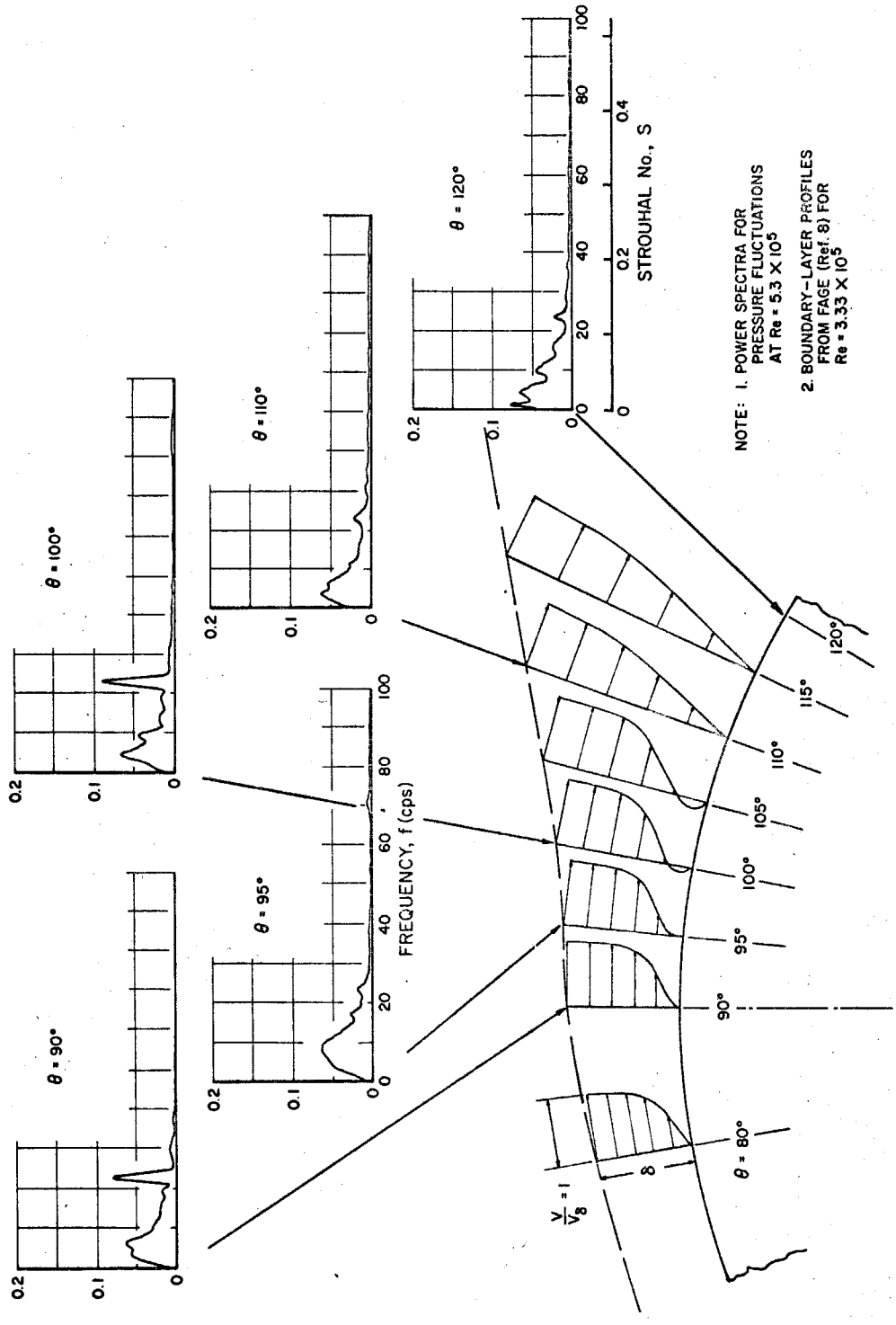

FIG. 35 POWER SPECTRA OF FLUCTUATING PRESSURES NEAR THE SEPARATION POINT